R. & M. No. 3786

PROCUREMENT EXECUTIVE, MINISTRY OF DEFENCE

AERONAUTICAL RESEARCH COUNCIL

REPORTS AND MEMORANDA

Iterative Method for Thick Cambered Wings in Subcritical Flow

By C. C. L. SELLS

Aerodynamics Dept., R.A.E., Farnborough

LONDON: HER MAJESTY'S STATIONERY OFFICE

1976

£4·50 NET

Iterative Method for Thick Cambered Wings in Subcritical Flow

By C. C. L. SELLS

Aerodynamics Dept., R.A.E. Farnborough

Reports and Memoranda No. 3786*

March, 1974

Summary

A method of computing the steady, inviscid flow around a thick, cambered and twisted wing (neglecting dihedral) is presented. The flow field is represented by distributions of sources and doublets in the chordal surface, the strengths of which are determined iteratively from the boundary conditions on the wing upper and lower surfaces. To save computing time, these conditions are transferred to the surface of the related uncambered wing (the 'thickness surface') by a two-term Taylor series expansion in the camber ordinate. This approximate boundary condition is now correct to second order. In order to improve the approximations for the singularity distributions at each stage, and so to speed up convergence, an inner iteration scheme is employed, based on a similar Taylor expansion centred on the mean chordal surface.

The method is extended to compressible (subcritical) flow with the help of the Prandtl-Glauert rule.

The method is tested on R.A.E. Wing 'B', a research wing with rapid spanwise changes in camber and twist near the root and tip. Results from two runs with different numbers of chordwise and spanwise stations agree well, which suggests that the method is well-conditioned and reliable; agreement with some results from the B.A.C. (Roberts) program is satisfactory; and the predictions of the latest version of the R.A.E. Standard Method agree with these reasonably well, in view of the marked spanwise deformation of the wing.

* Replaces R.A.E. Technical Reports 73047 and 74044—A.R.C. 34 959 and 35 354.

LIST OF CONTENTS

1. Introduction

Only in recent years, with the coming of large and fast computers, has it been possible to obtain fairly accurate numerical solutions for the steady inviscid incompressible flow around a given finite body immersed in a moving stream. The pioneering work was done by Smith and Hess[1] who calculated non-lifting solutions by distributing sources over the surfaces of such bodies, and showed how to include lifting effects in two-dimensional aerofoils and cascades. The flow around a finite wing at incidence can alternatively be represented by distributions of singularities (sources and doublets) on the wing chordal surface, and in this Report we describe the development of a computer program to perform the calculations for this method.

The method is based on the full second-order small-perturbation theory due to Weber[2], and proceeds by iteration as follows. We obtain approximations for the singularity distributions and compute the flow fields due to these singularities using the Ledger[3]–Sells[4] computer subroutine. In general these flow fields violate the boundary conditions of zero normal flow at certain points (collocation points) on the upper and lower wing surfaces; the amounts of these violations are computed and interpreted as residual errors in upwash. These residual errors are added and subtracted to give a symmetrical part and an antisymmetrical part, and can then be used to generate new source and doublet distributions to add to those already stored, in order approximately to cancel the respective errors. The velocity components may now be recomputed, and the iteration cycle continued.

The present method is judged important for the following reasons:

(1) For many years wing research workers have used linear theory, which is sufficiently accurate for some purposes; however, as time goes on greater accuracy is needed in some applications, and the present method can help to provide it.

(2) Some second-order terms can be conveniently added to the methods of linear theory, leading to the R.A.E. Standard Method[5,6] and its modification as in equation (3) of Ref. 7 (due originally to Lock[13]); see also Appendix E, Ref. 2, and Appendix B, Ref. 11; these methods are fairly quick to apply, and the present method can be used to check them when there is reason to be doubtful of their accuracy. To some degree, this will also be true for compressible subcritical flow when the local Mach number is sufficiently small for the Prandtl–Glauert rule to work well.

(3) In recent years a surface source distribution method, similar to that of Hess and Smith[1] but extended to lifting three-dimensional configurations, has been successfully designed and programmed at B.A.C., Weybridge, and is described by Roberts and Rundle[15]. This method, though time-consuming, is the best available for complicated body, or wing-and-body, shapes, but for wings alone it is considered worthwhile to have another method which might require less computing time for similar accuracy. Such a method would at least provide a compromise for anyone who desires more accurate knowledge of the flow field than the R.A.E. Standard Method can provide, without the expenditure of computer time on the scale of Roberts' program. The present method has the further advantage of providing a 'feel' for the physics of the flow, as the iterates (printed out by the program) can be examined at each stage.

(4) Possibilities are envisaged for extending the present method to deal with a wing mounted on a fuselage (and ultimately to a tailplane and engine nacelles also), still within the computing time-scale of the Roberts' program[15] and still with a 'feel' for the physics of the flow. This appears to be both important and possible, as Weber has shown (*see*, for example, Ref. 16) that there are wing-fuselage interaction effects which are not negligible but on the other hand not necessarily so large that such an extension is doomed to failure.

(5) The method can also be adapted as a wing design tool, as shown by Weber[2] and partially implemented by Sells[23]. Such an extension could also be used to design wings in combination with a fuselage or nacelles as in (4) above, or starting from a nearby solution obtained by other means. This may represent an advantage over the Roberts' method[15] which cannot be used economically as a direct design tool.

We now have to consider the most suitable way to compute the velocity fields due to the singularities. When the wing is symmetrical, it is sufficient to do this (for each collocation point) at one value of the local cartesian coordinate z (measured normal to the wing chordal surface), namely the section thickness ordinate $z = z_t$, and then to apply the symmetry and antisymmetry properties. For a cambered wing, two different values of z are relevant in general and to compute velocity fields at both values would effectively double the run times. We might do the computations on the chordal surface $z = 0$ and obtain the wing surface values by Taylor series expansions about $z = 0$ (Maclaurin series), as suggested by Weber[2]. This would save some computing time but would very likely fail near the tip, and near the root of a swept wing[2]. A better method seems to be still to compute velocity fields at $z = z_t$ and then to obtain the values on the wing surface using the first two terms of the Taylor series expansions about the 'thickness surface' $z = \pm z_t$. One advantage of this method (over the Maclaurin series approach) is that the 'thickness surface' will be nearer to at least one of the actual wing

surfaces than the chordal surface, and may be nearer to the other one also if the camber is sufficiently small, so that this Taylor series should be more accurate than the corresponding Maclaurin series. These matters are discussed more fully in Section 3, and the problem of calculating the necessary velocity field derivatives with respect to z is tackled in Section 4.

The basic first-order source distribution is easily obtained as twice the local 'thickness surface' slope (this follows from the first-order boundary condition). Determination of the basic first-order doublet (thin-wing loading) distribution is the classical problem of lifting-surface theory; the desirable attributes of any method of solution are speed, accuracy and mathematical rigour, in that order, and with this in mind the choice fell on the vortex lattice method as developed by Carr–Hill[19]. This method is indeed fairly quick for the first calculation on a given grid—a collocation matrix has to be set up and inverted—and very quick thereafter as the inverse matrix can be stored on magnetic tape for future use. It has been shown to give accurate answers in two-dimensions[20], and for the comparisons that have been made with other methods on three-dimensional wings so far the accuracy is generally sufficient for our purposes, and—most important—any local inaccuracies will be corrected along with second-order effects when the boundary condition error is evaluated.

For the success of the method, and because of the time scale involved in computing velocity fields, it is almost essential that the process converge adequately in at most two iterations. This means that the best possible singularity distributions must be sought at each iteration. Now, it is not essential to begin with an exact solution of linear theory. Simple improvements to the basic distributions determined as above are available from the Standard Method[5*], and have been found sufficient for uncambered wings; but for cambered wings there are extra cross-coupling terms in the boundary conditions, and these slow down convergence unacceptably. To recover from this, we have devised a fast inner-iteration technique, again based on the Maclaurin series[2] and the Standard Method[5], which generated still better singularity distributions and enabled us to realize our goal of convergence almost everywhere in two iterations, even for wings with quite large camber or variations in camber. The details are set down in Section 5; some results for particular wings are discussed in Section 6.

To obtain meaningful results near the wing leading edge, where linear theory predicts singularities in certain velocity components, we employ a device suggested by Lighthill[10] which in effect terminates the singularity distributions at a small finite distance behind the actual leading edge. Details appear in Appendix C.

In the course of the iterations a problem was encountered: having made the best available first guess for the singularity distributions, comparatively large errors in the boundary conditions appeared at the root section (on our swept wings), and these errors were at first reduced only slowly as the iterations proceeded. One difficulty is, that in the vortex-lattice scheme no collocation point can be placed at the centre line of a swept wing, so that no information from the centre line can be used for defining the planar-doublet distributions. A more general flaw is that no distribution of singularities could ever produce outside of itself a stream surface with a ridge line, which is always present at the root of a swept wing with constant-section geometry; and this affects both source and doublet calculations. What happens in practice is that at the root we require a rapid spanwise variation of these distributions which cannot be represented easily by parabolic interpolation on their values at the grid points, as is required for the Ledger–Sells method[3,4]. To overcome this difficulty we tried introducing a line-source and line-doublet distribution along the centre chordline (still strictly inside the wing surface). From the boundary-condition errors near the root, we can calculate the approximate strengths of these line singularities, and then calculate the velocity fields due to them and add to those due to the planar singularities; the boundary-condition errors can then be recalculated and the iteration cycle continued. The details are set out in Appendix D. This device was successful in reducing the boundary-condition errors so that they did not vary too rapidly near the root, and so the calculations with the planar distributions became more reliable, and convergence was improved. Of course, the ridge-line obstacle is not completely overcome in this way, and when the errors were checked in between the root and the first outboard collocation station, some fluctuation was observed in a sample case; however, the pressure coefficients turned out to be relatively insensitive to these fluctuating errors, once they had been reduced to second order, so that the problem is likely to be well-conditioned in practice.

Since the method would normally be run for at least two iterations, in terms of perturbation velocities it is a second-order method in the sense of Weber[2]. Also, since each perturbation velocity field is expanded to two terms in Taylor series, the boundary conditions to be satisfied, and the final pressure coefficients, are formally correct to second order in terms of section ordinates, twist angle and incidence. Thus, an assumption of the

---

* Still further improvement can be sought on the lines of Appendices A and E of Ref. 2, which give further higher-order terms. Allowing for differences in the basic lifting-surface theories, these terms should be equivalent to the second inner iteration of the technique described herein.

method is that the field errors due to the approximations by Taylor series are tolerably small. Moreover, since the Ledger–Sells subroutine applies only to singularities in a plane, we shall assume further that, when the wing is twisted, the singularity distributions in the mean chordal surface can be transferred to the unbanked plane containing the local chordline at each collocation section, without affecting the accuracy of the computed velocity fields to second order. This assumption requires[2] that any wing dihedral be of second-order magnitude, and that any chordwise local dihedral due to non-zero rate of change of twist $d\alpha_T/dy$ at the root be also of second-order magnitude. The method does not provide an internal *a posteriori* check on these assumptions, and it would be well to bear in mind, in any particular case, that they have been made. For untwisted symmetrical wings, of course, the assumptions are correct and then the final accuracy of the solution depends principally on the distribution of collocation points.

For subcritical flow, in which the free-stream Mach number is sufficiently small so that the local Mach number does not exceed about 0·8, the Prandtl–Glauert rule is used; the downstream (x) coordinate is uniformly stretched, leaving the transverse coordinates unchanged (affine transformation), so that the wing is transformed into the so-called analogous wing, and computations are performed in the affine coordinate system. The results are not the same as those for the analogous wing in incompressible flow, because the boundary conditions on the thick wing are changed by the affine transformation. The details are set out in Appendix E. For subcritical flow the method is no longer fully second-order, as the Prandtl–Glauert rule takes only the first-order compressibility perturbations into account.

An overall view of the program is provided in a résumé in Section 7, for the reader who wishes to know roughly how the program operates without going into the detailed exposition of the main text. The résumé is cross-referenced, and a flow diagram is also provided.

The program is written in Fortran and occupies just over 40K words of core store on a computer of the ICL 1900 series, with the storage requirements of most of the calculations reported in Section 6.

2. The Boundary Conditions on the Wing Surface

We consider a finite wing at a reference angle of incidence α in a free stream with speed unity. We take cartesian coordinates x^*, y, z^* with origin 0^* at the apex of the wing, with the x^*-axis in the reference downstream direction, the y-axis to starboard and the z^*-axis upwards; the free stream makes an angle α with the x^*-axis.

We intend to represent the flow field by distributions of sources and doublets on the wing chordal surface, which is generated by the chordlines between the leading and trailing edges at each value of y. When the wing is untwisted the chordal surface lies in a plane, which can be taken to be the plane $z^* = 0$; in general, however, the chordal surface is non-planar. Then we proceed as follows. At any spanwise 'control' station y, where the boundary conditions are to be satisfied, we consider the local plane Π which contains the local chordline and has normals parallel to the (x^*, z^*)-plane, that is to say, the plane is unbanked and makes an angle $\alpha_T(y)$ (the local twist angle) with the x^*-axis, *see* Fig. 1. α_T is reckoned positive in the sense in which the local angle of incidence is increasing, that is, clockwise in a view along the positive y-axis. Thus, in this representation we shall ignore dihedral effects. We define local cartesian coordinates (x, z) such that the x-axis is the intersection of the local plane Π with the central plane of symmetry $y = 0$, so that the x-axis is parallel to the local chordline, and the z-axis is in the central plane $y = 0$ and is directed upwards, completing a right-handed set with the x and y-axes; the local plane Π is the plane $z = 0$. The origin 0 is the z-projection of the apex 0^* on Π. The (x, z)-axes can be got by rotating the (x^*, z^*)-axes through the angle $\alpha_T(y)$. Wing thickness and camber are given for each spanwise station, y = constant, in the form used for two-dimensional sections, i.e. as ordinates z_w normal to the chord

$$z_w(x, y) = \pm z_t(x, y) + z_s(x, y). \tag{1}$$

z_t is the thickness distribution and z_s the camber distribution. Both z_t and z_s vanish at leading and trailing edges. $z_t/c(y)$, $z_s/c(y)$, α_T and the incidence α will all be taken as at least first-order small quantities, where $c(y)$ is the local chord.

Following Weber[2], we now assume that a singularity distribution on the plane $z = 0$ produces the same velocity field—to second-order accuracy—at this control station, as would the singularity distribution on the twisted chordal surface. Such an assumption has to be made here, since we intend to employ the Ledger–Sells[3,4] computer subroutine which applies only to singularity distributions in a plane. The assumption is not unreasonable, because the most significant contribution to the integral for a velocity component comes from spanwise stations near the control station, which lies in both surfaces, and moreover the two surfaces are nearly

parallel at this station, depending on the local behaviour of the (assumed small) quantity $d\alpha_T/dy^*$. As remarked by Weber[2] the assumption fails at the centre line of a wing with dihedral of first-order magnitude, and so any dihedral will be assumed to be of at most second-order magnitude, so that we can ignore it. (Overall dihedral can be treated if and when necessary, by considering singularity distributions in two half-planes).

Source and doublet distributions are placed, then, in the wing chordal surface, and we shall assume that at a particular value of y with an associated local plane Π, the velocity field would be approximately the same if the aforementioned distributions were placed instead in the projection of the wing on Π. The shape of this projection, the apex of which is at 0 (*see* Fig. 1), is independent of α_T to first order, and can be taken as that of the projection on the basic reference plane $z^* = 0$. Let the perturbation velocities due to these distributions be (in the xyz-coordinate system)

$$\begin{aligned}\mathbf{u}_t &= [u_t(x, y, z_s \pm z_t),\ v_t(x, y, z_s \pm z_t),\ w_t(x, y, z_s \pm z_t)\\ &= [u_t(x, y, z_t \pm z_s),\ v_t(x, y, z_t \pm z_s),\ \pm w_t(x, y, z_t \pm z_s)]\end{aligned} \tag{2}$$

and

$$\begin{aligned}\mathbf{u}_l &= [u_l(x, y, z_s \pm z_t),\ v_l(x, y, z_s \pm z_t),\ w_l(x, y, z_s \pm z_t)]\\ &= [\pm u_l(x, y, z_t \pm z_s),\ \pm v_l(x, y, z_t \pm z_s),\ w_l(x, y, z_t \pm z_s)],\end{aligned} \tag{3}$$

where the upper and lower signs correspond to upper and lower wing surfaces, respectively.

The incident free stream makes an angle $\alpha + \alpha_T(y)$ with the local x-axis, *see* Fig. 1, and so in the local (x, y, z) coordinates it has components

$$\mathbf{U}_\infty = [\cos(\alpha + \alpha_T),\ 0,\ \sin(\alpha + \alpha_T)]. \tag{4}$$

The surface boundary condition of vanishing normal velocity is

$$(\mathbf{U}_\infty + \mathbf{u}_t + \mathbf{u}_l) \,.\, \mathrm{grad}\,[z_w(x, y) - z] = 0. \tag{5}$$

Substituting for all quantities in equation (5), we have

$$U\left(\frac{\partial z_s}{\partial x} \pm \frac{\partial z_t}{\partial x}\right) + V\left(\frac{\partial z_s}{\partial y} \pm \frac{\partial z_t}{\partial y}\right) - W = 0 \tag{6}$$

where

$$\left.\begin{aligned} U &= \cos(\alpha + \alpha_T) + u_t(x, y, z_t \pm z_s) \pm u_l(x, y, z_t \pm z_s),\\ V &= \qquad\qquad v_t(x, y, z_t \pm z_s) \pm v_l(x, y, z_t \pm z_s)\end{aligned}\right\} \tag{7}$$

and

$$W = \sin(\alpha + \alpha_T) \pm w_t(x, y, z_t \pm z_s) + w_l(x, y, z_t \pm z_s).$$

We have obtained equation (6) by a simple method based on the geometry of Fig. 1, but it is derived rigorously (to second order) by Weber[2], both at and away from the centre section $y = 0$.

The sign convention of equations (2) and (3) implies the assumption that the upper surface lies entirely above the local chordline and that the lower surface lies entirely below it; that is, $|z_s| < z_t$ for all (x, y) on the planform. However, for two-dimensional flow the derived formulae can be given a meaning and can produce meaningful results, even for a section with large camber so that part of the chordline lies outside the section. It is reasonable to expect similar behaviour in three dimensions.

---

* By a quasi-two-dimensional analysis, it can be shown that the errors in u_t and w_l due to this assumption are of the order $(z_w/c)(d\alpha_T/dy)$ times integrals of the source and doublet distributions respectively, i.e. 3rd order, and in general that the errors in w_t and u_l are smaller still.

3. Taylor Series Expansion in the Camber Ordinate

Let us assume that we have determined approximate source and doublet distributions and are ready to compute their velocity fields at collocation points for insertion into the boundary conditions (6), either to obtain better approximations or to check the accuracy of the solution. Equation (6) may be considered in several ways.

(1) Velocity components may be computed at the wing surfaces $z = z_s \pm z_t$ for each collocation point. In principle, for untwisted wings this would give the residual error in the boundary condition exactly. But whereas a single computation at $z = z_t$ (and use of equations (2) and (3)) suffices for these wings, with $z_s = 0$, when $z_s \neq 0$ the resulting velocity field computation at two values of z would approximately double the run times (because this computation takes up most of the total time), which is undesirable in itself and would also render the whole method less competitive. Moreover, when the wing camber is so large that the chordal (singularity) surface intersects the wing surface, z_w might become very small at some points; the Ledger–Sells[3,4] subroutine for $z \neq 0$ would become ill-conditioned there, and the rather different (and larger) subroutines for $z = 0$ would have to be incorporated; this would increase the program size—a minor but still significant detail. If any such points (of small $|z_w|$) were to lie on the centre line of a swept wing, a further problem would arise since in general w_l would have a logarithmic singularity there.

(2) Some velocity components (u_t, v_t, w_l) may be computed on the chordal surface ($z = 0$) and the boundary condition transferred there by Taylor (Maclaurin) series expansions. (u_l, v_l and w_t are immediately available in terms of the singularity distributions.) This approach has been thoroughly discussed by Weber[2] who points out that the method will fail at the root $y = 0$ of a swept wing, where neither w_t nor w_l may be expanded in Maclaurin series, and does not recommend it near a wing tip either. She has suggested a hybrid method in which computations near root and tip are performed on the surface $z = z_w$ instead, as in (1) above, and makes out a case also for surface computations near the leading edge. As remarked above, this method would encounter difficulties for a wing with large root or tip camber; further, if the singularity distribution is such that the velocity field computed at the surface $z = z_w$ differs significantly from that found by Maclaurin series (and computations at $z = 0$), then there may be a numerical mismatch between the respective computation regions; this may lead to irregular behaviour in the corrections to the singularity distributions, and this in turn to spurious fluctuations in the computed velocity fields at the next iteration cycle. While not necessarily serious, this situation should preferably be avoided if possible.

However, we shall show later (Section 5) that despite the regional limitations, Maclaurin series can be advantageously employed to reduce the number of iterations required in our procedure.

(3) In an earlier pilot program for symmetrical wings which has been proven reasonably accurate and fast, field computations were done on the surface $z = z_t$. A simple extension suggests itself in which these are done in conjunction with two-way Taylor expansions about the 'thickness surface' $z = \pm z_t$ for the velocity components on the actual wing upper and lower surfaces. This method partly shares the advantage of wing-surface computation over Maclaurin series, because the 'thickness surface' will be nearer to at least one of the actual surfaces than the chordal surface, and may be nearer to the other one also (if $|z_s| < \frac{1}{2}z_t$), so that this Taylor series should be more accurate than the corresponding Maclaurin one. This advantage will be particularly marked near the leading edge $\xi = 0$, because (for conventional sections with rounded noses) z_s goes to zero faster than z_t does, as $\xi \to 0$.

The proposed Taylor series method also shares the advantage of the Maclaurin series approach over wing-surface computations, of computing at only one value of z; all three components of $\mathbf{u}_t$ or $\mathbf{u}_l$ must still be computed by double integration, but as the Ledger–Sells subroutine now computes all three in parallel, with a saving in arithmetic, there would not be much difference in computing times between Maclaurin series and Taylor series methods.

Further, although w_t and w_l do not possess Maclaurin expansions at the root of a swept wing, they still possess Taylor expansions valid in some neighbourhood of $z = z_t > 0$, and so the method can be applied at the root. From a strict mathematical viewpoint, Taylor expansion is valid only up to the nearest singularity which in this approach is $z = 0$, and so we should require $|z_s| < z_t$; for $|z_s| > z_t$ the full infinite Taylor series would diverge; but as computation of an infinite number of terms is not practicable, we shall content ourselves with the first two terms only, which will exhibit the local behaviour sufficiently near $z = z_t$, i.e. for sufficiently small z_s, and which will provide a continuous formal extension, which cannot diverge, to larger values of z_s. We can argue that $z = 0$ is not a real singularity of the physical flow (which is unique outside the wing surface, and only changes inside the surface according to the type *and position* of the singularities representing it), and thus the results of our two-term Taylor expansion can indeed be meaningful for some $|z_s| \geqslant z_t$.

This argument also makes it easy to justify the sign convention in equations (2) and (3), starting with the remark that (since $z_t > 0$) both these equations are correct on the 'thickness surface' $z = \pm z_t$.

In a neighbourhood of $z = z_t$, then, we formally write the two-term Taylor expansion for a typical velocity component, say u_t:

$$u_t(x, y, z_t \pm z_s) = u_t(x, y, z_t) \pm z_s \frac{\partial u_t}{\partial z}(x, y, z_t) + 0(z_s^2) \tag{8}$$

with similar expressions for v_t, w_t, u_l, v_l, w_l. From now until further notice, we shall work with these quantities at $z = z_t$ and drop the brackets (x, y, z). We then have for the complete velocity $\mathbb{U} = \mathbb{U}_\infty + \mathbb{u}_t + \mathbb{u}_l = (U, V, W)$ (*see* equation (7)) on the wing surface, the relations

$$U = \cos(\alpha + \alpha_T) + \left(u_t + z_s \frac{\partial u_l}{\partial z}\right) \pm \left(z_s \frac{\partial u_t}{\partial z} + u_l\right), \tag{9}$$

$$V = \left(v_t + z_s \frac{\partial v_l}{\partial z}\right) \pm \left(z_s \frac{\partial v_t}{\partial z} + v_l\right) \tag{10}$$

and

$$W = \sin(\alpha + \alpha_T) + \left(z_s \frac{\partial w_t}{\partial z} + w_l\right) \pm \left(w_t + z_s \frac{\partial w_l}{\partial z}\right). \tag{11}$$

These equations can now be used in equation (6) and will also be needed to obtain the pressure coefficients

$$C_p = 1 - (U^2 + V^2 + W^2). \tag{12}$$

Within second-order theory, for both equations (6) and (12) we can write $\sin(\alpha + \alpha_T) \doteqdot \alpha + \alpha_T$ in equation (11), and for the boundary condition (6) (but not for equation (12)) we can write $\cos(\alpha + \alpha_T) \doteqdot 1$ in equation (9). Making these changes, we have

$$\left.\begin{aligned} U &= Q_0 \pm Q_1, \\ V &= Q_2 \pm Q_3 \\ W &= Q_5 \pm Q_4 \end{aligned}\right\} \tag{13}$$

with

$$Q_0 = 1 + u_t + z_s \frac{\partial u_l}{\partial z}, \tag{14}$$

$$Q_1 = z_s \frac{\partial u_t}{\partial z} + u_l, \tag{15}$$

$$Q_2 = v_t + z_s \frac{\partial v_l}{\partial z}, \tag{16}$$

$$Q_3 = z_s \frac{\partial v_t}{\partial z} + v_l, \tag{17}$$

$$Q_4 = w_t + z_s \frac{\partial w_l}{\partial z} \tag{18}$$

and

$$Q_5 = \alpha + \alpha_T + z_s \frac{\partial w_t}{\partial z} + w_l. \tag{19}$$

Substituting values (13) into the corresponding square brackets in equation (6), we have

$$(Q_0 \pm Q_1)\left(\frac{\partial z_s}{\partial x} \pm \frac{\partial z_t}{\partial x}\right) + (Q_2 \pm Q_3)\left(\frac{\partial z_s}{\partial y} \pm \frac{\partial z_t}{\partial y}\right) - (Q_5 \pm Q_4) = 0. \tag{20}$$

Multiplying out, equation (20) becomes

$$R_l \pm R_t = 0$$

whence we obtain the symmetric part of the boundary condition

$$R_t = 0 \tag{21}$$

and the antisymmetric part

$$R_l = 0 \tag{22}$$

where

$$R_t = Q_0\frac{\partial z_t}{\partial x} + Q_1\frac{\partial z_s}{\partial x} + Q_2\frac{\partial z_t}{\partial y} + Q_3\frac{\partial z_s}{\partial y} - Q_4 \tag{23}$$

and

$$R_l = Q_0\frac{\partial z_s}{\partial x} + Q_1\frac{\partial z_t}{\partial x} + Q_2\frac{\partial z_s}{\partial y} + Q_3\frac{\partial z_t}{\partial y} - Q_5. \tag{24}$$

R_t and R_l are called *residuals*, for a reason which will become clear later.

It is convenient here to introduce the local coordinate system used. The local percentage chord ξ is given by

$$x = x_L(y) + c(y)\xi \tag{25}$$

where $x_L(y)$ is the leading edge ordinate and $c(y)$ is the local chord. We can define a variable $\bar{\eta} = y$ to go with ξ, and use $\partial/\partial\bar{\eta}$ to denote partial derivatives with respect to $\bar{\eta}$ along lines of constant percentage chord ξ. Then from equation (25)

$$\frac{\partial}{\partial x} = \frac{1}{c}\frac{\partial}{\partial \xi} \tag{26}$$

and, writing $x_L' = dx_L/dy$, $c' = dc/dy$

$$\frac{\partial}{\partial y} = \frac{\partial}{\partial \bar{\eta}} - (x_L' + c'\xi)\frac{\partial}{\partial x} = \frac{\partial}{\partial \bar{\eta}} - \tan\Lambda\frac{\partial}{\partial x} \tag{27}$$

where $\Lambda = \arctan(x_L' + c'\xi)$ is the local sweep angle.

4. Determination of the Velocity Field Derivatives

4.1 General

We assume that at this point in an iteration cycle, we have obtained approximate source and doublet distributions and that we have computed their velocity fields $\mathbf{u}_t$, $\mathbf{u}_l$ at discrete collocation points $[x, y, z_t(x, y)]$, following the procedure of Section 3. The next step is to substitute $\mathbf{u}_t$ and $\mathbf{u}_l$ into the expressions (24) and (25) for the residuals. To do this, the z-derivatives occurring in $Q_0 \ldots Q_5$ given by equations (14) to (19) must also be determined numerically, and this is not a trivial matter.

It may be enquired, whether we can simplify the problem by making use of the values of w_t, u_l and v_l which are known on $z = 0$, being simply related to the source and doublet distributions. There are two reasons for not

doing this. At the root, we intend to make use of line source and doublet distributions on $y = z = 0$, to improve the quality of the solution there (*see* Appendix D); thus we do not have this information at all at the root. Also, near the leading edge $\xi = 0$, w_t, u_t and v_t (on $z = 0$) generally become large like $\xi^{-\frac{1}{2}}$, and (following Lighthill's theory; *see* Appendix C) we intend to make the solution uniformly valid near the leading edge by stretching the ξ-coordinate; these two facts would impose an intolerable strain on numerical differentiation between $z = z_t$ and $z = 0$.

We therefore want to determine the derivatives from the values of $\mathbf{u}$ computed on $z = z_t(x, y)$. To attack the problem, we draw two families of curves on the thickness surface $z = z_t$. One family is generated by the intersections of the thickness surface with sectional planes $y =$ constant, and we may call these, chordwise curves. The other family is generated by the intersections of the thickness surface with the (not necessarily planar) surfaces $\xi =$ constant; these we may call spanwise curves. Let the arclength along a chordwise curve, measured from the leading edge to some point P, be s_1, and that along a spanwise curve (measured from the root) be s_2; also, let $\mathbf{t}_1$ be the unit vector tangent to the chordwise curve at P, and $\mathbf{t}_2$ the unit vector tangent to the spanwise curve (Fig. 2). If a typical velocity field component u has been computed at the intersections of the two families of chordwise and spanwise curves, then by regarding u as a function of s_1 and s_2 we can obtain the surface derivatives, $\partial u/\partial s_1$ along $\mathbf{t}_1$ and $\partial u/\partial s_2$ along $\mathbf{t}_2$, at each point P by numerical differentiation.

We remark that the program has been arranged to compute the chordwise derivative $\partial u/\partial s_1$ by cubic spline fit, and the spanwise derivative $\partial u/\partial s_2$ by a simple quadratic fit through three points at a time. We chose the latter technique because we discovered that in a simple case with some variation along a spanwise curve near root and tip but hardly any in mid-semispan, the spanwise cubic spline fit produced a small oscillation in the (presumed smooth) mid-semispan region. This is an occupational hazard for the user of cubic spline fits; it can frequently be tolerated if the oscillations are small enough compared with the intrinsic variations, but otherwise we prefer not to have them. We do not claim complete accuracy in the numerical derivatives either way, and particularly not in the chordwise derivatives near the leading edge (we have checked these for two analytic functions). The leading edge is a sensitive region but we do not know how to improve the treatment there, apart from the crude acquisition of more data; we have tried suitable reflection of the data in the axis $s_1 = 0$ but we found surprisingly that this only made matters worse. However, we bear in mind that the end results of the present computation are derivatives like $\partial u/\partial z$ which will be multiplied by the local camber z_s, and since $z_s \to 0$ as the leading edge is approached, larger errors may perhaps be tolerated in this region than elsewhere.

Returning to the task at hand, we consider first the chordwise curves. Let θ_1 be the angle between the tangent vector $\mathbf{t}_1$ and the x-axis (Fig. 2), so that $\tan\theta_1$ is the local chordwise slope of the thickness surface:

$$\tan\theta_1 = \frac{\partial z_t}{\partial x}.$$

By resolution along $\mathbf{t}_1$, or by rotating coordinate axes, we have

$$\frac{\partial u}{\partial x}\cos\theta_1 + \frac{\partial u}{\partial z}\sin\theta_1 = \frac{\partial u}{\partial s_1}. \tag{28}$$

Similarly, if $\mathbf{u} = (u, v, w)$ stands for either $\mathbf{u}_t$ or $\mathbf{u}_b$, v and w satisfy the equations

$$\frac{\partial v}{\partial x}\cos\theta_1 + \frac{\partial v}{\partial z}\sin\theta_1 = \frac{\partial v}{\partial s_1} \tag{29}$$

and

$$\frac{\partial w}{\partial x}\cos\theta_1 + \frac{\partial w}{\partial z}\sin\theta_1 = \frac{\partial w}{\partial s_1} \tag{30}$$

We can establish similar relations among the derivatives by considering the spanwise curves. Let a typical spanwise surface length element ds_2, aligned with the vector $\mathbf{t}_2$ be resolved into length elements dx, dy, dz, let θ_2 be the angle between $\mathbf{t}_2$ and the (x, y)-plane and let Λ be the angle between the y-axis and the projection of

$\mathbf{t}_2$ on the (x, y)-plane (Fig. 3). Thus $\tan \theta_2$ is the local slope of the thickness surface along the spanwise curves:

$$\tan \theta_2 = \frac{\partial z_t}{\partial \bar{\eta}}.$$

Also Λ is the local sweep angle, as before. From Fig. 3, we have

$$\frac{\partial x}{\partial s_2} = \cos \theta_2 \sin \Lambda \equiv (\mathbf{t}_2)_x,$$

$$\frac{\partial y}{\partial s_2} = \cos \theta_2 \cos \Lambda \equiv (\mathbf{t}_2)_y \tag{31}$$

and

$$\frac{\partial z}{\partial s_2} = \sin \theta_2 \equiv (\mathbf{t}_2)_z.$$

Hence, for the field quantity u

$$\frac{\partial u}{\partial x} \cos \theta_2 \sin \Lambda + \frac{\partial u}{\partial y} \cos \theta_2 \cos \Lambda + \frac{\partial u}{\partial z} \sin \theta_2 = \frac{\partial u}{\partial s_2}. \tag{32}$$

Similarly

$$\frac{\partial v}{\partial x} \cos \theta_2 \sin \Lambda + \frac{\partial v}{\partial y} \cos \theta_2 \cos \Lambda + \frac{\partial v}{\partial z} \sin \theta_2 = \frac{\partial v}{\partial s_2} \tag{33}$$

and

$$\frac{\partial w}{\partial x} \cos \theta_2 \sin \Lambda + \frac{\partial w}{\partial y} \cos \theta_2 \cos \Lambda + \frac{\partial w}{\partial z} \sin \theta_2 = \frac{\partial w}{\partial s_2}. \tag{34}$$

The six equations obtained thus are completed by the relations for irrotational flow (curl $\mathbf{u} = \mathbf{0}$):

$$\frac{\partial w}{\partial x} = \frac{\partial u}{\partial z}, \tag{35}$$

$$\frac{\partial w}{\partial y} = \frac{\partial v}{\partial z}, \tag{36}$$

$$\frac{\partial u}{\partial y} = \frac{\partial v}{\partial x} \tag{37}$$

and the relation for conservation of mass in incompressible flow (div $\mathbf{u} = 0$):

$$\frac{\partial u}{\partial x} + \frac{\partial v}{\partial y} + \frac{\partial w}{\partial z} = 0. \tag{38}$$

We now have a total of ten linear equations for the nine unknowns $\partial u/\partial x$, etc. However, the first nine equations are not linearly independent. Let us write [grad $\mathbf{u}$] for the second-order tensor whose components are $\partial u_i/\partial x_j$, where $u_i \equiv (u, v, w)$ and $x_j \equiv (x, y, z)$. Since the tensor is symmetric, $\partial u_i/\partial x_j = \partial u_j/\partial x_i$, the two double scalar products with $\mathbf{t}_1$ and $\mathbf{t}_2$ are equal:

$$[\mathbf{t}_1 \,.\, \text{grad}\, \mathbf{u}] \,.\, \mathbf{t}_2 = [\mathbf{t}_2 \,.\, \text{grad}\, \mathbf{u}] \,.\, \mathbf{t}_1$$

or, in suffix notation with summation over repeated suffices:

$$\left(t_{1j}\frac{\partial u_i}{\partial x_j}\right)t_{2i}=\left(t_{2i}\frac{\partial u_j}{\partial x_i}\right)t_{1j}. \tag{39}$$

The unit vector $\mathbf{t}_1$ has components $(\cos\theta_1, 0, \sin\theta_1)$ and $\mathbf{t}_2$ has components given by equations (31). Thus the components of $\mathbf{t}_1$. grad $\mathbf{u}$ are given by the left sides of equations (28) to (30) and the components of $\mathbf{t}_2$. grad $\mathbf{u}$ are given by the left sides of equations (32) to (34). Equation (39) now tells us that a linear combination of equations (28) to (30) is equal to a linear combination of equations (32) and (34) (the coefficient $(\mathbf{t}_1)_y$ for (33) is zero). For consistency the same linear combinations of the right sides ought to be equal, which gives on substituting into equation (39)

$$\frac{\partial u}{\partial s_1}\cos\theta_2\sin\Lambda+\frac{\partial v}{\partial s_1}\cos\theta_2\cos\Lambda+\frac{\partial w}{\partial s_1}\sin\theta_2=\frac{\partial u}{\partial s_2}\cos\theta_1+\frac{\partial w}{\partial s_2}\sin\theta_1. \tag{40}$$

In fact, because of discretization errors in calculating the field derivatives with respect to s_1 and s_2, the consistency condition (40) is not in general satisfied. However, if the error represented by the difference between the two sides of equation (40) is not large compared with the largest of $|\partial u/\partial z|$, $|\partial v/\partial z|$ and $|\partial w/\partial z|$, then this gives us a measure of confidence in these values. This difference is in fact output by the program along with the z-derivatives, for both $\mathbf{u}_t$ and $\mathbf{u}_l$, as a check.

Despite the linear dependence, it turns out that we cannot safely ignore any one of the equations and simply solve the rest. We can examine two cases.

(1) At the points of chordwise maximum thickness $\theta_1=0$; invoking equations (35) to (37) here and throughout the analysis, equations (28) to (30) give

$$\frac{\partial u}{\partial x}=\frac{\partial u}{\partial s_1};\qquad \frac{\partial v}{\partial x}=\frac{\partial v}{\partial s_1};\qquad \frac{\partial u}{\partial z}=\frac{\partial w}{\partial s_1}.$$

Substituting in equation (32), we get

$$\frac{\partial u}{\partial s_1}\cos\theta_2\sin\Lambda+\frac{\partial v}{\partial s_1}\cos\theta_2\cos\Lambda+\frac{\partial w}{\partial s_1}\sin\theta_2=\frac{\partial u}{\partial s_2}$$

which is the consistency equation (40) for this case, $\theta_1=0$. Thus, if we keep equations (28) to (30), equation (32) is redundant; we shall then need the other equations, in particular (34).

(2) At the leading edge $\theta_1=\pi/2$; equations (28) to (30) give

$$\frac{\partial u}{\partial z}=\frac{\partial u}{\partial s_1};\qquad \frac{\partial v}{\partial z}=\frac{\partial v}{\partial s_1};\qquad \frac{\partial w}{\partial z}=\frac{\partial w}{\partial s_1}.$$

Substituting in equation (34), we find

$$\frac{\partial u}{\partial s_1}\cos\theta_2\sin\Lambda+\frac{\partial v}{\partial s_1}\cos\theta_2\cos\Lambda+\frac{\partial w}{\partial s_1}\sin\theta_2=\frac{\partial w}{\partial s_2}$$

which is the consistency equation (40) for $\theta_1=\pi/2$. Thus if we keep equations (28) to (30), equation (34) is redundant; we shall then need the other equations, in particular (32).

It follows that if we keep (32) and ignore (34), the equations will become ill-conditioned near the maximum thickness positions $\theta_1\doteqdot 0$; and if we keep (34) and ignore (32), the equations will become ill-conditioned near the leading edge, $\theta_1\doteqdot\pi/2$.

This immediately suggests that we seek a linear combination of equations (32) and (34), possibly depending on θ_1, which will produce the appropriate equation in each of these neighbourhoods. Let us then multiply (32)

by λ and (34) by μ, where λ and μ are to be determined, and add. This gives

$$(\lambda \sin\theta_2+\mu\cos\theta_2\sin\Lambda)\frac{\partial u}{\partial z}+\mu\cos\theta_2\cos\Lambda\frac{\partial v}{\partial z}+\mu\sin\theta_2\frac{\partial w}{\partial z}+$$

$$+\lambda\cos\theta_2\sin\Lambda\frac{\partial u}{\partial x}+\lambda\cos\theta_2\cos\Lambda\frac{\partial v}{\partial x}=\lambda\frac{\partial u}{\partial s_2}+\mu\frac{\partial w}{\partial s_2}. \tag{41}$$

Eliminating $\partial v/\partial y$ between equations (33) and (38):

$$\frac{\partial v}{\partial z}\sin\theta_2-\frac{\partial w}{\partial z}\cos\theta_2\cos\Lambda-\frac{\partial u}{\partial x}\cos\theta_2\cos\Lambda+\frac{\partial v}{\partial x}\cos\theta_2\sin\Lambda=\frac{\partial v}{\partial s_2}. \tag{42}$$

The five equations (28), (29), (30), (41) and (42) for the five unknowns $\partial u/\partial z$, $\partial v/\partial z$, $\partial w/\partial z$, $\partial u/\partial x$, $\partial v/\partial x$, possess a matrix A whose transpose A' (written thus to save space) is

$$A'=\begin{bmatrix} \sin\theta_1 & 0 & \cos\theta_1 & \lambda\sin\theta_2+\mu\cos\theta_2\sin\Lambda & 0 \\ 0 & \sin\theta_1 & 0 & \mu\cos\theta_2\cos\Lambda & \sin\theta_2 \\ 0 & 0 & \sin\theta_1 & \mu\sin\theta_2 & -\cos\theta_2\cos\Lambda \\ \cos\theta_1 & 0 & 0 & \lambda\cos\theta_2\sin\Lambda & -\cos\theta_2\cos\Lambda \\ 0 & \cos\theta_1 & 0 & \lambda\cos\theta_2\cos\Lambda & \cos\theta_2\sin\Lambda \end{bmatrix}. \tag{43}$$

The determinant of A', $\det A' \equiv \det A$, can be expanded about its fourth column and written as the sum of two determinants:

$$\det A' = \lambda D_\lambda + \mu D_\mu$$

where

$$D_\lambda = \begin{vmatrix} \sin\theta_1 & 0 & \cos\theta_1 & \sin\theta_2 & 0 \\ 0 & \sin\theta_1 & 0 & 0 & \sin\theta_2 \\ 0 & 0 & \sin\theta_1 & 0 & -\cos\theta_2\cos\Lambda \\ \cos\theta_1 & 0 & 0 & \cos\theta_2\sin\Lambda & -\cos\theta_2\cos\Lambda \\ 0 & \cos\theta_1 & 0 & \cos\theta_2\cos\Lambda & \cos\theta_2\sin\Lambda \end{vmatrix}$$

$$=\sin\theta_1[\sin^2\theta_1\cos^2\theta_2+\cos^2\theta_1(\cos^2\theta_2\cos^2\Lambda+\sin^2\theta_2)-2\sin\theta_1\sin\theta_2\cos\theta_1\cos\theta_2\sin\Lambda]$$

$$=\sin\theta_1[1-(\sin\theta_1\sin\theta_2+\cos\theta_1\cos\theta_2\sin\Lambda)^2]$$

and

$$D_\mu = \begin{vmatrix} \sin\theta_1 & 0 & \cos\theta_1 & \cos\theta_2\sin\Lambda & 0 \\ 0 & \sin\theta_1 & 0 & \cos\theta_2\cos\Lambda & \sin\theta_2 \\ 0 & 0 & \sin\theta_1 & \sin\theta_2 & -\cos\theta_2\cos\Lambda \\ \cos\theta_1 & 0 & 0 & 0 & -\cos\theta_2\cos\Lambda \\ 0 & \cos\theta_1 & 0 & 0 & \cos\theta_2\sin\Lambda \end{vmatrix}$$

$$=-\cos\theta_1[1-(\sin\theta_1\sin\theta_2+\cos\theta_1\cos\theta_2\sin\Lambda)^2]$$

whence

$$\det A' = (\lambda\sin\theta_1-\mu\cos\theta_1)[1-(\sin\theta_1\sin\theta_2+\cos\theta_1\cos\theta_2\sin\Lambda)^2] \tag{44}$$

We observe that D_λ and D_μ are the determinants of the systems of equations got by omitting (34) and (32) respectively, and that D_λ vanishes when $\theta_1 = 0$, and D_μ when $\theta_1 = \pm \pi/2$, which leads to the conclusions already established about these two systems.

Now, since $|\Lambda| < \pi/2$, the quantity

$$\sin\theta_1 \sin\theta_2 + \cos\theta_1 \cos\theta_2 \sin\Lambda$$

lies strictly between the two expressions

$$\sin\theta_1 \sin\theta_2 - \cos\theta_1 \cos\theta_2 = -\cos(\theta_1 + \theta_2)$$

and

$$\sin\theta_1 \sin\theta_2 + \cos\theta_1 \cos\theta_2 = \cos(\theta_1 - \theta_2)$$

which themselves lie between -1 and 1. Hence the square bracket in equation (44) is always positive. By choosing

$$\lambda = \sin\theta_1, \qquad \mu = -\cos\theta_1 \tag{45}$$

we make

$$\lambda \sin\theta_1 - \mu \cos\theta_1 = 1 \qquad \text{(for all } \theta_1\text{)}$$

and this ensures

$$\det A' > 0$$

so that the matrix A is non-singular, and the equations are made as well-conditioned as they can be. The final form of equation (41) is thus

$$\begin{aligned}(\sin\theta_1 \sin\theta_2 - \cos\theta_1 \cos\theta_2 \sin\Lambda)\frac{\partial u}{\partial z} - \cos\theta_1 \cos\theta_2 \cos\Lambda \frac{\partial v}{\partial z} \\ -\cos\theta_1 \sin\theta_2 \frac{\partial w}{\partial z} + \sin\theta_1 \cos\theta_2 \sin\Lambda \frac{\partial u}{\partial x} + \sin\theta_1 \cos\theta_2 \cos\Lambda \frac{\partial v}{\partial x} \\ = \sin\theta_1 \frac{\partial u}{\partial s_2} - \cos\theta_1 \frac{\partial w}{\partial s_2}.\end{aligned} \tag{46}$$

4.2 The Centre Section

When the wing is unyawed and flying without bank, so that the flow is symmetrical about $y = 0$, we have $v = 0$ on this plane and hence

$$\frac{\partial v}{\partial x} = 0, \qquad \frac{\partial v}{\partial z} = 0. \tag{47}$$

However, because of discretization errors in the numerical computation of the derivatives $\partial u/\partial s_1$, etc., if we were to solve equations (28) to (30), (46) and (42) at $y = 0$ the computed values of $\partial v/\partial x$ and $\partial v/\partial z$ would not in general be precisely zero. Instead of blindly using the computed values of the other variables we need, $\partial u/\partial z$ and $\partial w/\partial z$ on $y = 0$, it seems advisable to make use of the information (47) in the solution. This is quite likely to be an improvement, because in general when there is some doubt as to the exact values of quantities inferred from given information, the more information we have at our disposal, the better.

The equation (29) is satisfied automatically by (47) and this leaves four equations for the three unknowns $\partial u/\partial z$, $\partial w/\partial z$, $\partial u/\partial x$. These equations can be solved approximately by least squares. The coefficients of the least-squares equations are combinations of the elements of the matrix (43), and as these elements have to be

coded in the program anyway, it is most economical (in coding effort, compilation and program size) not to write down or explicitly to code the coefficients as functions of θ_1, θ_2 and Λ, but to code the combinations instead. The details as programmed are set out in Appendix A.

5. Iterative Calculation of the Planar Source and Doublet Distributions

In this section we show how to derive initial source and doublet distributions $q^{(1)}(x, y)$, $l^{(1)}(x, y)$ to start the iteration cycle. To improve the quality of these initial approximations, and thus to reduce the number of iterations required for adequate convergence, an inner iteration scheme is employed. The same technique is used subsequently, when from singularity distributions $q^{(n)}$, $l^{(n)}$ at the nth iteration we have computed velocity fields $\mathbf{u}_t^{(n)}$, $\mathbf{u}_l^{(n)}$ and residuals $R_t^{(n)}$, $R_l^{(n)}$ from equations (23) and (24); we can similarly derive additional perturbation distributions $\Delta q^{(n)}$, $\Delta l^{(n)}$ to yield the next set of singularity distributions

$$q^{(n+1)} = q^{(n)} + \Delta q^{(n)}$$

and

$$l^{(n+1)} = l^{(n)} + \Delta l^{(n)}.$$

The iteration cycle will then be closed.

5.1 Basic Solutions

If we start out from the situation where there is just the uniform free stream and neither source nor doublet distribution, $\mathbf{u}_t^{(0)}$ and $\mathbf{u}_l^{(0)}$ are both zero and from equations (14), (19) and (23), (24) we have

$$R_t^{(0)} = \frac{\partial z_t}{\partial x} \tag{48}$$

and

$$R_l^{(0)} = \frac{\partial z_s}{\partial x} - (\alpha + \alpha_T). \tag{49}$$

In linear theory, both these conditions are transferred from the wing surface to the chordal plane $z = 0$. Following the classical procedure as in Ref. 2, we can regard $R_t^{(0)}$ as a deficiency in the symmetrical (source) velocity component $w_t(x, y, 0)$ and add the basic source distribution

$$q_B(x, y) = 2R_t^{(0)} = 2\frac{\partial z_t}{\partial x} \tag{50}$$

to cancel this deficiency. This satisfies the boundary condition (21) to the first order, but not exactly. We also regard $R_l^{(0)}$ as a deficiency in the antisymmetrical (doublet) velocity component $w_l(x, y, 0)$ and add a basic doublet distribution $l_B(x, y)$ which satisfies the double integral equation of classical lifting-surface theory

$$\frac{1}{8\pi} \iint_{\text{planform}} \frac{l_B(x', y')}{(y - y')^2} \left\{ 1 + \frac{x - x'}{[(x - x')^2 + (y - y')^2]^{\frac{1}{2}}} \right\} dx'\, dy' = R_l^{(0)}$$

$$= \frac{\partial z_s}{\partial x} - (\alpha + \alpha_T). \tag{51}$$

Assuming that the solution of this equation exists, the boundary condition (22) is now satisfied to the first order, but likewise not exactly.

In subsequent iterations, R_t and R_l can likewise be thought of as deficiencies in w_t and w_l which can, as in linear theory, be transferred to $z = 0$ and approximately cancelled by extra source and doublet distributions Δq and Δl satisfying equations similar to (50) and (51):

$$\Delta q(x, y) = 2R_t \tag{52}$$

and

$$\frac{1}{8\pi}\iint_{\text{planform}} \frac{\Delta l(x', y')}{(y-y')^2}\left\{1+\frac{x-x'}{[(x-x')^2+(y-y')^2]^{\frac{1}{2}}}\right\} dx'\,dy' = R_l \tag{53}$$

Since we actually have to compute $\mathbf{u}_t$ and $\mathbf{u}_l$ on the thickness surface $z = z_t$, the boundary conditions are still not quite satisfied next time, but the residual error fields $R_t^{(n)}$, $R_l^{(n)}$ hopefully become smaller as n increases.

The task of solving equation (53), or the special case (51), exactly for a swept wing is very difficult. Moreover, as equation (53) will have to be solved for several different right sides as the iterations proceed, it is most undesirable that any method of doing this should consume much computer time, compared with that needed to evaluate velocity components. On the other hand, if equation (53) can be solved quickly and fairly accurately, then any errors in this first-order solution will accompany those due to the evaluation of velocity components on the surface, and will be taken into account at the next pass. This can be done by the vortex lattice method, which has been programmed by Carr–Hill[19]. In this method, each half wing is divided into M_v panels by lines y = constant, and the panels may be of any convenient widths except that the last panel before the wing tip should have a width four times its distance from the tip. These panels are bisected by other lines y = constant = $Y_{k+1}(1 \leq k \leq M_v)$, say. These spanwise stations are the collocation stations at which computations will actually be done; thus the distribution of spanwise collocation stations ought to be compatible with a spanwise vortex-lattice panelling suitably tailored to the wing planform. The value $y = Y_1 = 0$ is reserved for the centre line. We use a version of the subroutine with a Multhopp chordwise distribution of alternating vortex and downwash stations, in order to cope with camber variations near the leading edge. With a number L_v of chordwise panels, the vortices are placed at the chordwise stations

$$\xi_v = \frac{1}{2}\left[1-\cos\frac{(2P-1)\pi}{2L_v+1}\right] \quad (1 \leq P \leq L_v)$$

and the downwash sensing stations at

$$\xi_D = \frac{1}{2}\left[1-\cos\frac{2P\pi}{2L_v+1}\right] \quad (1 \leq P \leq L_v).$$

Now the downwash field due to a vortex element is directly proportional to the strength of the element, so by calculating the downwash at every sensing point due to every vortex element per unit strength, a matrix A of order L_vM_v can be set up to give the downwash field in terms of the vortex elements. The matrix A can be inverted once for all, and then the vortex element strengths can be found for any downwash field. Finally the loading coefficients ΔC_p (doublet strengths l) can be calculated and output at the mid-points of the vortex elements, i.e. again on the bisecting lines $y = Y_{k+1}$.

The Ledger–Sells subroutine requires singularity data at the Weber points (L in number)

$$\xi_w = \frac{1}{2}\left[1-\cos\frac{(P-1)\pi}{L}\right] \quad (1 \leq P \leq L)$$

and, except for the leading edge $P = 1$, it outputs velocity fields at the same stations. So the residual field R_l is calculated at ξ_w and interpolated to ξ_D for input to the vortex lattice subroutine, and the resulting doublet field l output at ξ_v is factored with $[\xi/(1-\xi)]^{\frac{1}{2}}$ to remove the end-point singularities and interpolated back to ξ_w. Both interpolations are done by a cubic spline fitting subroutine.

The method is reasonably quick for the first pass with a given vortex lattice grid, the calculation and inversion of a typical matrix of order 80 taking about 100 mill s on an ICL 1907 computer, and is very quick thereafter as the inverted matrix is available for subsequent iterations and can also be stored on magnetic tape for future use.

5.2 Modification by Inner Iteration with Maclaurin Series

Although it may be mathematically quite satisfactory to construct an iteration scheme and to demonstrate that it converges, in a program of this kind with a large iteration cycle time, it is almost essential to keep the number of cycles as small as possible. We can expect that to attain accuracy to within a few per cent at least two

cycles will be needed (for wings with thickness ratios typically of the order of 10 per cent, the first order solution is not good enough), and the pilot program for uncambered wings typically required 3 cycles for acceptable accuracy. For such wings, if the basic doublet distribution l_B is assumed to be of flat-plate-at-incidence character, the theory of the R.A.E. Standard Method[6] enables us to modify l_B into a better approximation $l^{(1)}$ by a simple factor; the source distribution q_B can be modified with slightly more labour, using a Maclaurin series expansion, and then the number of iteration cycles needed for the same accuracy is typically reduced to 2. For cambered wings the simple modification to l_B fails, but we can instead extend the Maclaurin series approach to derive both source and doublet modifications, including the extra terms due to camber.

In a preliminary run, on a wing with admittedly large camber, this approach turned out to be insufficient. The difficulty is in the cross-coupling between the symmetrical and antisymmetrical boundary conditions, which presents a further set of error terms in the residuals (23) and (24) when these are worked out from the velocity fields due to the singularity distributions derived from the previous residual errors; this adversely affects the convergence ratios and the number of iterations needed for a given accuracy. Still further improvement to the singularity distributions is required, and having set down the modifications to the basic approximations q_B, l_B for cambered wings, we show how to extend our treatment so as partly to counterbalance the cross-coupling effect and again to attain the accuracy we desire with only two iterations.

We return to the ordinary (exact) boundary condition, keeping it in the form of equation (6) for compactness, and construct an inner iteration sequence. Let $\mathbf{u}^{(n,p)} = \mathbf{u}_t^{(n,p)} + \mathbf{u}_l^{(n,p)}$ be the complete perturbation field at the nth main (outer) iteration and pth inner iteration. Then the residual $R^{(n,p)}$ in the ordinary boundary condition is

$$R^{(n,p)} = \frac{\partial z_w}{\partial x}[\cos(\alpha+\alpha_T) + u^{(n,p)}(x, y, z_w)] + \frac{\partial z_w}{\partial y} v^{(n,p)}(x, y, z_w) - w^{(n,p)}(x, y, z_w) - \sin(\alpha+\alpha_T). \tag{54}$$

Now, let us suppose that corresponding to $\mathbf{u}^{(n,p)}$ we have an estimate for the residual field $R^{(n,p)}$, either from the main iteration (at the start of the inner iteration) or from a previous inner iteration. Using the techniques described in the previous sub-section, we compute additional source and doublet distributions $\Delta q, \Delta l$ producing additional velocity fields $\Delta\mathbf{u} = \Delta\mathbf{u}_t + \Delta\mathbf{u}_l$, so that on the plane $z = 0$

$$\Delta w(x, y, 0) \simeq R^{(n,p)}. \tag{55}$$

Equality will not hold precisely because the vortex lattice technique used for the lifting-surface theory is not exact. The new velocity field

$$\mathbf{u}^{(n,p+1)} = \mathbf{u}^{(n,p)} + \Delta\mathbf{u}$$

produces the residual field

$$R^{(n,p+1)} = \frac{\partial z_w}{\partial x}[\cos(\alpha+\alpha_T) + u^{(n,p)}(x, y, z_w) + \Delta u(x, y, z_w)] + \frac{\partial z_w}{\partial y}[v^{(n,p)}(x, y, z_w) + \Delta v(x, y, z_w)]$$
$$- [\sin(\alpha+\alpha_T) + w^{(n,p)}(x, y, z_w) + \Delta w(x, y, z_w)].$$

Following Weber[2], we now expand $\Delta\mathbf{u}$ in Maclaurin series (about $z = 0$) in regions where this is valid, and also use equation (54) to get (all quantities evaluated here at $z = 0$)

$$R^{(n,p+1)} = R^{(n,p)} - \left[\Delta w + z_w \frac{\partial \Delta w}{\partial z} + 0(z_w^2 \Delta\mathbf{u})\right] + \frac{\partial z_w}{\partial x}\Delta u + 0(z_w^2\Delta\mathbf{u}) + \frac{\partial z_w}{\partial y}\Delta v + 0(z_w^2\Delta\mathbf{u}).$$

Neglecting the higher order terms and using the continuity equation to eliminate $\partial\Delta w/\partial z$, we have

$$R^{(n,p+1)} \doteqdot R^{(n,p)} - \Delta w + \frac{\partial}{\partial x}(z_w \Delta u) + \frac{\partial}{\partial y}(z_w \Delta v). \tag{56}$$

Substituting from equation (1) and the analogues of equations (2) and (3) on the chordal surface,

$$R^{(n,p+1)} = R^{(n,p)} - [\pm \Delta w_t + \Delta w_l] + \frac{\partial}{\partial x}[(\pm z_t + z_s)(\Delta u_t \pm \Delta u_l)] + \frac{\partial}{\partial y}[(\pm z_t + z_s)(\Delta v_t \pm \Delta v_l)]$$

so that (with $R = \pm R_t + R_l$)

$$R_t^{(n,p+1)} = R_t^{(n,p)} - \Delta w_t + \frac{\partial}{\partial x}(z_t \Delta u_t + z_s \Delta u_l) + \frac{\partial}{\partial y}(z_t \Delta v_t + z_s \Delta v_l) \tag{57}$$

and

$$R_l^{(n,p+1)} = R_l^{(n,p)} - \Delta w_l + \frac{\partial}{\partial x}(z_t \Delta u_l + z_s \Delta u_t) + \frac{\partial}{\partial y}(z_t \Delta v_l + z_s \Delta v_t). \tag{58}$$

In the same way as for the basic source distribution (50) or for the source distributions derived from exact residuals (on the thickness surface) (52), $\Delta w_t \equiv \Delta w_t(x, y, 0)$ can be made precisely equal to $R_t^{(n,p)}$ so that the first two terms in equation (57) cancel; and by using vortex lattice technique as for the solution of equations (51) or (53) we can approximately cancel Δw_l against $R_l^{(n,p)}$ in equation (58). (We observe that for the error in this cancellation to be of the same order as the terms neglected in deriving equation (58), the numerical error in the vortex lattice method should be of third order magnitude in z_w/c, $\Delta \mathbf{u}$. A shortcoming of the scheme is that at present this cannot be guaranteed in practice, for example near the root of a highly swept wing.)

With certain expressions or estimates for Δu_t, Δv_t, Δu_l, Δv_l, equations (57) and (58) now furnish new estimates for the residual field $R^{(n,p+1)}$ corresponding to $\mathbf{u}^{(n,p+1)}$, and the inner iteration cycle is complete.

These equations are of course not new. With $\Delta \mathbf{u} = \mathbf{u}_{tB} + \mathbf{u}_{lB}$, $\mathbf{u}_{lB}$ being derived by simple two-dimensional and sheared-wing solutions of the lifting-surface equation (51), they lead to the second-order terms of the R.A.E. Standard Method. With $\Delta \mathbf{u} = \mathbf{u}^{(1)}$, equations (57) and (58) are also derived and discussed in Ref. 2, for the purpose of a single second-order calculation. As remarked in Section 3 above, to implement Weber's approach *via* Maclaurin series we should now need the Ledger–Sells subroutines for $z = 0$, in order to compute u_t, v_t and w_l precisely by double integration; however, to do so here would imply a very lengthy inner iteration which would defeat its own object.

When q_B is known from equation (50), the work of Küchemann and Weber[5] as amplified by the Standard Method[6] provides quick estimates for u_{tB} and v_{tB}. We can treat the general perturbation source distribution $\Delta q = 2R_t^{(n,p)}$ in exactly the same way. We first calculate a generalization in terms of local percentage chord ξ, $\sigma(\xi, y)$, of the function $S^{(1)}(\xi)$ (Ref. 5):

$$\sigma^{(n,p)}(\xi, y) = \frac{1}{\pi} \int_0^1 R_t^{(n,p)}(\xi', y) \frac{d\xi'}{\xi - \xi'}. \tag{59}$$

A subroutine for evaluating this Cauchy principal-value integral at the Weber points ξ_w is incorporated in the program. The estimates we seek are now given by

$$\Delta u_t = K_3 \sigma^{(n,p)} \cos \Lambda - K_2 f(\Lambda) \cos \Lambda R_t^{(n,p)} \tag{60}$$

and

$$\Delta v_t = -(1 - |K_2|)\sigma^{(n,p)} \sin \Lambda \tag{61}$$

where

$$f(\Lambda) = \frac{1}{\pi} \ln \frac{1 + \sin \Lambda}{1 - \sin \Lambda}$$

and $K_2(y)$ is an interpolation function which is zero over the mid-semi-span (sheared wing) region, rises to one at the root and takes negative values near the tip. We write, as in Ref. 6 or 7

$$K_2 = K_c - K_T.$$

K_T is the contribution from the tip, and we adopt Wooller's formula given in Addendum 1 to Ref. 6:

$$K_T = \begin{cases} \dfrac{0{\cdot}073 - 0{\cdot}098u'}{0{\cdot}104 + u'} & u' < 0{\cdot}745 \\ 0 & u' > 0{\cdot}745 \end{cases}$$

where $u' = (s-y)/c_T, s$ being the semi-span and c_T the tip chord. If the actual tip chord is zero, as for a curved-tip wing, c_T is taken as 0·4 times the chord at 75 per cent semi-span.

K_c is the contribution from the root (centre line). Wooller gives a formula for K_c also, but examination of preliminary results for a 45 degrees swept constant-chord wing indicated that better values of K_2 could be found and would agree well with those suggested by Carr-Hill [2]. The author fitted a rectangular hyperbola to these values, and the result was

$$K_c = \begin{cases} \dfrac{0{\cdot}1611 - 0{\cdot}3052u}{0{\cdot}1611 + u} & u < 0{\cdot}528 \\ 0 & u > 0{\cdot}528 \end{cases}$$

where $u = y/c_R$, c_R being the root chord. This choice of K_2 is not claimed to be the best possible, and it is quite likely that the optimum choice varies from one wing to another, taper effects being especially likely to prove significant; but we hope it is a good mean choice over the range of most practical wings.

The calculation of the other interpolation function $K_3(y)$ is complicated[6], and since it does not normally differ much from 1, the approximation $K_3 = 1$ is used here.

When Δl is known (approximately) from the vortex lattice subroutine, we have also

$$\Delta u_l = \tfrac{1}{4}\Delta l \tag{62}$$

and since $\Delta \mathbf{u}_l$ is irrotational, making use of equation (27)

$$\Delta v_l = \int (\partial \Delta u_l/\partial y)\, dx = \frac{\partial}{\partial \bar{\eta}}\left(\int_{x_L}^{x} \tfrac{1}{4}\Delta l\, dx\right) - \Delta u_l \tan \Lambda. \tag{63}$$

We can now examine equations (57) and (58) to see if they will maintain the correct behaviour near the leading edge $\xi = 0$. We consider wings for which $z_t = 0(\xi^{\frac{1}{2}})$ and $z_s = 0(\xi)$ for $\xi \to 0$. Let us assume as an induction hypothesis that away from the centre section, $R_t^{(n,p)}$ and hence Δq are $0(\xi^{-\frac{1}{2}})$ and that $R_l^{(n,p)}$ is 0(1). The induction starts, because $R_t^{(0,0)} = \partial z_t/\partial x = 0(\xi^{-\frac{1}{2}})$ and $R_l^{(0,0)} = \partial z_s/\partial x - (\alpha + \alpha_T) = 0(1)$. Then $\sigma(n, p)$ from equation (59) is 0(1) and Δl and Δu_l, Δv_l from equations (62) and (63) are $0(\xi^{-\frac{1}{2}})$. From equation (61) $\Delta v_t = 0(1)$. From equation (60) Δu_t has one part 0(1) and the other part, with the factor $R_t^{(n,p)}$, $0(\xi^{-\frac{1}{2}})$. The part 0(1) now gives $R_t^{(n,p+1)} = 0(\xi^{-\frac{1}{2}})$ and $R_l^{(n,p+1)} = 0(1)$, and as far as this part goes the induction proof is complete. The other part $0(\xi^{-\frac{1}{2}})$ would not disturb $R_t^{(n,p+1)}$ (it would give a contribution 0(1) but we always extrapolate R_t to the leading edge on a $\xi^{-\frac{1}{2}}$ basis anyway), but it would give $R_l^{(n,p+1)} = 0(\xi^{-\frac{1}{2}})$ and thus break down the induction proof and damage the convergence of the inner iteration.

We must therefore modify the second term of equation (60) so that Δu_t has both parts 0(1). This can be done by generalizing the 'Riegels rule'[2] and re-writing equation (60) in the form (*compare* Ref. 7)

$$\Delta u_t = \sigma^{(n,p)} \cos \Lambda - K_2 f(\Lambda) \cos \Lambda \frac{R_t^{(n,p)}}{[1 + R_t^{(n,p)2}]^{\frac{1}{2}}}. \tag{64}$$

We have now only to compute some derivatives of equations (64), (59), (62) and (63) for insertion in equations (57) and (58) to close the inner iteration cycle. The calculations are straightforward and are set out in Appendix B.

We comment that when $z_s = 0$, the Δu_l and Δv_l terms drop out of equation (57) and for the first inner iteration of the first main iteration ($n = p = 0$) we recover the expression used in the pilot program for uncambered wings, for $q^{(1)} = q_B + \Delta q$. We expect to do better with our inner iteration cycle, employed not just as the first main iteration but for the next one or two also.

As remarked in Section 3, the Maclaurin series approach fails at the root of a swept wing, and so, after the first inner iteration, Δq is extrapolated to the root (by a parabolic fit from the first three outboard stations). The root values of Δw_l are not required by the vortex lattice subroutine, but the output doublet distributions Δl are also extrapolated to the root. Both Δq and Δl are further extrapolated to the last spanwise data station before the tip, at which computations of $\mathbf{u}_t(x, y, z_t)$ and $\mathbf{u}_l(x, y, z_t)$ by the Ledger–Sells subroutine[3,4] would probably not be accurate and so are not performed, nor are vortex lattice calculations.

From equations (55) and (56) we expect that

$$R^{(n,p+1)} = 0[R^{(n,p)} z_w/c(y)] \tag{65}$$

and hence that for sufficiently small z_w/c the successive residuals will decrease. We generally exit from the inner iteration after 5 cycles or when $|R_t|, |R_l| < 0{\cdot}001$. (It is arguable whether as many as 5 cycles are worthwhile; but the computation time per cycle is very small compared with the main iteration cycle time.)

It should not be thought that inner iteration, with a sequence of residuals decaying in the manner of equation (65), is a means of restoring the neglected terms $0(z_w^2 \Delta \mathbf{u})$ in equation (56). If we repeat the analysis leading to this equation, keeping the neglected terms, we find that they are still present in the next residual approximation, along with the next set of otherwise neglected terms, so that as the inner iterations proceed, they will accumulate. What the inner iteration does is to take into account the effect of repeatedly transferring successive simple approximations to the true residual error from the wing surface to the chordal surface; the effect of transferring the errors in the approximations is lost. But this is where the main iteration comes to our aid, for this effect will reappear when we evaluate the residual errors properly, on the thickness surface. The point is that if the errors in the approximations are of higher order than the approximations themselves, then the remaining residual errors in the main iteration will be of higher order than they would have been without the inner iteration scheme.

Other errors, which accumulate invisibly as the inner iteration proceeds, are: in R_l, the successive true field values of the lifting surface approximation error $(R_l^{(n,p)} - \Delta w_l)$; in both R_t and R_l, the difference between true values of $\Delta \mathbf{u}_t$ and approximate values derived from the Standard Method (with a very *ad hoc* Riegels rule), and in these, the errors due to numerical integration of the Cauchy integral (59) for $\sigma^{(n,p)}$; numerical integration of (63) for Δv_l; numerical differentiation of Δu_t, Δv_t, Δu_l, Δv_l; and possibly the extrapolations to the root and near-tip stations. The root extrapolations have the virtue of maintaining smooth spanwise behaviour of the singularity distributions and so satisfying an implicit condition for the accuracy of the Ledger–Sells subroutines[3,4]; since no account is taken of the residuals at $y = 0$ in the inner iteration, we can expect comparatively large values there when we evaluate them in the main iteration, but we can improve the situation substantially by placing a line source and line doublet distribution on the root line $y = z = 0$. (*See* Appendix D.) So all these errors are likewise taken into account in the main iteration scheme.

6. Results

6.1 High Aspect Ratio Unswept Wing

As a first test of the accuracy of the Taylor series expansions, calculations were made for an unswept, untapered wing with a constant spanwise section. The aspect ratio was taken as 60, this being judged sufficiently large to produce two-dimensional flow conditions at the centre section to at least three significant figures, enough for graphical accuracy. The section was a 'medium' camber Karman–Trefftz aerofoil, as studied by Foster[12], for which the two-dimensional flow is known analytically; the thickness/chord ratio was 13 per cent, the camber ratio 9 per cent, and the trailing-edge angle 10 degrees. The section ordinates at 72 points are listed in Foster's report, and the section is shown at the top of Fig. 4. We see that the camber ordinate z_s is larger than the thickness ordinate z_t over most of the chord, being about twice as large around $\xi = 0{\cdot}7$, and so this is quite a severe test case for the hypothesis, put forward on physical grounds in Section 4, that the region of validity of our Taylor series is not restricted to $|z_s| \leq z_t$.

We consider first the predictions for the chordwise distribution of pressure coefficient C_p at zero incidence. Fig. 4 shows the analytic result and also the successive results from three iterations of the present method. We see that the present method converges quickly over most of the chord, the second and third iterations being indistinguishable except near the leading edge. We also see that the level of absolute error is acceptable except at the three stations near $\xi = 0{\cdot}3$ on the upper surface, where it is around 4 per cent; this corresponds to about 3 per cent error in perturbation velocity. This final error has been investigated with the help of the analytic solution (the Karman–Trefftz transformation), which we have continued across the upper surface to the upper thickness surface $z = z_t$ (we can do this as we do not cross a singularity of the circle transformation function).

Using this solution, we computed the velocity fields u, w and their derivatives $\partial u/\partial z$, $\partial w/\partial z$ on the upper and lower thickness surfaces, and then in order to see whether the two-term Taylor series was everywhere adequate, we inserted these analytic values into the Taylor series to calculate the surface velocities. The resulting values of C_p are shown as the dashed curve in Fig. 4, and it is evident that this Taylor series is indeed in error near the peak in C_p on the upper surface, and that, except near the trailing edge on the lower surface, this error is very similar to the error in the converged results from the present method.

The remaining difference between these two sets of results could be due to the rather sparse distribution of chordwise data points, to some inaccuracy in computing velocity field derivatives at these points from the spline fits along the thickness surfaces, but also to the velocity field being forced to satisfy a surface boundary condition which is not quite correct because the two-term Taylor series used in it is inadequate. (This difference happens to be beneficial in mid-chord, for this case.) Thus, although comparison of our converged results with the exact values on the thickness surface reveals certain differences in the velocity fields and their derivatives, it is difficult to apportion error to particular sources. (But from our experience with the pilot program for symmetrical wings, the error on the lower surface near the wedge-shaped trailing edge is probably caused by a deficiency in the local source solution for such an edge.)

To demonstrate the need for an inner iteration scheme (or some other improvement), we have plotted in Fig. 4 the results from the first iteration when the basic singularity distributions are only modified once as in Section 5.2 and thus no inner iteration is performed. The convergence of the main iteration (not shown) is very slow, and the prediction for the upper surface is considerably in error compared with the corresponding result when inner iteration is employed.

In Fig. 4 we also show the predictions of a simplified version of Lock's method[7,13] (*see also* Appendix G) which for two-dimensional flow reduces to the classical method of Weber[17], assuming that the vortex lattice technique reproduces the camber solution of linear theory and that the methods of computing the thickness solutions of linear theory produce nominally identical results. We see that by this method the pressure distribution is predicted best on the lower surface; on the upper surface, the suction is considerably under-estimated in mid-chord—not as badly as it was by the present method first time without inner iteration, as above, but the full present method does much better. Near the leading edge, on the other hand, the suction is overpredicted. For camber ratios of this size, second-order effects are of course important, and Foster has shown[12] that full second-order (Gretler) theory, which is essentially the two-dimensional form of the Maclaurin series approach[2], gives considerable improvement for this section; about 5 per cent accuracy is found, compared with 4 per cent accuracy by the present method.

The corresponding results are shown for the section at incidence 10 degrees in Fig. 5. Again the present method converges very well, two iterations sufficing over most of the section, and the correct pressure distribution on the lower surface and the rear half of the upper surface is well represented, but the results oscillate about the exact curve over the front half of the upper surface, with a maximum error of about 4 per cent. The causes of error are probably similar to those for the zero incidence case, exacerbated by the very rapid changes of velocity in that region.

In this case too, Foster has shown[12] that full second-order theory produces marked improvement on first-order theory, and so we are not surprised to see from Fig. 5 that on the upper surface the results from the first main iteration, when no inner iteration is set, are again further from the exact solution than those of the full present method, and that the results from the method of Lock (Weber) are only slightly better, though excellent agreement obtains on the lower surface (not shown here, for clarity). A second-order method (at least) is essential for wings with camber ratio of this order.

6.2 Uncambered Constant Chord Wing

We now consider an untwisted, undihedralled constant chord wing with aspect ratio 6, leading-edge sweep 45 degrees, and uncambered 9 per cent thick R.A.E. 101 section. Computations were made using an 8×10 grid (with seven chordwise collocation stations and nine spanwise), and for the lifting-surface calculations a 10×8 vortex lattice grid with the eight outboard spanwise stations (not including the root) as before, and chordwise stations as defined in Section 5.1 with $L_v = 10$. The computer storage required, including that for the program, was 40K words, and each iteration took about 350 central processor seconds (cps); thus the total time for two iterations was about 750 cps.

We have also obtained results (denoted 'previous results') for this wing with our pilot program in which the Standard Method was used once to improve the basic singularity distributions at the first iteration. We compare the two sets of results in some detail, in order to show the effect of the inner iteration scheme with Maclaurin expansions.

Fig. 6 shows the residual errors R_t from both methods, near the root and near the tip, at first and second iterations. We have also plotted the basic thickness slope, divided by ten, as a dotted line to provide a background scale. It is clear that, for the source solution, the present method converges much better than the previous method; the error field from both methods resembles a chordwise wave, and the amplitude of this wave is reduced by about 75 per cent, compared with 50 per cent previously. We also see that the errors at the first iteration are improved by the inner iteration, everywhere except near the apex and possibly the trailing edge; it is likely that in both these regions, the Maclaurin series method is a little doubtful, and the fact that near a wedge-shaped trailing edge u_t shows a logarithmic infinity according to linear theory probably also inhibits convergence there. Overall, however, the improvement due to the inner iteration is substantial.

Fig. 7 shows the corresponding results for the pressure coefficient C_p at zero incidence. We see that the results from the first iteration with the present method are generally closer to the final results than those with the previous method, and that the final results from both methods do not differ much. This suggests that even if we were able to satisfy the boundary condition $R_t = 0$ precisely, the resulting change in C_p would be very small, and so after our two iterations the only practical uncertainty in our results is the error due to our rather sparse chordwise partitioning for $L = 8$. (Since the chordal surface of this wing is unwarped and all the velocity components are calculated on the exact wing surface which coincides with the 'thickness surface', the solutions generated are free of errors due to Taylor expansions as well as the planar approximation to a warped chordal surface.)

In Fig. 8 we show the results for the other residual error R_l. This time we see that near the root the previous method was better, the present method still having a final maximum residual error of almost 5 per cent of the incidence field (with corresponding results for the first iteration). This is probably because the Maclaurin series (58), used in the inner iteration, is increasingly in error as we approach the logarithmic singularity in w_l at the root $y = z = 0$. (The computed doublet distribution has a kink at the root.) Near the tip the situation is reversed and the present method reduces the error field to a negligible level. As we approach the leading edge, the residuals from the present method at the first iteration tend to increase. This suggested at first that the finite-difference representation of $\partial u_l/\partial x$ was slightly ill-conditioned, but an alternative programming technique failed to improve matters; it is now thought that the residual may be an accumulation of leading-edge downwash errors in the vortex-lattice technique as the inner iterations proceed. However, this effect disappears at the second iteration.

Finally, in Fig. 9 we show how the doublet function $e_l = l \sin \phi$ varies, near the root and near the tip. (We use e_l in order to demonstrate results for the leading edge $\xi = 0$; we remember that on the chordal surface $u_l(x, y, 0) = \frac{1}{4} e_l(x, y)/\sin \phi$. Also we wish to keep the doublet effects separate from the source effects in this comparison.) Here we note that near the root, the final values from the two methods are similar except for a 5 per cent difference just downstream of the apex, and that the values from the present method do not change much from the first to the second iteration except near the leading edge, which we expect to be a sensitive region from the discussion of Fig. 8. However, near the tip the first iterate from the present method is much closer to the final result than that from the previous method, and so it is likely that lifting effects will be better represented near the tip by the present method.

We can conclude from this study that the inner iteration scheme is beneficial everywhere except perhaps for the doublet distribution near the root. For a cambered wing, the benefit will be still greater, as shown by the results for the Karman–Trefftz section, since the inner iteration now includes the camber terms.

6.3 R.A.E. Wing 'B'

R.A.E. Wing 'B' is a research wing designed by Jones and Grey-Wilson[14] (with the aid of the R.A.E. Standard Method) to have a roof-top near-sonic chordwise pressure distribution on its upper surface at free-stream Mach number 0·8 and zero incidence. The wing planform and thickness distribution are the same as those of R.A.E. Wing 'A': aspect ratio 6, taper ratio $\frac{1}{3}$, mid chord sweep angle 30 degrees, and 9 per cent thick R.A.E. 101 section at all spanwise stations. The wing has substantial variations in both camber and twist, near the root and also near the tip; analytic formulae are given in Ref. 14, and the twist distribution and some camber shapes are shown in Fig. 10.

Computations were made for this wing at zero incidence (in incompressible flow) with two grids, the comparatively coarse 8×10 grid as employed for the constant-chord wing already discussed, and a finer 12×20 grid with one extra station in each interval between consecutive spanwise stations. The corresponding vortex lattice grids used were 10×8 and 8×18 respectively; for the fine grid, eight chordwise collocation stations was a compromise between equivalent chordwise accuracy and computer storage; with $8 \times 18 = 144$ collocation points, a 144×144 matrix already requires about 42K words of core store, unless time-consuming

magnetic tape or disc operations are demanded. (Another 40K words were needed to hold the rest of the data for the fine grid, and the program; the upper limit of available core store on the ICL 1907 at R.A.E. is 96K.)

Three iterations were run with the coarse grid, only two with the fine grid to save computing time. Fig. 11 shows how well the method converges for both grids on the root section, which was likely to be very sensitive because of the rapid changes in camber and twist on this wing. Over much of the section, the second and third iteration results from the coarse grid are graphically identical, and the results from the second iteration are then omitted for clarity. Except near the apex on the upper surface, the results from the first and second iteration with the fine grid are also very satisfactorily close together. We also observe that the difference between the final results for the coarse and fine grids is very small, except near the apex, and this tells us that despite the rapid spanwise changes near the root, the overall discretization error is sufficiently small for practical purposes, with respect to both chordwise and spanwise variations in grid size. Also it seems likely that we can tolerate a reduced accuracy near the apex without impairing the quality of the solution downstream.

Next, we compare the final results from coarse and fine grids with the results from the B.A.C. program of Roberts[15], near the root, in mid-semispan and near the tip, in Figs. 12, 13, 14 respectively. Again noteworthy is the excellent agreement between the two sets of results from the present method, indicating that (except near the apex and tip leading corner) the present method is everywhere well-conditioned with respect to grid size. Also the good convergence of the present method found at the root in Fig. 11 was maintained everywhere on the wing, and so even for this seemingly difficult case two iterations with either grid would have sufficed. At mid-semispan the Roberts method agrees well with the present method, and also over most of the near-tip section, with the exception of the forward upper surface. Near the root the two methods disagree somewhat in mid-chord. We do not know how well the Roberts solution has converged with respect to spanwise grid size; Roberts took 17 spanwise stations for this run (and 27 chordwise over each complete section), but his method at the time of writing does not have a collocation station at the root $\eta = 0$ precisely. If we take the Roberts solution as near-accurate on this scale, then we are left with an error of about 5 per cent in the present method. Since discretization and convergence errors are small, we may consider two other possible sources of error:

(i) Inadequacy in the two-term Taylor series, as already noted for the Karman–Trefftz wing. Since we have neglected terms $0(z_s^2)$, this particular relative error is likely to be proportional to the square of the maximum camber ratio; on this basis the 4 per cent error found for the Karman–Trefftz wing with 9 per cent camber ratio would reduce to 0·2 per cent for Wing 'B' with 1·8 per cent root camber ratio. This takes no account of the rapid spanwise changes on Wing 'B', and a more conservative estimate of the error from this source would be 1 per cent, which is still small compared with the error shown in Fig. 12. There may be a similar effect near the tip, already mentioned (Fig. 14), but we expect some disagreement there because of the finite area of the wing tip section; neither method imposes zero normal velocity there, and hence, not only is neither method exactly right, but also the tip flow field due to a surface source distribution (Roberts) will not be the same as that due to our chordal plane source distribution, and hence in a neighbourhood of the tip the two methods must produce different results. In mid-semispan the excellent agreement between the two methods (Fig. 13) may owe much to the relatively small forward camber on that section (Fig. 10).

(ii) Local dihedral at the root, here largely due to the rate of change of twist. If the chordal surface is $z^* = z_c(x, y)$ and we take the wing trailing-edge to lie in the plane $z^* = 0$, then the local dihedral is found as arctan $(\partial z_c/\partial y)$ where

$$\frac{\partial z_c}{\partial y} = \tan \Lambda_{TE} \tan \alpha_T(0) + \frac{d\alpha_T}{dy}(0) \sec^2 \alpha_T(0).c(0)(1-\xi)$$

where Λ_{TE} is the trailing-edge sweep angle. For Wing 'B' this gives about $-0{\cdot}30$ at the apex $\xi = 0$, and about $-0{\cdot}13$ in mid-chord. These values are clearly not of second-order magnitude, which violates the assumption we made in Section 2 when replacing the chordal surface by a plane for the singularity integrations. Although the dihedral is local only, intuitively speaking the contributions to these integrals can depend significantly on these local values; it is quite likely that this accounts for most of the remaining error in Fig. 12. As Wing 'B' is a research wing, and practical wings are not expected to exhibit local dihedral on this scale, it is not now proposed to extend the program to deal with purely local dihedral effects.

The predictions of the simplified version of Lock's method are also shown in Figs. 12–14. At mid-semispan very good agreement obtains, except possibly at mid-chord on the upper surface. Near the tip the Lock results are higher than the Roberts results but agree with those from the present method with the coarse grid, on the forward upper surface, and they come out lower than the Roberts results on the lower surface; thus Lock's method will slightly overpredict the tip sectional lift. Near the root the Lock results are too high over most of the upper surface and also on the forward lower surface, but fall between the present method and Roberts

method results over the rear lower surface. The sectional lift is underestimated by about 4 per cent, compared with the present method. From our studies with the pilot program, we would expect some overprediction of root thickness and incidence effects on the forward upper surface, but the overprediction seems greater than we would have expected, especially over the rear, and we can attribute this part of the error largely to camber effects. However, the error on the forward lower surface is likely to be an overestimate of the thickness effect.

A similar method to Lock's, known variously as SPERT or the BAC thin wing method, has been developed at B.A.C., Warton, and is compared with the Roberts method in Ref. 15, also for R.A.E. Wing 'B' at zero incidence and Mach number. The differences between these two methods are everywhere similar to the differences shown here between Lock's method and the present method.

6.4 R.A.E. Wing 'A' in Subcritical Flow

To demonstrate the program's action for flows at low Mach number M_∞, we have computed the flow past the symmetrical R.A.E. Wing 'A' at 10 degrees incidence with $M_\infty = 0{\cdot}4$, and the results (after two iterations) are compared with the results from Roberts' program in Fig. 15. Roberts' program also operates in the Prandtl–Glauert (affine) space, and so the two methods are expected to agree except perhaps near the tip, as noted earlier. Very good agreement is found in mid-semispan, good agreement near the root, and fair agreement near the tip. This is not considered as a particularly interesting or even difficult exercise, but it does check out the modifications (for the affine space) set down in Appendix E; the affine scaling factor $\sqrt{1-M_\infty^2}$ is 0·916 so that any programming errors would be expected to show up on the scale of Fig. 15.

7. Résumé

In this section we summarize briefly the action of the program to give the reader an overall view. A flow diagram of the program is provided in Figs. 16a–h.

The number of chordwise collocation stations (*see* Section 5.1) and of spanwise collocation stations, and the free-stream Mach number M_∞ are input. The leading-edge ordinate x_L and local chord of the planform (the analogous wing planform in compressible flow, by the transformation $x = \tilde{x}\sqrt{1-M_\infty^2}$; *see* Appendix E) are input, and also any outboard-crank-station ordinates. The twist distribution α_T, normalized thickness distribution $z_t/c(y)$ and camber distribution $z_s/c(y)$ are specified along with $\partial z_t/\partial x$, $\partial z_s/\partial x$ at the collocation stations, the thickness distribution z_t is cubic-spline-fitted against the angular chordwise coordinate ϕ at each spanwise station, and the chordwise arclength s_1 on the 'thickness surface' $z = z_t(x, y)$ is determined. z_t and z_s are also cubic-spline-fitted spanwise along lines of constant ϕ, and values of $\partial z_t/\partial\bar{\eta}$ and $\partial z_s/\partial\bar{\eta}$ (derivatives along these lines) are determined, also the spanwise arclength s_2 on $z = z_t$.

The function $2(\partial z_t/\partial\tilde{x})\sin\phi$ is extrapolated to $\phi = 0$ and used to determine the leading-edge Lighthill ξ-shift at each spanwise station (*see* Appendix C) to make the solution uniformly valid near the leading edge. The values of K_2 and $\mathrm{d}|K_2|/\mathrm{d}y$ (see Section 5.2) are also stored.

If the number of spanwise stations is large, it is possible to read in a set of integers corresponding to stations where the velocity fields $\mathbf{u}_t$ and $\mathbf{u}_l$ are to be computed by the Ledger–Sells subroutine, and then at the remaining stations $\mathbf{u}_t$ and $\mathbf{u}_l$ can be found by spanwise interpolation along lines of constant ϕ (spanwise curves). This facility can save some computing time, but should be used sparingly and in any event not near the root or near the tip.

If final pressure distributions are required at any further spanwise stations, these stations are read in here.

For the symmetrical residual R_t the basic residual error R_{tB} is set:

$$R_{tB} = \partial z_t/\partial x \qquad \text{(equation (48))}$$

which gives the corresponding basic source function

$$e_{tB} = 2R_{tB}\sin\phi.$$

The incidence α is read in, and then at each spanwise station the camber distribution z_s is cubic-spline-fitted chordwise and the derivative $\partial z_s/\partial x$ is determined at the downwash sensing stations in the vortex lattice method (*see* Section 5.1). For the other residual R_l the basic residual error field R_{lB} is set:

$$R_{lB} = \partial z_s/\partial x - (\alpha + \alpha_T). \qquad \text{(equation (49))}$$

Here the main iteration cycle begins. The vortex lattice subroutine is entered, where on this first entry the vortex lattice matrix is either computed or read in from magnetic tape; and the card input and magnetic tape peripherals are released. The subroutine returns values of the doublet function $e_l = l \sin \phi$ at the vortex stations, and these are interpolated chordwise to the Weber points. This first entry produces the basic doublet function $e_{lB} = l_B \sin \phi$.

At this point the inner iteration cycle begins. From R_t we compute approximations to u_t and v_t on $z = 0$ based on the R.A.E. Standard Method:

$$u_t \simeq \sigma \cos \Lambda - \frac{K_2}{\pi} \ln \frac{1+\sin \Lambda}{1-\sin \Lambda} \cos \Lambda \frac{R_t}{(1+R_t^2)^{\frac{1}{2}}} \qquad \text{(equation (64))}$$

and

$$v_t \simeq -(1-|K_2|)\sigma \sin \Lambda \qquad \text{(equation (61))}$$

where Λ is the local sweep angle and

$$\sigma(\xi, y) = \frac{1}{\pi} \int_0^1 R_t(\xi', y) \frac{d\xi'}{\xi - \xi'}. \qquad \text{(equation (59))}$$

With e_l equal to the basic doublet function e_{lB}, we also compute (on $z = 0$)

$$u_l = \tfrac{1}{4} l = \tfrac{1}{4} e_l / \sin \phi \qquad \text{(equation (62))}$$

and

$$v_l = \frac{\partial}{\partial \bar{\eta}} \left[c(\bar{\eta}) \int_0^{\xi} u_l(\xi', \bar{\eta})\, d\xi' \right] - u_l \tan \Lambda. \qquad \text{(equation (63))}$$

With the aid of Maclaurin series expansions, we have estimates for the next set of residual error fields: (for $M_\infty = 0$)

$$R_t \simeq \frac{\partial}{\partial x}(z_t u_t + z_s u_l) + \frac{\partial}{\partial y}(z_t v_t + z_s v_l) \qquad \text{(equation (57))}$$

and

$$R_l \simeq \frac{\partial}{\partial x}(z_t u_l + z_s u_t) + \frac{\partial}{\partial y}(z_t v_l + z_s v_t). \qquad \text{(equation (58))}$$

From R_t an extra source function $\Delta e_t = 2R_t \sin \phi$ is derived, and is added to the basic source function to produce an accumulated source function which is stored separately. From R_l and the vortex lattice subroutine an extra doublet function Δe_l is derived; R_l is also added to the basic vortex-lattice input field to produce an accumulated vortex-lattice input field which is likewise stored separately.

The Maclaurin series are not used at the root, at the last spanwise station before the tip or at the leading edge. The source and doublet functions are instead extrapolated to these stations.

With the new R_t in place of R_{tB}, and the new Δe_l in place of e_{lB}, the inner iteration cycle is repeated and further residual errors are computed approximately, the further source functions and vortex lattice input fields being likewise accumulated. The inner iteration is terminated after a fixed number of cycles (2 to 5) or when the residual errors become sufficiently small.

From the accumulated vortex lattice input field the doublet function e_l corresponding to the doublet distribution $l^{(1)}$ is derived, and input to the Ledger–Sells subroutine which computes $\mathbf{u}_l$ on the 'thickness surface' $z = z_t$. Then the accumulated source function e_t corresponding to the source distribution $q^{(1)}$ is input to the Ledger–Sells subroutine which now computes $\mathbf{u}_t$, likewise on $z = z_t$. These computations are performed at ξ-values stretched so as to give the Lighthill shift near the leading edge.

Both velocity fields are differentiated numerically with respect to s_1 (chordwise) and s_2 (spanwise) at each collocation point. From these, by resolution of derivatives in the s_1 and s_2 directions, we have to compute values of their derivatives with respect to z. Making use of the equation of conservation of mass and the

equations of irrotational flow, the number of unknown derivatives for any velocity field in incompressible flow is reduced to five ($\partial u/\partial z$, $\partial v/\partial z$, $\partial w/\partial z$, $\partial u/\partial x$, $\partial v/\partial x$) and the equations for them read:

$$\frac{\partial u}{\partial z}\sin\theta_1+\frac{\partial u}{\partial x}\cos\theta_1=\frac{\partial u}{\partial s_1}, \qquad \text{(equation (28))}$$

$$\frac{\partial v}{\partial z}\sin\theta_1+\frac{\partial v}{\partial x}\cos\theta_1=\frac{\partial v}{\partial s_1}, \qquad \text{(equation (29))}$$

$$\frac{\partial u}{\partial z}\cos\theta_1+\frac{\partial w}{\partial z}\sin\theta_1=\frac{\partial w}{\partial s_1}, \qquad \text{(equation (30))}$$

$$(\sin\theta_1\sin\theta_2-\cos\theta_1\cos\theta_2\sin\Lambda)\frac{\partial u}{\partial z}-\cos\theta_1\cos\theta_2\cos\Lambda\frac{\partial v}{\partial z}-\cos\theta_1\sin\theta_2\frac{\partial w}{\partial z}+$$

$$+\sin\theta_1\cos\theta_2\sin\Lambda\frac{\partial u}{\partial x}+\sin\theta_1\cos\theta_2\cos\Lambda\frac{\partial v}{\partial x}=\sin\theta_1\frac{\partial u}{\partial s_2}-\cos\theta_1\frac{\partial w}{\partial s_2} \qquad \text{(equation (46))}$$

and

$$\frac{\partial v}{\partial z}\sin\theta_2-\frac{\partial w}{\partial z}\cos\theta_2\cos\Lambda-\frac{\partial u}{\partial x}\cos\theta_2\cos\Lambda+\frac{\partial v}{\partial x}\cos\theta_2\sin\Lambda=\frac{\partial v}{\partial s_2} \qquad \text{(equation (42))}$$

where θ_1 and θ_2 are the slope angles between the s_1, s_2 directions and the plane $z=0$. The matrix of these five equations is inverted and then used to obtain the z-derivatives for both $\mathbf{u}_t$ and $\mathbf{u}_l$. At the root $y=0$, where we have already $\partial v/\partial x=\partial v/\partial z=0$, a least squares solution is taken.

The residual errors R_t, R_l can now be computed from Taylor series expansions about $z=z_t$, using the numerically accurately computed values of $\mathbf{u}_t$ and $\mathbf{u}_l$: for $M_\infty=0$

$$R_t=Q_0\frac{\partial z_t}{\partial x}+Q_1\frac{\partial z_s}{\partial x}+Q_2\frac{\partial z_t}{\partial y}+Q_3\frac{\partial z_s}{\partial y}-Q_4 \qquad \text{(equation (23))}$$

$$R_l=Q_0\frac{\partial z_s}{\partial x}+Q_1\frac{\partial z_t}{\partial x}+Q_2\frac{\partial z_s}{\partial y}+Q_3\frac{\partial z_t}{\partial y}-Q_5 \qquad \text{(equation (24))}$$

with

$$\left.\begin{aligned} Q_0&=1+u_t+z_s\,\partial u_l/\partial z,\\ Q_1&=u_l+z_s\,\partial u_t/\partial z,\\ Q_2&=v_t+z_s\,\partial v_l/\partial z,\\ Q_3&=v_l+z_s\,\partial v_t/\partial z,\\ Q_4&=w_t+z_s\,\partial w_l/\partial z \end{aligned}\right\} \qquad \text{(equations (14) to (19))}$$

and

$$Q_5=\alpha+\alpha_T+w_l+z_s\,\partial w_t/\partial z.$$

Actually, at first R_t and R_l are only computed at the wing root and the first outboard spanwise station. Then an attempt is made to reduce the errors at the root by placing line source and line doublet distributions along the centre line $y=z=0$ as explained in Appendix D. The velocity fields $\mathbf{u}_Q$ and $\mathbf{u}_D$ due to these distributions are computed on $z=z_t$, added to $\mathbf{u}_t$ and $\mathbf{u}_l$ respectively, and also (in subsequent iterations) accumulated with previously computed $\mathbf{u}_Q$ and $\mathbf{u}_D$, to be added to velocity fields $\mathbf{u}_t$, $\mathbf{u}_l$ from the Ledger–Sells subroutine.

Next, the residuals R_t, R_l and the pressure coefficients C_{pu}, C_{pl} on upper and lower surfaces, are computed at all collocation stations, and output as printed tables.

This marks the end of the main iteration cycle. If more cycles are to be done, a new extra source function Δe_l is derived from R_l and is also added to the accumulated source function, while R_l is added to the accumulated vortex–lattice input field. Then R_l itself is input to the vortex-lattice subroutine, and the inner iteration cycle is entered as already described.

If the required number of cycles has been done, the absolute local Mach number is printed out (for compressible flow). As the Prandtl–Glauert rule is not sufficiently accurate for regions with local Mach number near unity, if such regions are observed in this print-out the solution should be regarded as qualitative only.

Finally, if output is required at any further spanwise stations, C_{pu} and C_{pl} are interpolated to these stations along lines of constant ϕ, allowance being made for the presence of any crank stations.

8. Conclusion

A program has been written to determine iteratively the pressure distribution on a thick, cambered, twisted wing in incompressible or subcritical flow.

The computing time is dominated by the time to calculate the velocity fields due to planar source and doublet distributions; with an 8×10 computing grid this requires about 350 central processor seconds (cps) per iteration on an ICL 1907 computer (which has a cycle time of $1{\cdot}00$ μs). Excellent convergence is obtained with two iterations, giving a total time of about 750 cps. This excellent convergence was attained with the help of a fast inner iteration scheme to improve the initial approximations for the planar source and doublet distributions.

The method has been tested on a research wing, R.A.E. Wing 'B', with severe camber and twist near root and tip; the results from two different computing grids agree very well, and so the discretization errors due to finite grid size are likely to be small and thus it may be assumed that the method is well-conditioned. These results agree well also with the results from the B.A.C. method due to Roberts and Rundle[15], except near the root where it is thought that local dihedral effects impair the accuracy (at the root) of the integrations over the wing chordal surface in the present method.

The computing time for the coarse grid was about one-third of that required by the Roberts method[15]. This gave the results at one incidence; to obtain results for a range of incidences, as the Roberts method can already do, a second run would be necessary so that the factor would rise to two-thirds. But this will be immaterial for the extensions of the method, recently programmed by the author[23] and considered to be potentially still more useful, to some wing design problems—for which the Roberts method cannot readily be adapted.

LIST OF SYMBOLS

$c, c(y)$	Local chord
c'	dc/dy
C_p	Pressure coefficient
K_2	Spanwise interpolation function in R.A.E. Standard Method
l	Planar doublet (loading) distribution
L	Number of chordwise intervals in computing grid
M	Number of spanwise intervals in computing grid
M_∞	Free-stream Mach number
L_v	Number of chordwise panels in vortex-lattice subroutine
q	Planar source distribution
$Q_0 \ldots Q_5$	$U = Q_0 \pm Q_1$, $V = Q_2 \pm Q_3$, $W = Q_5 \pm Q_4$
R	Residual error in boundary condition
s	Semispan
s_1	Arclength along a chordwise curve (section)
s_2	Arclength along a spanwise curve
$\mathbf{t}_1$	Unit vector tangent to chordwise curve
$\mathbf{t}_2$	Unit vector tangent to spanwise curve
$\mathbf{u}$	General (perturbation) velocity vector
u, v, w	Components of $\mathbf{u}$
$\mathbf{U}_\infty$	Free-stream velocity vector
$\mathbf{U}$	Complete velocity vector: $\mathbf{U}_\infty + \mathbf{u}_t + \mathbf{u}_l$
U, V, W	Components of $\mathbf{U}$
x, y, z	Local Cartesian coordinates in wing chordal singularity plane
$\tilde{x}$	$x/\sqrt{1-M_\infty^2}$
x^*, y, z^*	Cartesian coordinates referred to apex
$x_L, x_L(y)$	Leading-edge ordinate
x'_L	dx_L/dy
z_t	Wing thickness ordinate
z_s	Wing camber ordinate
z_w	Wing section ordinate, $z_s \pm z_t$
α	Incidence
$\alpha_T(y)$	Wing twist, reckoned positive clockwise viewed along starboard y-axis
$\Delta q, \Delta l$	Planar source and doublet increments
η	y/s
$\bar{\eta}$	y; but $(\partial/\partial\bar{\eta})$ denotes differentiation along line of constant ξ
θ_1	Local chordwise slope of 'thickness surface'
θ_2	Local spanwise slope of thickness surface; local slope of spanwise curve
Λ	Local (geometric) sweep angle
ξ	Percentage chord; $x = x_L(y) + c(y)\xi$
ξ_w	Weber points $\xi_w = \frac{1}{2}\left[1 - \cos\frac{(p-1)\pi}{L}\right]$ $(1 \leqslant p \leqslant L)$
ξ_v, ξ_D	Vortex points and downwash sensing stations in vortex-lattice method: $\xi_v = \frac{1}{2}\left[1 - \cos\frac{(2p-1)\pi}{2L_v+1}\right]$ $(1 \leqslant p \leqslant L_v)$ $\xi_D = \frac{1}{2}\left[1 - \cos\frac{2p\pi}{2L_v+1}\right]$
$\sigma(\xi, y)$	$\frac{1}{\pi}\int_0^1 R_t(\xi', y)\frac{d\xi'}{\xi - \xi'}$
ϕ	Angular chordwise coordinate

Subscripts

B	Basic (first-order theory)
l	Due to planar doublets (loading)
t	Due to planar sources

Superscripts

(n)	Outer iteration number
(n, p)	Inner iteration numbers

REFERENCES

No.	Author(s)	Title, etc.
1	A. M. O. Smith and J. L. Hess	*Calculation of potential flow about arbitrary bodies.* *Progress in Aeronautical Sciences*, Vol. 8 Pergamon Press, London (1967).
2	J. Weber	Second-order small-perturbation theory for finite wings in incompressible flow. A.R.C. R. & M. 3759 (1972).
3	J. A. Ledger	Computation of the velocity field induced by a planar source distribution, approximating a symmetrical non-lifting wing in subsonic flow. A.R.C. R. & M. 3751 (1972).
4	C. C. L. Sells	Calculation of the induced velocity field on and off the wing plane for a swept wing with given load distribution. A.R.C. R. & M. 3725 (1970).
5	D. Küchemann and J. Weber	The subsonic flow past swept wings at zero lift without and with body. A.R.C. R. & M. 2908 (1956).
6	—	Method for predicting the pressure distribution on swept wings with subsonic attached flow. *R. Aero Soc. Transonic Data Memorandum 6312* (1963).
7	—	Method for predicting the pressure distribution on swept wings with subsonic attached flow. *Revised version of Ref. 6 Eng. Sci. Data Unit Item* 73012 (1973).
8	H. C. Garner and G. F. Miller	Analytical and numerical studies of downwash over rectangular planforms. *Aero. Quarterly*, XXIII, pp. 169–180 (1972).
9	P. F. Jordan	Exact solutions for lifting surfaces. *J. A.I.A.A.* **11** (8), pp. 1123–1129 (1973).
10	M. J. Lighthill	A new approach to thin-aerofoil theory. *Aero. Quarterly*, III, pp. 193–210 (1951).
11	H. C. Garner	Low-speed theoretical and experimental aerodynamic loading on highly-swept curved-tipped wings of two thicknesses. A.R.C. R. & M. 3735 (1972).
12	D. N. Foster	Note on methods of calculating the pressure distribution over the surface of two-dimensional cambered wings. R.A.E. Technical Report 67095 (1967).

No.	Author(s)	Title, etc.
13	R. C. Lock	Revised compressibility corrections in subsonic swept wing theory, with applications to wing design. N.P.L. Aero Memorandum 64, A.R.C. 31310 (1969).
14	A. F. Jones and P. V. Grey-Wilson ..	The design and definition of a particular three-dimensional swept wing. Unpublished M.O.D.(P.E.) material.
15	A. Roberts and K. Rundle	The computation of first-order compressible flow about wing-body configurations. Report Aero M.A. 20, B.A.C., Weybridge (1973).
16	J. Weber and M. Gaynor Joyce	Interference problems for wing-fuselage combinations in inviscid, incompressible flow. A.R.C. R. & M. 3781 (1974).
17	J. Weber	The calculation of the pressure distribution on the surface of thick cambered wings and the design of wings with given pressure distribution. A.R.C. R. & M. 3026 (1957).
18	R. C. Lock	An equivalence law relating three- and two-dimensional pressure distributions. A.R.C. R. & M. 3346 (1964).
19	G. A. Carr-Hill	A critical assessment of the vortex lattice method for calculating velocities on lifting wings in linearized subsonic flow. Unpublished M.O.D.(P.E.) material.
20	R. M. James	On the remarkable accuracy of the vortex lattice discretization in thin-wing theory. Douglas Aircraft Co., Report D.A.C. 67211, Feb. 1969.
21	G. A. Carr-Hill	The effective sweep of a tapered wing. *Engineering Sciences Data Unit T.*215, April 1970.
22	J. Weber and G. G. Brebner	Low speed tests on 45 deg. swept-back wings. A.R.C. R. & M. 2882, Part I (1958).
23	C. C. L. Sells	Iterative design techniques for thick cambered wings in subcritical flow. R.A.E. Technical Report 76027 (1976).

APPENDIX A

Solution of Linear Equations by Least Squares

The task at hand is to solve equations (28), (29), (30), (46) and (42) for the five quantities ($\partial u/\partial z$, $\partial v/\partial z$, $\partial w/\partial z$, $\partial u/\partial x$, $\partial v/\partial x$) which may be represented by the vector ($\mathbf{X}_j$), $j = 1(1)5$. Since the first three of these are the quantities finally required, it is computationally convenient to have them in this order.

On the central symmetry plane $y = 0$, we have from equation (47)

$$X_2 = X_5 = 0 \tag{A-1}$$

and equation (29) is automatically satisfied. We arrange the system of equations for the X_j so that equation (29) comes last. (In order to ensure that the leading diagonal is free of zeros, so that row and column interchanges will never be needed when solving the straightforward set by a Gaussian elimination subroutine, we take the equations in the order (30), (46), (42), (28), (29); but this does not affect the least squares equations below). Let the matrix corresponding to the rearranged equations be (a_{ij}), and let the vector ($\mathbf{q}_i$) represent a set of typical right sides of these equations.

The straightforward set of equations would be

$$\sum_{j=1}^{5} a_{ij} X_j = q_i \qquad i = 1(1)5.$$

When (A-1) holds, we try to minimize the sum

$$2\sigma = \sum_{i=1}^{4} \left[\sum_{j=1,3,4} a_{ij} X_j - q_i \right]^2.$$

We have, for $s = 1, 3, 4$

$$\frac{\partial \sigma}{\partial X_s} = \sum_{i=1}^{4} a_{is} \left[\sum_{j=1,3,4} a_{ij} X_j - q_i \right] = 0$$

and hence

$$\sum_{\hat{\jmath}=1,3,4} \left(\sum_{i=1}^{4} a_{is} a_{i\hat{\jmath}} \right) X_{\hat{\jmath}} = \sum_{i=1}^{4} a_{is} q_i \qquad (s = 1, 3, 4). \tag{A-2}$$

The 3×3 matrix corresponding to (A-2) we call (b_{nj}), with

$$n = 1, 2, 3 \text{ corresponding to } s = 1, 3, 4$$

and

$$j = 1, 2, 3 \text{ corresponding to } \hat{\jmath} = 1, 3, 4.$$

This matrix can be inverted using the same Gaussian elimination subroutine as before.

APPENDIX B

Computation of Field Derivatives in the Plane $z=0$

We have to evaluate the velocity field derivatives occurring in the expressions (57), (58)

$$R_t^{(n,p+1)} = \frac{\partial}{\partial x}(z_t \Delta u_t + z_s \Delta u_l) + \frac{\partial}{\partial y}(z_t \Delta v_t + z_s \Delta v_l)$$

$$= z_t \nabla_2 \,.\, \Delta \mathbf{u}_t + z_s \nabla_2 \,.\, \Delta \mathbf{u}_l + \frac{\partial z_t}{\partial x} \Delta u_t + \frac{\partial z_s}{\partial x} \Delta u_l + \frac{\partial z_t}{\partial y} \Delta v_t + \frac{\partial z_s}{\partial y} \Delta v_l$$

with

$$\nabla_2 . \Delta \mathbf{u}_t = \frac{\partial \Delta u_t}{\partial x} + \frac{\partial \Delta v_t}{\partial y} \tag{B-1}$$

$$\nabla_2 . \Delta \mathbf{u}_l = \frac{\partial \Delta u_l}{\partial x} + \frac{\partial \Delta v_l}{\partial y}; \tag{B-2}$$

and

$$R_l^{(n,p+1)} \doteq \frac{\partial}{\partial x}(z_t \Delta u_l + z_s \Delta u_t) + \frac{\partial}{\partial y}(z_t \Delta v_l + z_s \Delta v_t)$$

$$= z_t \nabla_2 . \Delta \mathbf{u}_l + z_s \nabla_2 . \Delta \mathbf{u}_t + \frac{\partial z_t}{\partial x}\Delta u_l + \frac{\partial z_s}{\partial x}\Delta u_t + \frac{\partial z_t}{\partial y}\Delta v_l + \frac{\partial z_s}{\partial y}\Delta v_t.$$

The derivatives thus occur only through (B-1) and (B-2). To evaluate (B-1), we have the estimates (64), (61)

$$\Delta u_t = \sigma^{(n,p)} \cos \Lambda - K_2(y) f(\Lambda) \cos \Lambda \frac{R_t^{(n,p)}}{[1 + R_t^{(n,p)^2}]^{\frac{1}{2}}}$$

$$\Delta v_t = -[1 - |K_2(y)|]\sigma^{(n,p)} \sin \Lambda$$

where

$$\sigma^{(n,p)}(\xi, y) = \frac{1}{\pi} \int_0^1 R_t^{(n,p)}(\xi', y) \frac{d\xi'}{\xi - \xi'}.$$

$K_2(y)$ and $f(\Lambda)$ are defined in Section 5, and $R_t^{(n,p)}$ is the previous residual field. Substituting into (B-1), neglecting variations in the sweep angle Λ and making use of the derivative relations (26), (27)

$$\frac{\partial}{\partial x} = \frac{1}{c}\frac{\partial}{\partial \xi}$$

and

$$\frac{\partial}{\partial y} = \frac{\partial}{\partial \bar{\eta}} - \tan \Lambda \frac{1}{c}\frac{\partial}{\partial \xi} \tag{B-3}$$

where $\partial/\partial\bar{\eta}$ denotes the partial derivative with respect to $y = \bar{\eta}$ along lines of constant percentage chord ξ, we have

$$\nabla_2 . \Delta \mathbf{u}_t = \frac{1 - |K_2| \sin^2 \Lambda}{\cos \Lambda} \frac{1}{c} \frac{\partial \sigma^{(n,p)}}{\partial \xi} - K_2 f(\Lambda) \cos \Lambda \frac{\partial R_t^{(n,p)}/\partial \xi}{[1 + R_t^{(n,p)^2}]^{\frac{3}{2}}}$$

$$+ \frac{d|K_2|}{d(y/s)} \frac{1}{s} \sigma^{(n,p)} \sin \Lambda - (1 - |K_2|) \frac{\partial \sigma^{(n,p)}}{\partial \bar{\eta}} \sin \Lambda. \tag{B-4}$$

$R_t^{(n,p)}$ and $\sigma^{(n,p)}$ are stored at equal intervals in angular chordwise coordinate ϕ, with

$$\xi = \tfrac{1}{2}(1 - \cos \phi)$$

so that

$$\frac{\partial}{\partial \xi} = \frac{2}{\sin \phi} \frac{\partial}{\partial \phi}. \tag{B-5}$$

So the chordwise derivatives in (B-4) are calculated from central difference formulae in ϕ.

The spanwise derivative $\partial\sigma^{(n,p)}/\partial\bar{\eta}$ is found by differentiating a three-term Lagrange interpolation polynomial at one of the data points. Quite generally, if $f(\nu)$ is a function of ν which takes the value f_i at $\nu = \nu_i$ for $i = 1, 2, 3$, then f can be approximated by

$$f(\nu) \simeq \sum_{\substack{i,j,k \\ \varepsilon_{ijk}=1}} f_i \frac{(\nu-\nu_j)(\nu-\nu_k)}{(\nu_i-\nu_j)(\nu_i-\nu_k)}$$

(where ε_{ijk} is the alternating tensor). Hence at $\nu = \nu_1$

$$\frac{df}{d\nu}(\nu_1) \simeq f_1(t_3-t_2) - f_2(t_1+t_3) + f_3(t_2+t_1) \tag{B-6}$$

where

$$t_1 = \frac{1}{\nu_2-\nu_3},\ t_2 = \frac{1}{\nu_3-\nu_1},\ t_3 = \frac{1}{\nu_1-\nu_2}.$$

We also note that

$$\frac{d^2f}{d\nu^2} \simeq 2 \sum_{\substack{i,j,k \\ \varepsilon_{ijk}=1}} \frac{f_i}{(\nu_i-\nu_j)(\nu_i-\nu_k)}. \tag{B-7}$$

To evaluate (B-2), for a given doublet distribution Δl we have from equations (62) and (63)

$$\Delta u_l = \tfrac{1}{4}\Delta l$$

and

$$\Delta v_l = \frac{\partial I}{\partial \bar{\eta}} - \Delta u_l \tan\Lambda \tag{B-8}$$

where

$$I = \int_{x_L}^{x} \tfrac{1}{4}\Delta l(x', y)\, dx'.$$

In the program we work, not with Δl but with Δe_l given by

$$\Delta e_l = \sin\phi\ \Delta l$$

so that

$$\Delta u_l = \frac{1}{4}\frac{\Delta e_l}{\sin\phi} \tag{B-9}$$

and

$$I = \frac{1}{8}\int_0^{\phi} \Delta e_l(\phi', y)\, d\phi'. \tag{B-10}$$

The integral (B-10) is evaluated successively at each ϕ, starting at the leading edge $\phi = 0$, by Simpson's rule.

Applying (B-3) to (B-8), we have

$$\frac{\partial \Delta v_l}{\partial y} = \frac{\partial \Delta v_l}{\partial \bar{\eta}} - \frac{\partial \Delta v_l}{\partial x}\tan\Lambda = \frac{\partial^2 I}{\partial \bar{\eta}^2} - 2\tan\Lambda\frac{\partial \Delta u_l}{\partial \bar{\eta}} + \tan^2\Lambda\frac{\partial \Delta u_l}{\partial x}$$

so that for (B-2) we have

$$\nabla_2 . \Delta \mathbf{u}_l = \frac{\partial^2 I}{\partial \bar{\eta}^2} - 2 \tan \Lambda \frac{\partial \Delta u_l}{\partial \bar{\eta}} + (1 + \tan^2 \Lambda) \frac{\partial \Delta u_l}{\partial x}. \tag{B-11}$$

The x-derivative in (B-11) is worked out from (B-5) and (B-9) as

$$\frac{\partial \Delta u_l}{\partial x} = \frac{2}{c \sin \phi} \frac{\partial}{\partial \phi} \left(\frac{1}{4} \frac{\Delta e_l}{\sin \phi} \right) = \frac{2}{c \sin^2 \phi} \left(\frac{1}{4} \frac{\partial \Delta e_l}{\partial \phi} - \Delta u_l \cos \phi \right)$$

and the ϕ-derivative is calculated as a central difference.

The $\bar{\eta}$-derivatives in (B-11) are normally calculated from formulae (B-6), (B-7) with $\nu = \bar{\eta}$; with the exception of the last spanwise station used here. So far, we have assumed that the wing tip chord is finite and non-zero; then, except near the leading and trailing edges, the spanwise variation of near-tip doublet strength Δl ought to be elliptic (Ref. 8 is recent work in indirect support of this observation) and so it would be better to effect numerical differentiation with respect to

$$\nu = \sqrt{1 - \eta^2} \qquad (\eta = y/s)$$

rather than η or $\bar{\eta} = y$. We then obtain the $\bar{\eta}$ derivatives at the last spanwise station using the relations

$$\frac{\partial}{\partial \bar{\eta}} = \frac{1}{s} \frac{\partial \nu}{\partial \eta} \frac{\partial}{\partial \nu} = -\frac{1}{s} \frac{\eta}{\sqrt{1 - \eta^2}} \frac{\partial}{\partial \nu},$$

$$\frac{\partial^2}{\partial \bar{\eta}^2} = \frac{1}{s^2} \frac{\partial^2}{\partial \eta^2} = \frac{1}{s^2} \frac{\partial}{\partial \eta} \left[-\frac{\eta}{\sqrt{1 - \eta^2}} \frac{\partial}{\partial \nu} \right] = \frac{1}{s^2} \left[\frac{\eta^2}{1 - \eta^2} \frac{\partial^2}{\partial \nu^2} - \frac{1}{(1 - \eta^2)^{\frac{3}{2}}} \frac{\partial}{\partial \nu} \right].$$

For wings with rounded tips, Δl would not show this elliptic behaviour and so we should then continue to use $\nu = \bar{\eta}$ for numerical differentiation. (Jordan has shown[9] that the lift distribution near a curved tip is partly constant and partly varies as $(1 - \eta^2)^{\frac{1}{2}} \ln (1 - \eta^2)$. The singularity is weak and may be ignored in our numerical calculations, compared with the constant term).

We remark that formula (B-6) is also used to calculate the derivatives $\partial u / \partial s_2$, etc., on the thickness surface $z = z_t$ as set out in Section 4.

APPENDIX C

The Solution Rendered Uniformly Valid near the Leading Edge

It is well known that in a region of a rounded leading edge $\xi = 0$, linear theory breaks down, predicting infinite values $0(\xi^{-\frac{1}{2}})$ for u_l, v_l and w_l; and R_l contains the second-order term $u_l \, \partial z_t / \partial x$ (equation (24)) which is $0(\xi^{-1})$ in a straightforward higher-order thin-wing theory. What happens numerically is that all these quantities, even when actually computed on the thickness surface $z = z_t$, become large near the leading edge, it becomes very difficult to satisfy the boundary conditions and convergence is severely retarded in that region.

Fortunately, there is a way out. Lighthill has shown[10] that in two dimensions, the velocity field, found by straightforward expansions in first- and higher-order theory, can be rendered uniformly valid, in both first- and second-order approximations, by shifting the whole field downstream through a distance $\frac{1}{2}\rho_L$ where ρ_L is the leading-edge radius of curvature. Or, which amounts to the same thing, we may keep the velocity field fixed and move the surface upstream, which is more convenient as the sources and doublets which produce the velocity field can be left at the Ledger-Sells computing stations, and the velocity components calculated at different values of ξ, which is easy to arrange in the case $z \neq 0$.

For a swept wing, Weber[2] has shown further that the required leading-edge ξ-shift (scaled with respect to the local chord) becomes $(\frac{1}{2}\rho_L / c) H$ where

$$\left.\begin{aligned} H = H_0 = \cos^2 \Lambda_0(0) \text{ at the apex, and} \\ H = H_1 = 1/\cos^2 \Lambda_0(\eta) \text{ outboard.} \end{aligned}\right\} \tag{C-1}$$

$\Lambda_0(\eta)$ is the leading edge sweep angle. The question now arises, how to pass smoothly from H_0 to H_1 near the apex. In the program, we arbitrarily take a rational approximation

$$H = \frac{\eta H_1(\eta) + \eta_0 H_0}{\eta + \eta_0} \tag{C-2}$$

where η_0 is some positive constant at our disposal. In our early runs we determined η_0 by asking that $H(\eta)$ should be 1 percent away from its asymptotic value H_1 at the mid-semispan $\eta = 0{\cdot}5$. This yields, for a swept wing with $H_0 < 1 < H_1$

$$\eta_0 \doteqdot \frac{0{\cdot}005 H_1(0{\cdot}5)}{H_1(0{\cdot}5) - H_0}. \tag{C-3}$$

But we now prefer to choose η_0 so that the surface corresponding to the ξ-shifts is unswept at the root $\eta = 0$, corresponding to a streamsurface through the leading-edge stagnation point. This gives

$$\frac{d}{dy}[\tfrac{1}{2}\rho_L H(\eta)] = \tan \Lambda_0 \qquad \text{at} \quad \eta = 0.$$

If the section geometry is constant, $(\frac{1}{2}\rho_L/c)$ does not depend on η; thus, neglecting this dependence generally and writing c_0' for (dc/dy) at the root

$$c_0' H_0 + c_0 \frac{H_1 - H_0}{\eta_0} = \frac{s \tan \Lambda_0}{(\frac{1}{2}\rho_L/c)}$$

so if $\Lambda_0 \neq 0$

$$\eta_0 = \frac{c_0[H_1(0) - H_0]}{(\frac{1}{2}\rho_L/c)^{-1} s \tan \Lambda_0(0) - c_0' H_0}. \tag{C-4}$$

(C-4) is expected to be more consistent near the apex than (C-3), without losing anything far outboard, in virtue of the asymptotic form (C-2).

We remark that the radius of curvature ρ_L is simply related to the limiting behavior of the basic source strength q_B near the leading edge. Let us write

$$e_{tB} = q_B \sin \phi = 2 \frac{dz_t}{dx} \cdot 2\sqrt{\xi(1-\xi)}.$$

Then, near the leading edge z_t is approximately given by

$$\frac{z_t}{c} = \tfrac{1}{2}\xi^{\frac{1}{2}} e_{tB}(0)$$

where $e_{tB}(0)$ is the limit of e_{tB} as $\xi \to 0$. Hence

$$\frac{\rho_L}{2c} = \tfrac{1}{16}[e_{tB}(0)]^2.$$

Finally, we note that the Lighthill theory is not intended to apply at the trailing edge $\xi = 1$, and that if the sections are simply translated upstream relative to the source and doublet distributions, then some sources and doublets will appear inside the actual flow field near the trailing edge, and moreover the values of singularity strengths at the interior grid points near this edge will be incorrectly calculated. To overcome this, the sections are considered as being linearly stretched from the trailing edge, so that a typical grid point with percentage chord ξ, and hence distant $c(1-\xi)$ from this edge, becomes a point with percentage chord $\hat{\xi}$, distant $c(1-\hat{\xi})$

from this edge. The linear stretching equated to its leading-edge value gives

$$\frac{1-\hat{\xi}}{1-\xi} = 1+\tfrac{1}{2}\frac{\rho_L}{c}H$$

and hence

$$\hat{\xi} = 1-(1-\xi)[1+(\tfrac{1}{2}\rho_L/c)H]$$

so that $\hat{\xi} = -(\frac{1}{2}\rho_L/c)H$ at the leading edge, and $\hat{\xi} = 1$ at the trailing edge, as it should. The value of z input to the Ledger-Sells subroutine does not change.

Preliminary versions of the program were run with and without Lighthill stretching, and it was found that without stretching, large and persistent residual errors, around four times their mid-chord values, could be generated at the first chordwise station (this is at $\xi = 0{\cdot}0381$ when $L = 8$), but that these were reduced to around or even below the typical mid-chord values when Lighthill stretching was employed. For RAE Wing 'A' with a leading-edge sweep angle 36° 40′ and a 9 percent RAE 101 section, the mid-semi-span ξ-shift was approximately 0·004789. Subsequent runs have suggested further that the residuals are not highly sensitive to the form of interpolation function $H(\eta)$.

APPENDIX D

Calculation of Line Singularities at the Root of a Swept Wing

While the program was being developed, it was observed that the residuals in the boundary conditions tended to be comparatively large at the root section, and that these residuals were reduced only slowly as the iterations proceeded. In the case of the antisymmetric boundary condition (22) this is not surprising as the vortex lattice subroutine does not use information from the centre line (the root chord line), its downwash sensing points being perforce located outboard of this line for any distribution of panels over the half wing as described in Section 5; thus the root section residuals are not fed back for the second (and any subsequent) iterations. As a corollary, the doublet distributions l determined at each iteration have to be extrapolated towards the centre line somehow when input to the Sells subroutine for $\mathbf{u}_l$. Now if the lines of constant doublet strength (isobars) are kinked at the centre line, the upwash w_l exhibits a logarithmic singularity for $y, z \to 0$, and it might be thought necessary to extrapolate with 'rounded isobars' (meaning here, lines of constant l) in order to obtain sensible values of upwash on the root section and to increase the chances of small residuals. The difficulty here is, how to represent the resulting spanwise distribution of l in the form used by the subroutine. Sells[4] employs quadratic spanwise interpolation which is not really suitable for the type of distribution encountered near the apex of a thin wing, no matter how fine a grid is employed; and in one case (a 45 degree constant chord wing) it was found that when the 'rounded isobars' condition and the quadratic interpolation property were used to generate a root doublet distribution from data on the next two outboard spanwise stations $y = Y_2$, $y = Y_3$, then near the apex the value of l at the root bore no sensible relation to the obvious trend given by the values still further outboard ($y = Y_4, \ldots$). Thus, at and near the root the subroutine would have been working with unrealistic spanwise interpolations on the data for l, and the velocity field values output could not have been trusted.

The experimental results reported by Weber and Brebner[22] on a constant chord wing of aspect ratio 5 suggest that a quadratic extrapolation of the pressure difference ($-\Delta C_p$) due to life—which can be assumed to be a fair measure of our l—towards the root from the values at the next three outboard stations, would be a good fit to the measured values over most of the chord, and would not be seriously in error near the apex. Clearly the 'isobars' would be rounded so near the root that the difference is insignificant and cannot be picked up by the subroutine. So we judge it better to extrapolate l in this way, and thereby to ensure that the subroutine at least makes sense of its input near the root. Some details of this and other extrapolations are given in Appendix F.

The problem of the root residuals in equation (22) still remains. Moreover, there is a similar problem with the symmetric boundary condition equation (21). This might seem easier to deal with because here the root line *is* a collocation line on which equation (21) is to be satisfied iteratively. But in reality our method has a general drawback, which is that no distribution of sources and doublets can ever produce a kinked streamsurface outside of itself, whereas for a thick swept wing of constant section geometry the root section is always a ridge line. Thus it is mathematically impossible to satisfy the boundary conditions exactly at all points on the wing surface, and in particular near the root, with our planar distributions, and this fact makes itself felt in the slow convergence of both residuals R_t, R_l on the root section. The best we can do is to reduce the

residuals as much as possible at the given grid points by our iterative scheme, and to hope that these residuals will not be too large in between the grid points, in particular between the root section $y = 0$ and the first outboard station $y = Y_2$.

Since the awkward residuals R_t, R_l occur along an isolated gridline $y = 0$, it is natural to attempt to reduce them by placing, not planar, but line sources and line doublets respectively, on the centre line $y = z = 0$. There is no need to cancel the residuals precisely, so it is sufficient to find approximations to those line singularities which will bring the residuals down to about the same level as those outboard. The iteration scheme is easily adapted. We calculate the current velocity field $\mathbf{u}_c$ from the existing planar distribution. If it is not the first iteration, there is another velocity field $\mathbf{u}_Q^{(n-1)}$ due to previously determined line distributions, and this is added to $\mathbf{u}_c$. Residuals are computed, and an approximate line distribution derived. The velocity field $\mathbf{u}_Q^{(n)}$ due to this newly calculated line distribution is computed and added on, and the residuals are recomputed to continue the cycle.

In order to avoid sudden spanwise jumps in the residuals, which might cause trouble for the Ledger-Sells subroutine in integrating the resulting planar distributions, it has been found best to input (to the line distribution calculation) the difference between the residuals at the root and at the second spanwise station

$$\tilde{R} = R(\xi, Y_1 = 0) - R(\xi, Y_2)$$

rather than the whole residual at the root. In this way one hopes to keep the recomputed residuals sufficiently slowly varying that the parabolic interpolation functions employed by the Ledger-Sells subroutine will be reasonably good approximations.

Line Sources

The potential due to a line source distributed on $y = z = 0$ with local strength $4\pi Q(x)$ per unit length between $x = 0$ and $x = c$ is

$$\Phi_Q(x, y, z) = -\int_0^c Q(x')\, dx'/r \tag{D-1}$$

with

$$r^2 = (x - x')^2 + y^2 + z^2.$$

The components of the induced velocity $\mathbf{u}_Q = \nabla\Phi_Q$ are given by

$$u_Q = \int_0^c Q(x')\frac{x - x'}{r^3}\, dx', \tag{D-2}$$

$$v_Q = yI_Q \tag{D-3}$$

and

$$w_Q = zI_Q \tag{D-4}$$

with

$$I_Q = \int_0^c Q(x')\frac{dx'}{r^3}. \tag{D-5}$$

Suppose that we wish to estimate $Q(x)$ to cancel a residual $\tilde{R}_t(x, 0, z_t)$ in the boundary condition (21), so that approximately

$$u_Q\frac{\partial z_t}{\partial x} - w_Q = -\tilde{R}_t(x, 0, z_t). \tag{D-6}$$

To do this we have to estimate the integrals (D-2), (D-5). The latter is dominated by its behaviour for small r, i.e. near $x' = x$, and we write

$$I_Q = Q(x)\int_0^c \frac{dx'}{r^3} + \int_0^c [Q(x') - Q(x)]\frac{dx'}{r^3}. \tag{D-7}$$

Evaluating the first integral in (D-7), we find that w_Q from (D-4) is dominated by

$$\bar{w}_Q = Q(x)\left[\frac{x'-x}{r}\right]_0^c \Big/ z. \tag{D-8}$$

(The limits are values of x', of course.)

Similarly the integral u_Q in (D-2) is dominated by

$$\bar{u}_Q = Q(x)\left[\frac{1}{r}\right]_0^c. \tag{D-9}$$

Substituting from equations (D-8) and (D-9) into (D-6), and writing out the expressions in full with $z = z_t$, we arrive at an equation for $Q(x)$:

$$\tilde{R}_t(x, 0, z_t) = \frac{Q(x)}{c}\left[\frac{1}{z_t/c}\left\{\frac{1-x/c}{[(1-x/c)^2+(z_t/c)^2]^{\frac{1}{2}}} + \frac{x/c}{[(x/c)^2+(z_t/c)^2]^{\frac{1}{2}}}\right\} - \right.$$
$$\left. - \frac{\partial z_t}{\partial x}\left\{\frac{1}{[(1-x/c)^2+(z_t/c)^2]^{\frac{1}{2}}} - \frac{1}{[(x/c)^2+(z_t/c)^2]^{\frac{1}{2}}}\right\}\right] \tag{D-10}$$

A simplified form of (D-10) is used in deriving slender-body theory. The second term on the right side is usually neglected, but we retain it here since it might become significant near the apex. Equation (D-10) is displayed in the form in which it is actually programmed, in terms of percentage-chords $\xi = x/c$ (at $y = 0$) and the section geometry.

Equation (D-10) defines $Q(x)$ at discrete points $x_2, x_3, \ldots, x_L$. (x_1 is reserved for the leading edge.) To calculate the integrals (D-2) and (D-5) precisely, we define $Q(x)$ to be piecewise continuous in $x_2 \leqslant x \leqslant x_L$, and given by linear variation in each interval:

$$Q_i(x') = Q(x_{i-1}) + \frac{x'-x_{i-1}}{x_i - x_{i-1}}[Q(x_i) - Q(x_{i-1})] \qquad (x_{i-1} \leqslant x' \leqslant x_i)$$
$$= Q_B + (x'-x)Q_A \qquad (3 \leqslant i \leqslant L) \tag{D-11}$$

where

$$\left.\begin{aligned} Q_A &= \frac{Q(x_i) - Q(x_{i-1})}{x_i - x_{i-1}} \\ Q_B &= Q(x_{i-1}) - (x_{i-1} - x)Q_A. \end{aligned}\right\} \tag{D-12}$$

and

Then (D-2) can be written

$$u_Q = \sum_{i=3}^{L} \int_{x_{i-1}}^{x_i} Q_i(x')\frac{x-x'}{r^3}\,dx'$$
$$= \sum_{i=3}^{L} u_{Q_i} \tag{D-13}$$

with

$$u_{Q_i} = \int_{x_{i-1}}^{x_i} [Q_B + (x'-x)Q_A] \frac{x-x'}{r^3}\, dx'$$

$$= Q_B \left[\frac{1}{r}\right]_{x_{i-1}}^{x_i} + Q_A \left[\frac{x'-x}{r} - \ln(r+x'-x)\right]_{x_{i-1}}^{x_i}. \tag{D-14}$$

Similarly (D-5) gives

$$I_Q = \sum_{i=3}^{L} I_{Q_i} \tag{D-15}$$

with

$$I_{Q_i} = \int_{x_{i-1}}^{x_i} [Q_B + (x'-x)Q_A] \frac{dx'}{r^3}$$

$$= \frac{Q_B}{y^2+z^2} \left[\frac{x'-x}{r}\right]_{x_{i-1}}^{x_i} - Q_A \left[\frac{1}{r}\right]_{x_{i-1}}^{x_i}. \tag{D-16}$$

It is found that when $\mathbf{u}_Q$ is calculated in this way, the new residuals behave sufficiently smoothly chordwise and spanwise, and are acceptably reduced at the root, the near-apex and near-trailing-apex stations lagging behind the rest. This is notwithstanding the discontinuous gradients in the representation (D-11); we turn to advantage the continuous nature of the induced velocity field in regions exterior to the line distribution.

Line Doublets

The potential due to a line doublet distributed on $y = z = 0$ between $x = 0$ and $x = c$, with local strength $4\pi D(x)$ per unit length, is

$$\Phi_D = -\int_0^c D(x') \frac{\partial}{\partial z}\left(\frac{1}{r}\right) dx'$$

$$= -\frac{\partial}{\partial z} \int_0^c D(x')\, dx'/r.$$

The integral in Φ_D is the same as that for Φ_Q, with $D(x)$ written in place of $Q(x)$. It follows that the components of the induced velocity $\mathbf{u}_D = \nabla\Phi_D$ are

$$u_D = \frac{\partial}{\partial z} \int_0^c D(x') \frac{x-x'}{r^3}\, dx', \tag{D-17}$$

$$v_D = y \frac{\partial}{\partial z} I_D \tag{D-18}$$

and

$$w_D = \frac{\partial}{\partial z}(z I_D) \tag{D-19}$$

where

$$I_D = \int_0^c D(x') \frac{dx'}{r^3}. \tag{D-20}$$

We have to estimate $D(x)$ to cancel a residual $\tilde{R}_l(x, 0, z_t)$ in the boundary condition (22), so that approximately

$$u_D \frac{\partial z_t}{\partial x} - w_D = -\tilde{R}_l(x, 0, z_t). \tag{D-21}$$

Employing the technique of equation (D-7), we find that u_D and w_D are dominated by

$$\bar{u}_D = -D(x)\left[\frac{z_t}{r^3}\right]_0^c$$

and

$$\bar{w}_D = -D(x)\left[\frac{1}{z_t^2}\frac{x'-x}{r}+\frac{x'-x}{r^3}\right]_0^c.$$

Substituting into (D-21), we obtain the estimate for $D(x)$

$$D(x) = \frac{\tilde{R}_l(x, 0, z_t)}{\left[\frac{1}{z_t^2}\frac{x'-x}{r}+\frac{x'-x}{r^3}\right]_0^c - \frac{\partial z_t}{\partial x}\left[\frac{z_t}{r^3}\right]_0^c}. \tag{D-22}$$

We now have to calculate all the integrals arising in equations (D-17) to (D-20). As in the line sources case, we may define a piecewise continuous linear function in $x_2 \leqslant x' \leqslant x_L$ by

$$D_i(x') = D_B + (x'-x)D_A \qquad (x_{i-1} \leqslant x' \leqslant x_i;\ i = 3, 4, \ldots, L)$$

with D_B, D_A given by the analogues of (D-12)

$$D_A = \frac{D(x_i) - D(x_{i-1})}{x_i - x_{i-1}}$$

and

$$D_B = D(x_{i-1}) - (x_{i-1} - x)D_A.$$

With the help of equations (D-14), (D-17) can now be written in the form of equation (D-13)

$$u_D = -z\sum_{i=3}^{L}\left[\frac{D_B}{r^3}+\left\{\frac{1}{(r+x'-x)r}+\frac{x'-x}{r^3}\right\}D_A\right]_{x_{i-1}}^{x_i}. \tag{D-23}$$

Equations (D-18) and (D-19) can also be written in the form

$$v_D = y\sum_{i=3}^{L}\frac{\partial}{\partial z}I_{D_i} \tag{D-24}$$

and

$$w_D = \sum_{i=3}^{L}\left[I_{D_i} + z\frac{\partial}{\partial z}I_{D_i}\right] \tag{D-25}$$

where, similarly to equation (D-16)

$$I_{D_i} = \frac{D_B}{y^2+z^2}\left[\frac{x'-x}{r}\right]_{x_{i-1}}^{x_i} - D_A\left[\frac{1}{r}\right]_{x_{i-1}}^{x_i}$$

and

$$\frac{\partial}{\partial z}I_{D_i} = z\left\{D_A\left[\frac{1}{r^3}\right]_{x_{i-1}}^{x_i} - \frac{D_B}{y^2+z^2}\left[\frac{x'-x}{r^3}\right]_{x_{i-1}}^{x_i} - \frac{2D_B}{(y^2+z^2)^2}\left[\frac{x'-x}{r}\right]_{x_{i-1}}^{x_i}\right\}.$$

As in the sources case, when $\mathbf{u}_D$ is calculated thus and added to the existing $\mathbf{u}_l$, the new residuals are acceptably reduced at the root.

The recomputation of the residual errors means that near the root the calculations of surface derivatives as described in Section 4 have to be done twice for each singularity distribution: once on the velocity fields before the current line singularities are introduced, and once after. In an early run, we tried to avoid the first of these computations by dropping all the products with z_s in equations (14) to (19); but this did not represent the difference in root and outboard residuals sufficiently accurately, and the run did not converge so well at the root. The extra work is needed only on the first two spanwise collocation lines.

APPENDIX E

Modifications for Subcritical Compressible Flow

We briefly derive the Prandtl-Glauert equations here, and then show how the velocity fields and boundary conditions are modified in order to make the problem soluble by source and doublet distributions.

The density ρ is now a dependent space variable, and is connected to the pressure p and the velocity $\mathbf{U}$ by Bernoulli's equation:

$$\frac{\gamma}{\gamma-1}\frac{p}{\rho}+\frac{1}{2}\mathbf{U}^2=\text{const.}$$

We can normalize ρ and $\mathbf{U}$ so that at infinity $\rho_\infty=1$ and $|\mathbf{U}_\infty|=1$. Noting that the square of the free-stream speed of sound is

$$\frac{\gamma p_\infty}{\rho_\infty}=\frac{\mathbf{U}_\infty^2}{M_\infty^2}$$

we have

$$p_\infty=1/\gamma M_\infty^2$$

where M_∞ is the free-stream Mach number. Making use of the adiabatic equation of state, Bernoulli's equation becomes

$$\frac{\rho^{\gamma-1}}{(\gamma-1)M_\infty^2}+\frac{1}{2}\mathbf{U}^2=\frac{1}{(\gamma-1)M_\infty^2}+\frac{1}{2}.$$

Taking the gradient, there follows

$$\frac{1}{M_\infty^2}\rho^{\gamma-2}\nabla\rho+\mathbf{U}\,.\,\nabla\mathbf{U}=0. \tag{E-1}$$

The equation of conservation of mass reads:

$$\nabla\,.\,(\rho\mathbf{U})\equiv\rho\nabla\,.\,\mathbf{U}+\mathbf{U}\,.\,\nabla\rho=0.$$

Substituting for $\nabla\rho$ from (E-1),

$$\nabla\,.\,\mathbf{U}-\mathbf{U}\,.\,(\mathbf{U}\,.\,\nabla\mathbf{U})M_\infty^2/\rho^{\gamma-1}=0.$$

At this stage we linearize about the free-stream conditions: assuming that all departures from the unit flow in the x-direction are small, so that (with $\mathbf{U}=\mathbf{U}_\infty+\mathbf{u}$)

$$\mathbf{U}\,.\,\nabla\mathbf{U}\doteq\left(\frac{\partial u}{\partial x},0,0\right)$$

we have

$$\beta^2\frac{\partial u}{\partial x}+\frac{\partial v}{\partial y}+\frac{\partial w}{\partial z}=0 \tag{E-2}$$

with $\beta^2=1-M_\infty^2$.

We now transform into the affine (Prandtl-Glauert) space $(\tilde{x}, y, z)$ with the affine velocity perturbations $(\tilde{u}, v, w)$ by the relations

$$x=\tilde{x}\beta \tag{E-3}$$

and

$$u=\tilde{u}/\beta \tag{E-4}$$

and equation (E-2) becomes

$$\frac{\partial \tilde{u}}{\partial \tilde{x}}+\frac{\partial v}{\partial y}+\frac{\partial w}{\partial z}=0. \tag{E-5}$$

The equation of irrotational flow,

$$\nabla \mathbf{x}\mathbf{u}\equiv\left[\frac{\partial w}{\partial y}-\frac{\partial v}{\partial z},\frac{\partial u}{\partial z}-\frac{\partial w}{\partial x},\frac{\partial v}{\partial x}-\frac{\partial u}{\partial y}\right]=0$$

transforms to the set

and

$$\left.\begin{aligned}\partial w/\partial y-\partial v/\partial z&=0,\\ \partial \tilde{u}/\partial z-\partial w/\partial \tilde{x}&=0\\ \partial v/\partial \tilde{x}-\partial \tilde{u}/\partial y&=0.\end{aligned}\right\} \tag{E-6}$$

Equations (E-5) and (E-6) are the equations for incompressible flow in the affine space $(\tilde{x}, y, z)$ and can be satisfied by introducing velocity potentials due to suitable source and doublet distributions. The physical velocity component u is then found from the affine component $\tilde{u}$ by (E-4).

The boundary condition (5) transforms to

$$\left(U_\infty+\frac{\tilde{u}}{\beta}\right)\frac{1}{\beta}\frac{\partial z_w}{\partial \tilde{x}}+v\frac{\partial z_w}{\partial y}-(W_\infty+w)=0. \tag{E-7}$$

As in Section 3, this can be expanded in Taylor series about the thickness surface $z=z_t(\tilde{x}, y)$ and split into symmetrical and antisymmetrical parts

$$\pm R_t+R_l=0$$

where

$$R_t=\frac{\tilde{Q}_0}{\beta}\frac{\partial z_t}{\partial \tilde{x}}+\frac{\tilde{Q}_1}{\beta}\frac{\partial z_s}{\partial \tilde{x}}+Q_2\frac{\partial z_t}{\partial y}+Q_3\frac{\partial z_s}{\partial y}-Q_4$$

and

$$R_l=\frac{\tilde{Q}_0}{\beta}\frac{\partial z_s}{\partial \tilde{x}}+\frac{\tilde{Q}_1}{\beta}\frac{\partial z_t}{\partial \tilde{x}}+Q_2\frac{\partial z_s}{\partial y}+Q_3\frac{\partial z_t}{\partial y}-Q_5$$

with

$$\tilde{Q}_0 = 1 + \left(\tilde{u}_t + z_s \frac{\partial \tilde{u}_l}{\partial z}\right) \Big/ \beta$$

and

$$\tilde{Q}_1 = \left(z_s \frac{\partial \tilde{u}_t}{\partial z} + \tilde{u}_l\right) \Big/ \beta$$

$Q_{2\ldots5}$ are as defined by equations (16) to (19).

We remark that the basic first-order residuals are as in the incompressible flow problem:

$$R_{tB} = \frac{1}{\beta} \frac{\partial z_t}{\partial \tilde{x}} \equiv \frac{\partial z_t}{\partial x}$$

and

$$R_{lB} = -\sin(\alpha + \alpha_T) + \frac{1}{\beta} \frac{\partial z_s}{\partial \tilde{x}} = -\sin(\alpha + \alpha_T) + \frac{\partial z_s}{\partial x}.$$

The lifting-surface (vortex lattice) subroutine, on receiving the input R_l, outputs the affine doublet distribution $\tilde{l}$ which is connected to the pressure coefficient $-\Delta C_p$ in linearized thin-wing theory by the same relation as that between the physical and affine streamwise-velocity components in (E-4):

$$-\Delta C_p \doteqdot \tilde{l}/\beta.$$

Further, starting with the boundary condition (E-7) we can repeat the Maclaurin series analysis of Section 5 and derive at the pth inner iteration:

$$R^{(n,p+1)} = R^{(n,p)} - \Delta w + \frac{1}{\beta^2} \frac{\partial z_w}{\partial \tilde{x}} \Delta \tilde{u} + \frac{\partial z_w}{\partial y} \Delta v + z_w \left(\frac{\partial \Delta \tilde{u}}{\partial \tilde{x}} + \frac{\partial \Delta v}{\partial y}\right)$$

$$\doteqdot \frac{\partial}{\partial \tilde{x}}(z_w \Delta \tilde{u}) + \frac{\partial}{\partial y}(z_w \Delta v) + \left(\frac{1}{\beta^2} - 1\right) \frac{\partial z_w}{\partial \tilde{x}} \Delta \tilde{u}$$

so that

$$R_t^{(n,p+1)} = \frac{\partial}{\partial \tilde{x}}(z_t \Delta \tilde{u}_t + z_s \Delta \tilde{u}_l) + \frac{\partial}{\partial y}(z_t \Delta v_t + z_s \Delta v_l) + \left(\frac{1}{\beta^2} - 1\right) R_{ct}$$

and

$$R_l^{(n,p+1)} \doteqdot \frac{\partial}{\partial \tilde{x}}(z_s \Delta \tilde{u}_t + z_t \Delta \tilde{u}_l) + \frac{\partial}{\partial y}(z_s \Delta v_t + z_t \Delta v_l) + \left(\frac{1}{\beta^2} - 1\right) R_{cl}^*.$$

These are the expressions (57) and (58) for incompressible flow, with the compressibility correction terms

$$R_{ct} = \frac{\partial z_t}{\partial \tilde{x}} \Delta \tilde{u}_t + \frac{\partial z_s}{\partial \tilde{x}} \Delta \tilde{u}_l$$

and

$$R_{cl}^* = \frac{\partial z_s}{\partial \tilde{x}} \Delta \tilde{u}_t + \frac{\partial z_t}{\partial \tilde{x}} \Delta \tilde{u}_l.$$

We must ensure that the expressions used are uniformly valid near the wing leading edge $\xi = 0$. We require at worst

$$R_t = 0(\xi^{-\frac{1}{2}}), \qquad R_l = 0(1).$$

The expression R_{ct} is satisfactory, but the second term in R_{cl}^* is not. We introduce a Riegels-type factor and replace R_{cl}^* by

$$R_{cl} = \frac{\partial z_s}{\partial \tilde{x}} \Delta \tilde{u}_t + \frac{(\partial z_t/\partial \tilde{x}) \Delta \tilde{u}_l}{1 + [(\partial z_t/\partial \tilde{x}) \Delta \tilde{u}_l]^2}.$$

Further, when computing line singularity distributions at the root, corresponding to equation (E-7) the appropriate boundary condition, in place of equations (D-6) and (D-21) of Appendix D, reads:

$$\tilde{u}_{(\mathrm{D})} \frac{\partial z_t}{\partial \tilde{x}} \frac{1}{\beta^2} - w_{(\mathrm{D})} = -R_{(\mathrm{I})}(x, 0, z_t).$$

Finally, we need the standard relation between $\mathbf{u}^2$ and the pressure coefficient C_p in adiabatic flow:

$$C_p = \frac{[1 + \frac{1}{2}(\gamma - 1) M_\infty^2 (1 - \mathbf{u}^2)]^{\gamma/(\gamma-1)} - 1}{\frac{1}{2}\gamma M_\infty^2}.$$

Also the absolute local Mach number M_{loc} is given by

$$M_{loc}^2 = \frac{\mathbf{u}^2 M_\infty^2}{1 + \frac{1}{2}(\gamma - 1) M_\infty^2 (1 - \mathbf{u}^2)}.$$

Following Lock[18], we define the critical pressure coefficient C_p^* for flow normal to the local sweep line (in the physical plane) by the relation

$$\tfrac{1}{2}\gamma M_\infty^2 C_p^* = \left[\frac{2}{\gamma+1} + \frac{\gamma-1}{\gamma+1} M_\infty^2 \cos^2 \Lambda\right]^{\gamma/(\gamma-1)} - 1.$$

APPENDIX F

Extrapolations for Planar Source and Doublet Distributions

As explained in Subsection 5.1, the loading l cannot be determined directly on the centre line $y = 0$ from the vortex lattice subroutine, and so we extrapolate using a quadratic in y based on the next three outboard stations $y = Y_2, Y_3, Y_4$. The extrapolation is actually done on the loading function

$$L(\phi, Y) = l(x, y) c(y) \sin \phi$$

where ϕ is the angular chordwise coordinate. Lagrange's formula is programmed in the form

$$l(\xi, 0) = [l(\xi, Y_2) c_2 H_{01} + l(\xi, Y_3) c_3 H_{02} + l(\xi, Y_4) c_4 H_{03}]/c_1$$

where $c_n = c(Y_n)$ and

$$H_{0i} = Y_{j+1} Y_{k+1} / [(Y_{i+1} - Y_{j+1})(Y_{i+1} - Y_{k+1})]$$

with i, j, k an arrangement (permutation) of 1, 2, 3.

The distributions must also be extrapolated towards the wing tip. It is unwise[3,4] to compute $\mathbf{u}_t$ and $\mathbf{u}_l$ at the spanwise station nearest the tip and so no information is available at that station for the source or vortex lattice

calculations. Yet we need q and l there to repeat the u_t and u_l computations. As in linear theory[4] we assume that l depends on η through the square root $\sqrt{1-\eta^2}$ near the tip $\eta = 1$, and fit a quadratic through the two available values at Y_{M-2} and Y_{M-1} and the zero at Y_{M+1} (i.e. the tip). This gives

$$l(\xi, Y_M) = [l(\xi, Y_{M-1})h_2(h_0 - h_2) + l(\xi, Y_{M-2})h_1(h_1 - h_0)]h_0/[h_1 h_2(h_1 - h_2)]$$

with

$$h_i = (1 - Y_{M-i}^2/Y_{M+1}^2)^{\frac{1}{2}} \qquad i = 0, 1, 2.$$

On the other hand, the source distribution q does not tend to zero at the tip for a wing with constant section geometry. For the sources we extrapolate from Y_{M-3}, Y_{M-2} and Y_{M-1} to Y_M in the ordinary variable y:

$$q(\xi, Y_M) = \sum_{n=1}^{3} q(\xi, Y_{M-n})F_n$$

where

$$F_i = \frac{(Y_M - Y_{M-j})(Y_M - Y_{M-k})}{(Y_{M-i} - Y_{M-j})(Y_{M-i} - Y_{M-k})}$$

with i, j, k a permutation of 1, 2, 3.

This last formula can also be used for l, should the chord $c(\eta)$ show elliptic behaviour at the tip.

The Ledger-Sells subroutine also requires input data for $q \sin\phi$ or $l \sin\phi$ at the leading edge $\xi = 0$ (both are finite there). The doublet function is readily obtained along with all the other values along the chordline from the vortex lattice output at the stations ξ_v. The source function is available directly from the residuals at the stations ξ_w, where $z = z_t \neq 0$, but the residuals cannot be calculated at the leading edge because $z_t = 0$ there, and more especially $\partial z_t/\partial x$ is infinite. We could build in Ledger's other subroutine[3] for $z = 0$, to calculate u_t, v_t and the limit $R_t \sin\phi$ from equation (23), but it is simpler to extrapolate $e_t = q \sin\phi$ parabolically to the leading edge from its values at the first 2 stations ξ_w. We also know that $q = 0(\xi^{-\frac{1}{2}})$ near $\xi = 0$, and it follows that $\partial e_t/\partial\phi = 0$ at the leading edge. This leads to

$$e_t(0, y) = [4e_t(\xi_2, y) - e_t(\xi_3, y)]/3. \tag{F-1}$$

It has also been found advisable to use (F-1) to extrapolate the input data e_{tB} in order to compute the integral $S^{(1)}$. The program was used to calculate the flow past a swept uncambered wing with a blunt-nosed section (compared with the quasi-elliptical sections of the RAE 100 series) for which elliptical behaviour was effectively confined to the first 5 per cent or so of the chord. The input data $e_{tB} = q_B \sin\phi = 2(\partial z_t/\partial x)\sin\phi$ is specified at L chordwise points, and for $L \leqslant 12$ only the first two of these points, at the leading edge $\phi = 0$ and at $\phi = \pi/L$, lie in the first 5 per cent of the chord. From this input, the program calculates values of $S^{(1)}(\xi)$ as given by equation (59) with $R_t = \partial z_t/\partial x$:

$$\begin{aligned} S^{(1)}(\xi) &= \frac{1}{\pi}\int_0^1 \frac{\partial z_t}{\partial x}(\xi')\frac{d\xi'}{\xi - \xi'} \\ &= \frac{1}{2\pi}\int_0^\pi \frac{e_{tB}(\phi')\,d\phi'}{\cos\phi' - \cos\phi}. \end{aligned} \tag{F-2}$$

If the values of e_{tB} at the first *three* points on the chord are not numerically consistent with the condition $\partial e_{tB}/\partial\phi = 0$ at $\phi = 0$, the values of $S^{(1)}$ at these points are liable to quite serious error. This is not surprising because when this condition does not hold, the integral (F-2) shows a logarithmic singularity for $\phi \to 0$. This error would influence the approximate second-order terms in the first iteration and would seriously affect convergence near the leading edge. So, even though an analytic expression for $e_{tB}(0)$ may be available, it is better to calculate its value from the other data so that this difficulty does not appear.

APPENDIX G

Lock's Modification of the RAE Standard Method

The basic formula of the RAE Standard Method[6] for the velocity in incompressible flow may be written[13]

$$\mathbf{u}^2 = \frac{[\cos\alpha(1+u_t \pm u_c) \pm u_\alpha(1+S^{(3)}\sec\Lambda_m^*)]^2 + (v_t \pm v_c)\cos\alpha \pm v_\alpha(1+S^{(3)}\sec\Lambda_m^*)]^2}{D} +$$

$$+(1-K_2^2)\left(1-\frac{1}{D}\right)\sin^2\Lambda\cos^2\alpha \qquad \text{(G-1)}$$

where suffices t, c and α refer to thickness, camber and incidence respectively.

$$S^{(3)}(\xi) = \frac{1}{\pi}\int_0^1 \left[\frac{dz_t}{dx}(\xi') - \frac{2z_t(\xi')/c}{1-(1-2\xi')^2}\right]\frac{d\xi'}{\xi-\xi'}$$

$$D = 1+(\partial z/\partial x)^2\sec^2\Lambda^*$$

$$\Lambda^* = (1-|K_2|)\Lambda$$

and the expression,

$$\Lambda_m^* = (1-|K_2|)\Lambda_m$$

where Λ_m is the local sweep angle of the maximum thickness line, has been privately suggested by Lock for use in the incidence terms $\mathbf{u}_\alpha(1+S^{(3)}\sec\Lambda^*)$. It would not be right to use Λ_m^* in the definition of D, which is the Riegels leading-edge correction factor and should therefore contain the local value of sweep angle.

The vectors $\mathbf{u}_t$ and $\mathbf{u}_l$ (suffix l standing for c or α) are evaluated on the chordal plane $z = 0$. Although estimates for u_t and v_t are available from the original RAE Standard Method[6] (and quoted as equations (60) and (61) here), we are likely to achieve a worthwhile gain in accuracy by computing these using Ledger's subroutine[3] for $z = 0$. For similar reasons, we determine each u_l from the vortex lattice solution with equation (62), and then evaluate each v_l with expression (63):

$$v_l = \frac{\partial}{\partial\eta}\int_{x_L}^{x} u_l\,dx - u_l\tan\Lambda.$$

The integral is evaluated at the Weber points $\xi = \xi_w$ using Simpson's rule, and then the differentiation is carried out along lines of constant ξ using 3-point Lagrange formulae in η inboard, but in $\sqrt{1-\eta^2}$ near the tip. Although so simple a process may be in error near the root particularly, where the v_l rise quite rapidly from zero, it is unlikely to matter much since v_c, v_α enter (G-1) through squares and products with v_t.

The results quoted in the main text were obtained with this simplified version, in which camber and incidence effects are represented separately by the plain vortex lattice technique. In a more sophisticated version, developed since, these representations are improved by evaluating the downwash field due to each representing doublet distribution[4] and iterating on the residual errors.

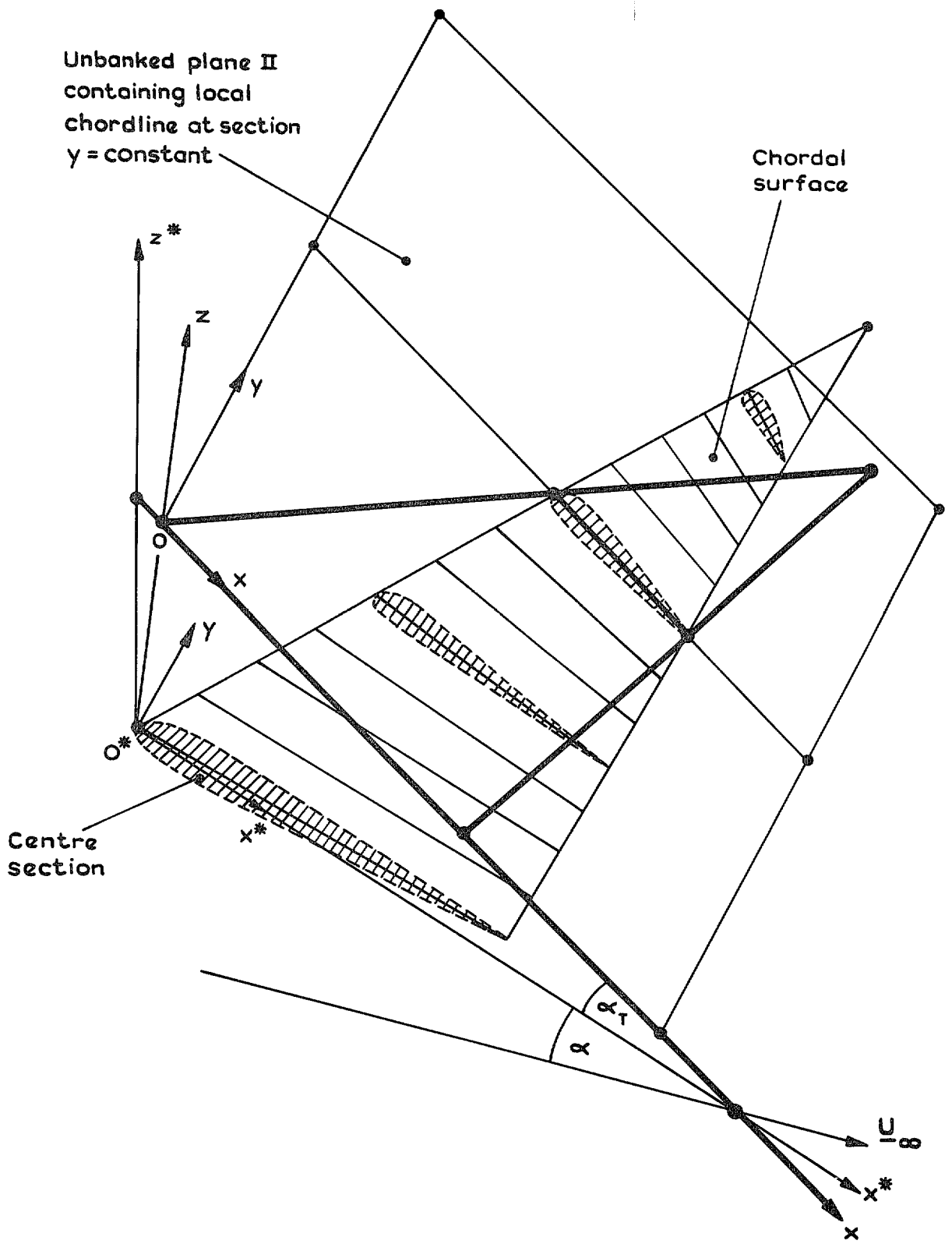

FIG. 1. Sketch of half wing and typical singularity plane.

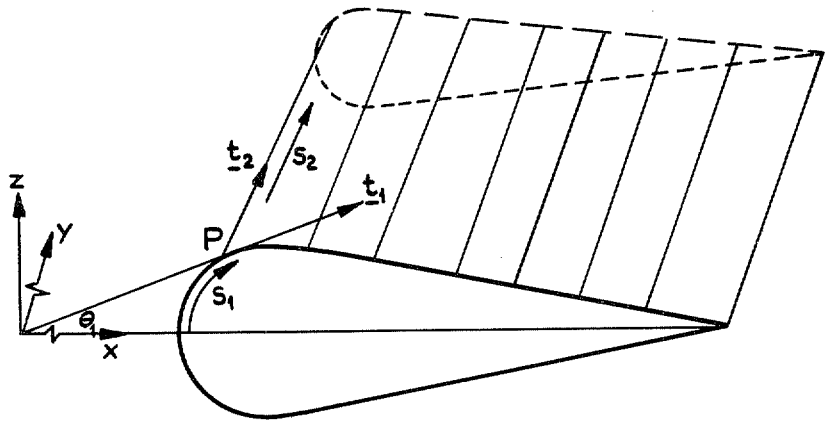

FIG. 2. Families of curves in thickness surface.

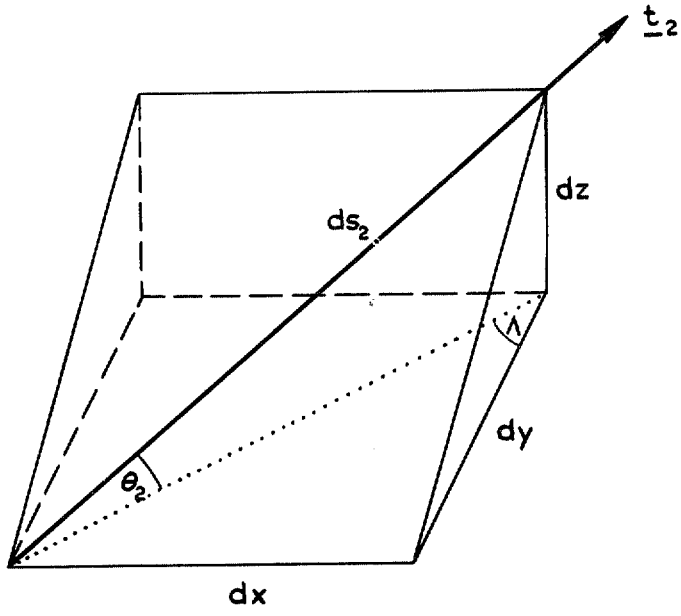

FIG. 3. Spanwise length element in thickness surface.

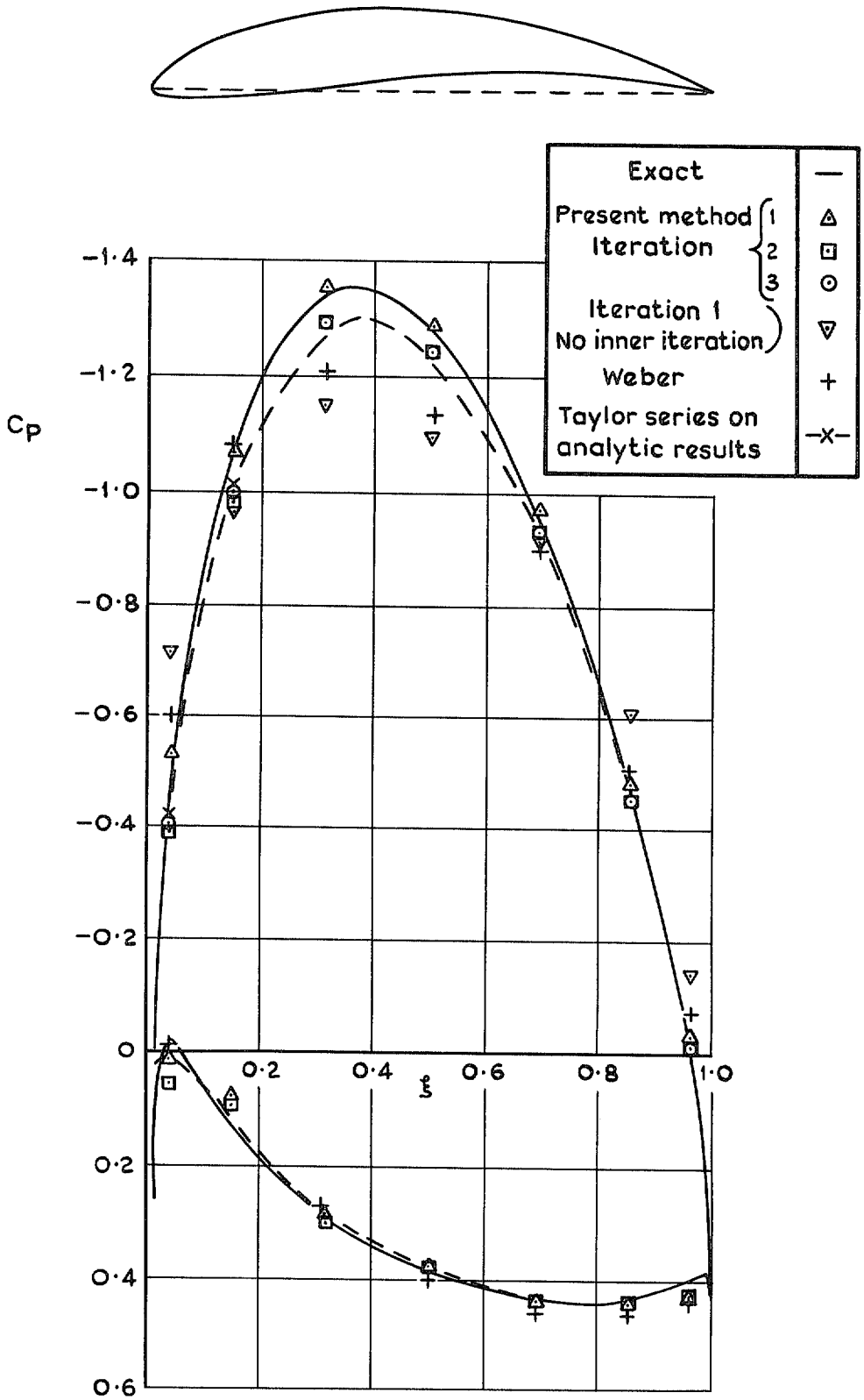

FIG. 4. Pressure distribution on medium camber Karman-Trefftz section at zero incidence; $M_\infty = 0$.

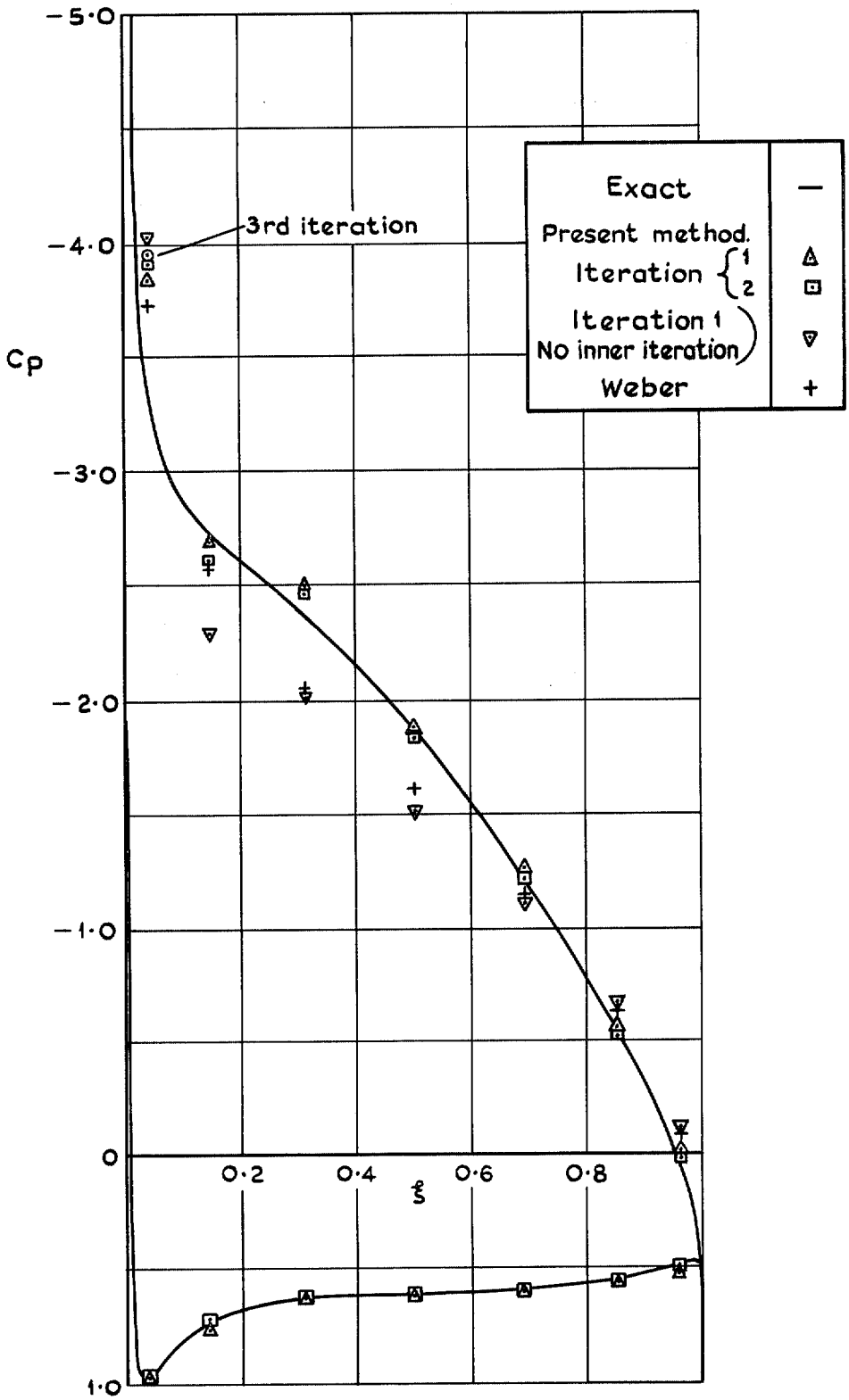

FIG. 5. Pressure distribution on medium camber Karman-Trefftz section. $\alpha = 10°$, $M_\infty = 0$.

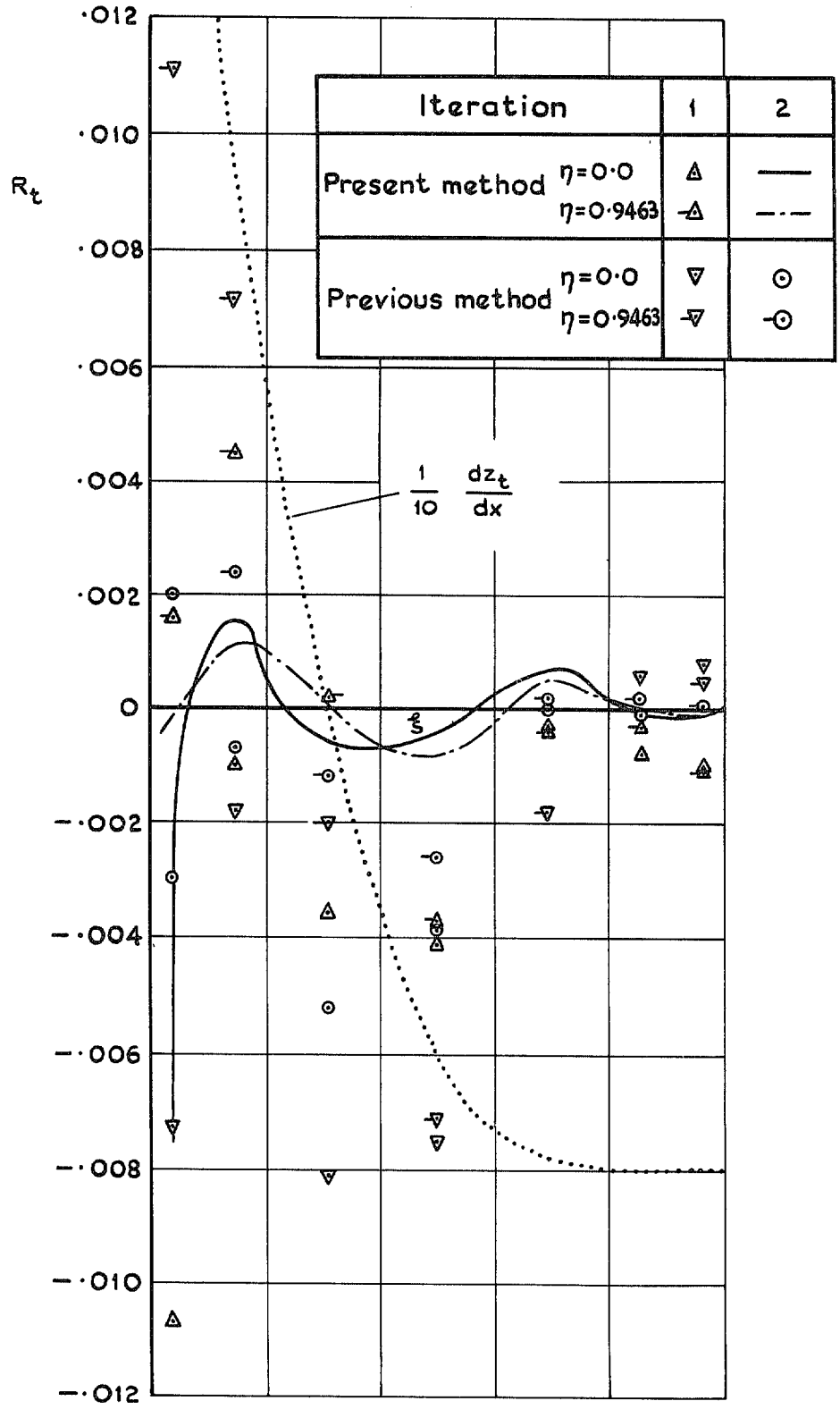

FIG. 6. Convergence comparisons at root and near tip for symmetrical residual R_t. Uncambered constant chord wing, aspect ratio 6, sweep 45°, 9% R.A.E. 101 section.

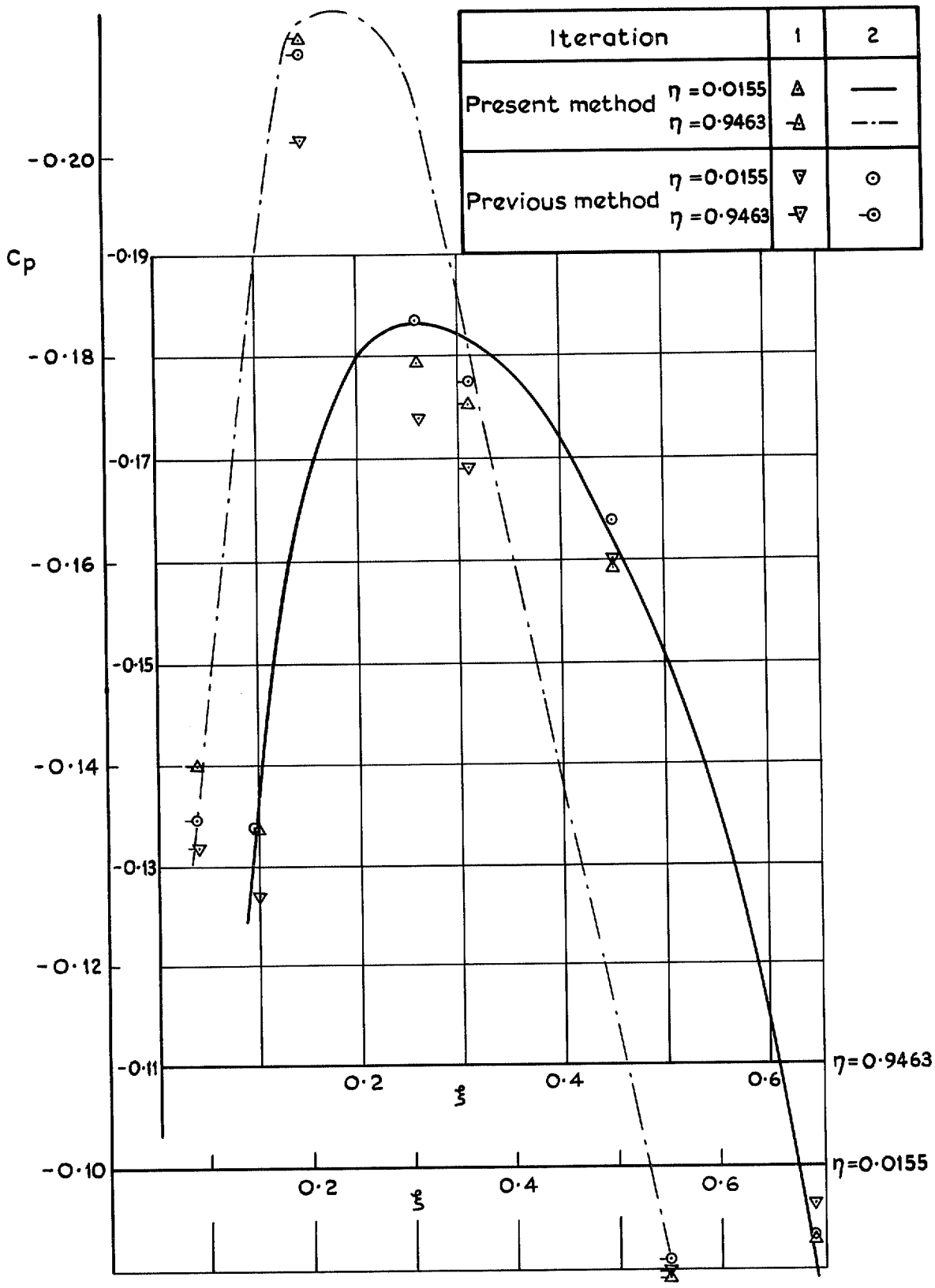

FIG. 7. Convergence comparisons near root and tip, for pressure coefficient. Uncambered constant chord wing, aspect ratio 6, sweep 45°, 9% R.A.E. 101 section, zero incidence, $M_\infty = 0$.

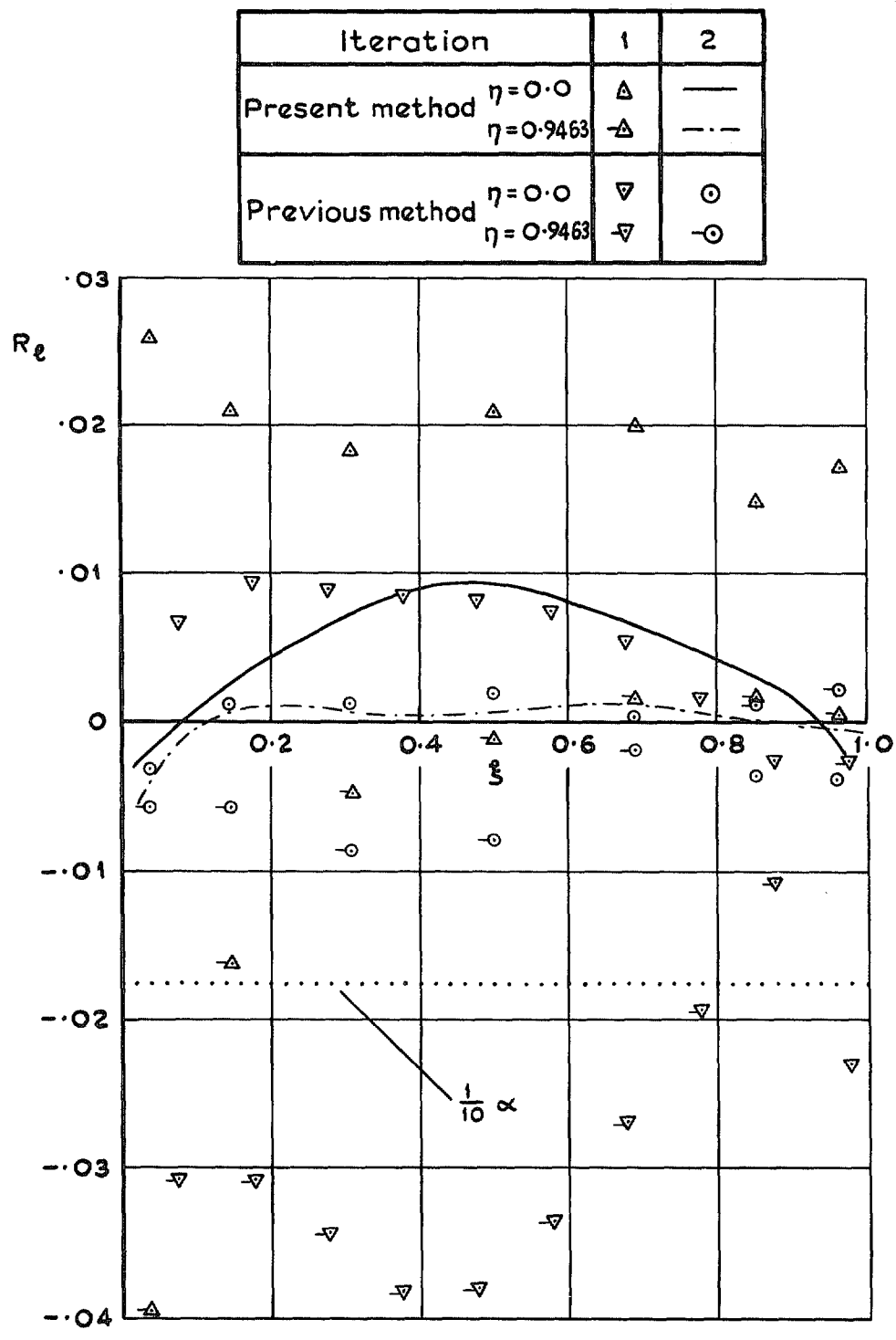

FIG. 8. Convergence comparisons at root and near tip for antisymmetrical residual R_l. Uncambered constant chord wing, aspect ratio 6, sweep 45°, 9% R.A.E. 101 section, $\alpha = 10°$.

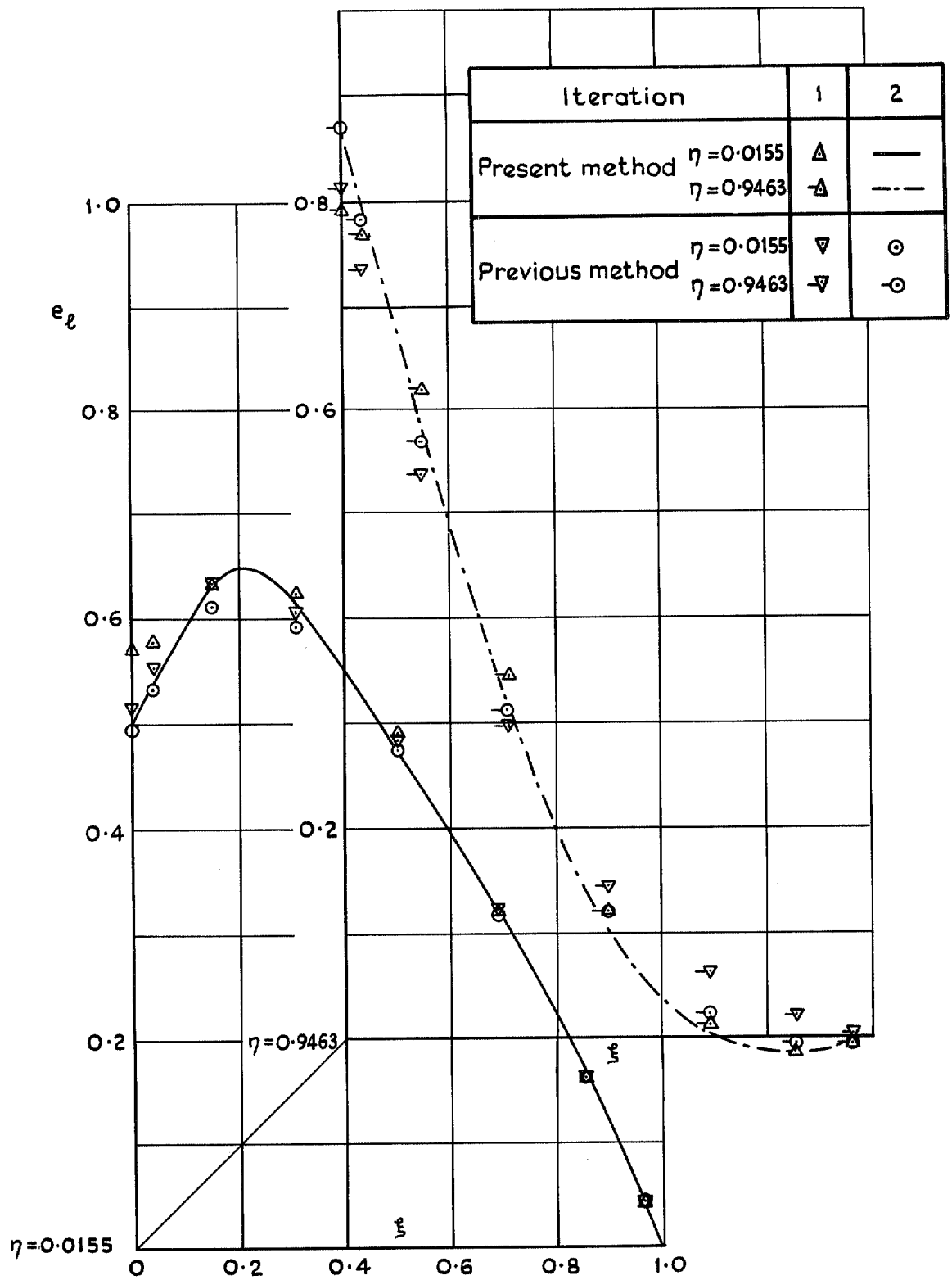

FIG. 9. Convergence comparisons near root and tip for load function. Uncambered constant chord wing, aspect ratio 6, sweep 45°, 9% R.A.E. 101 section, 10° incidence, $M_\infty = 0$.

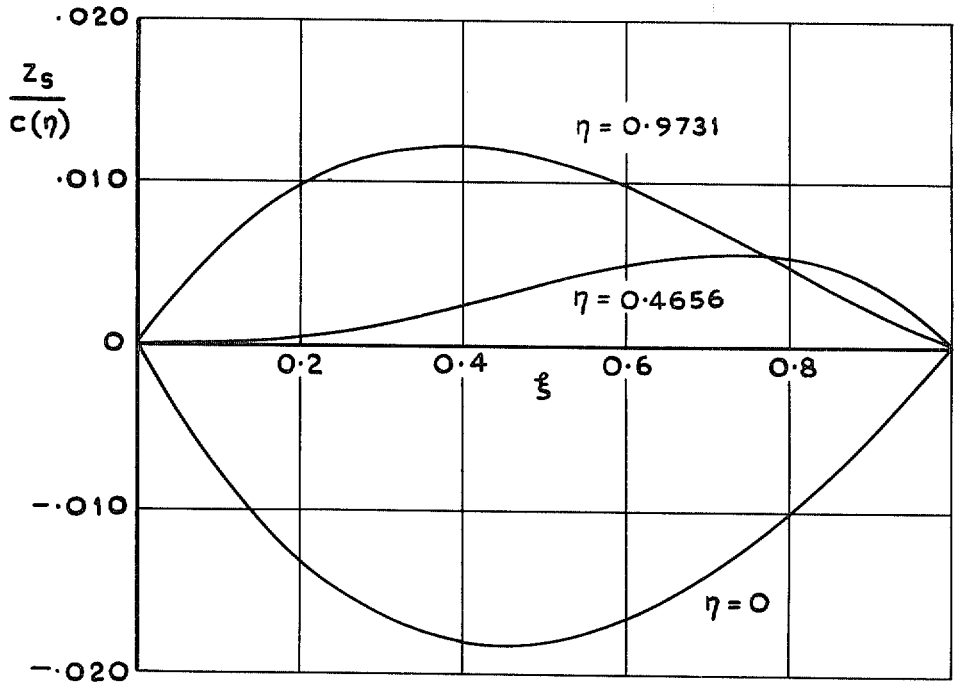

FIG. 10a. Camber distribution on R.A.E. wing 'B'.

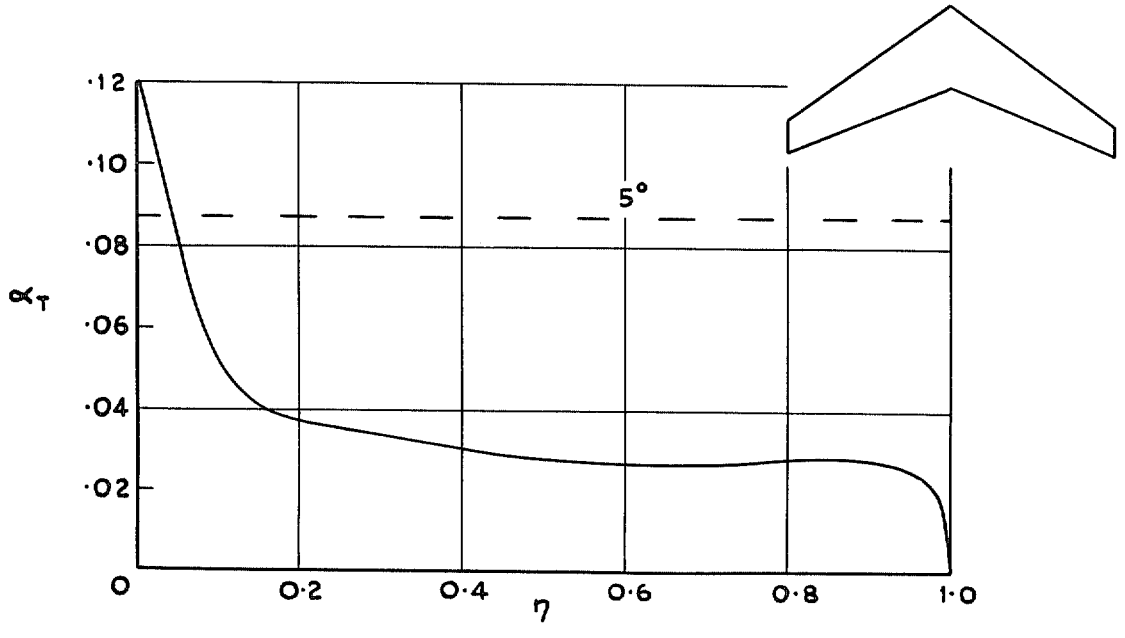

FIG. 10b. Twist distribution on R.A.E. wing 'B'.

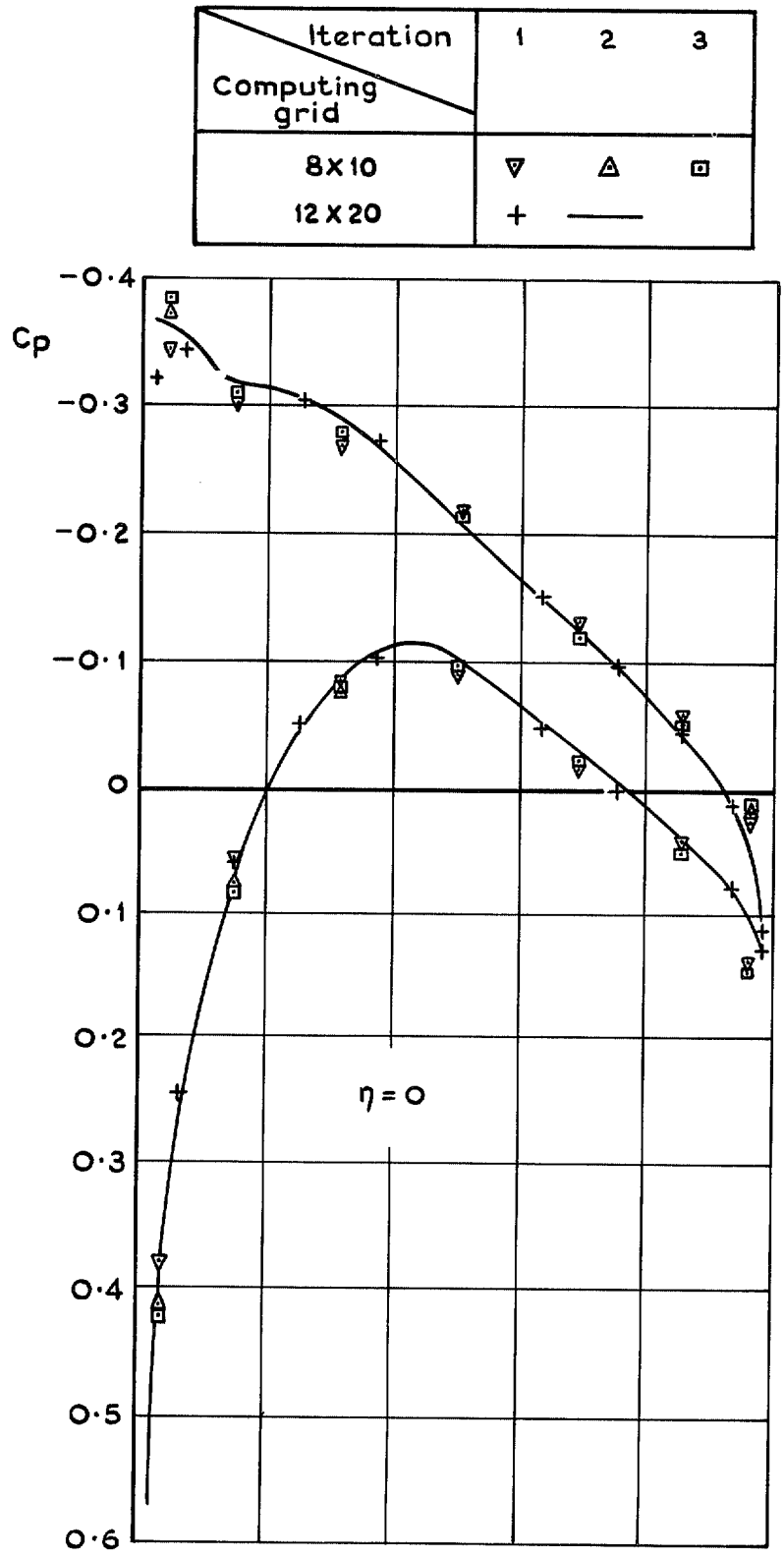

FIG. 11. Iterative convergence at root for coarse and fine computing grids. R.A.E. wing 'B', $\alpha = 0$, $M_\infty = 0$.

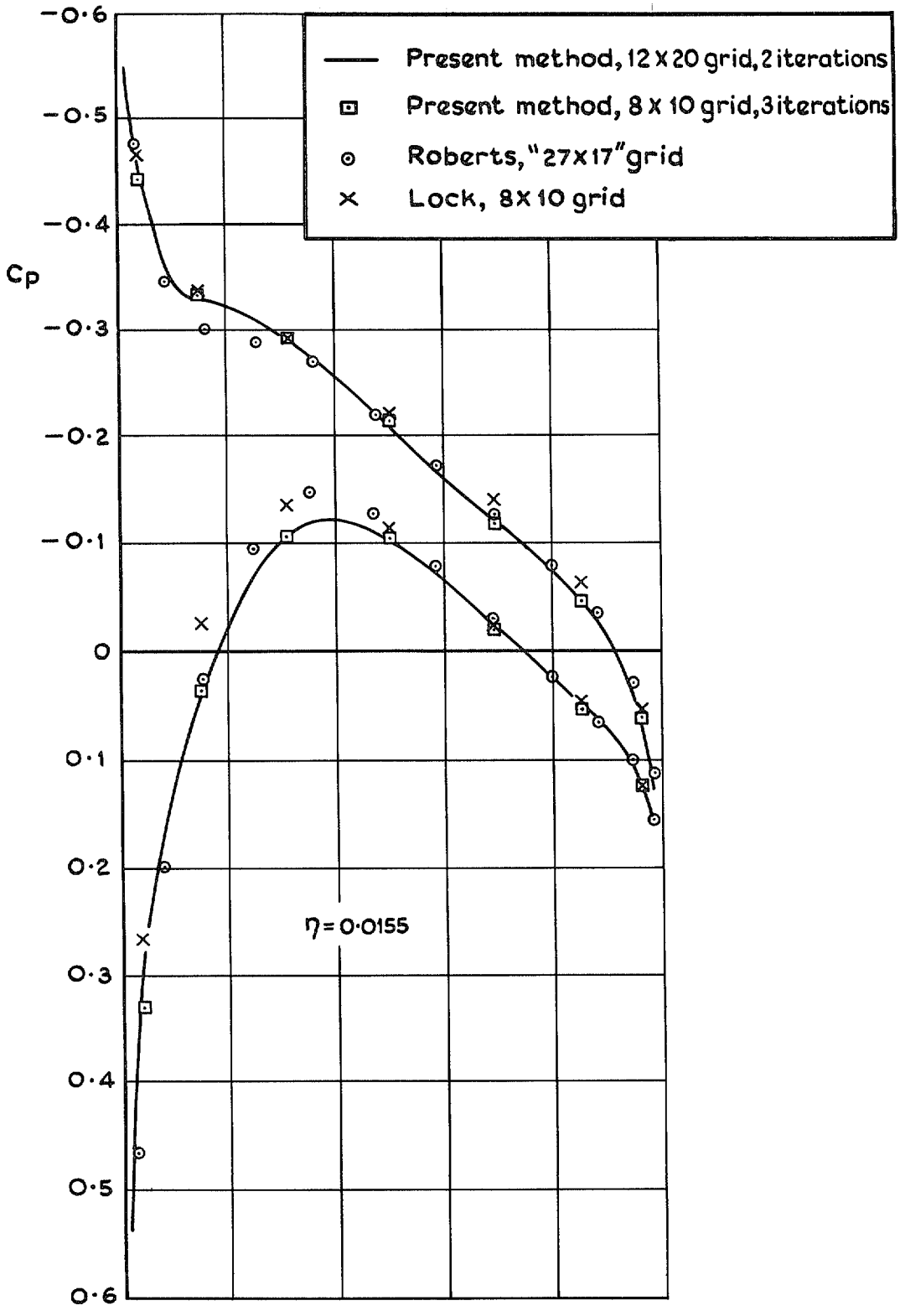

FIG. 12. Comparison of methods near root for R.A.E. wing 'B' at zero incidence, $M_\infty = 0$.

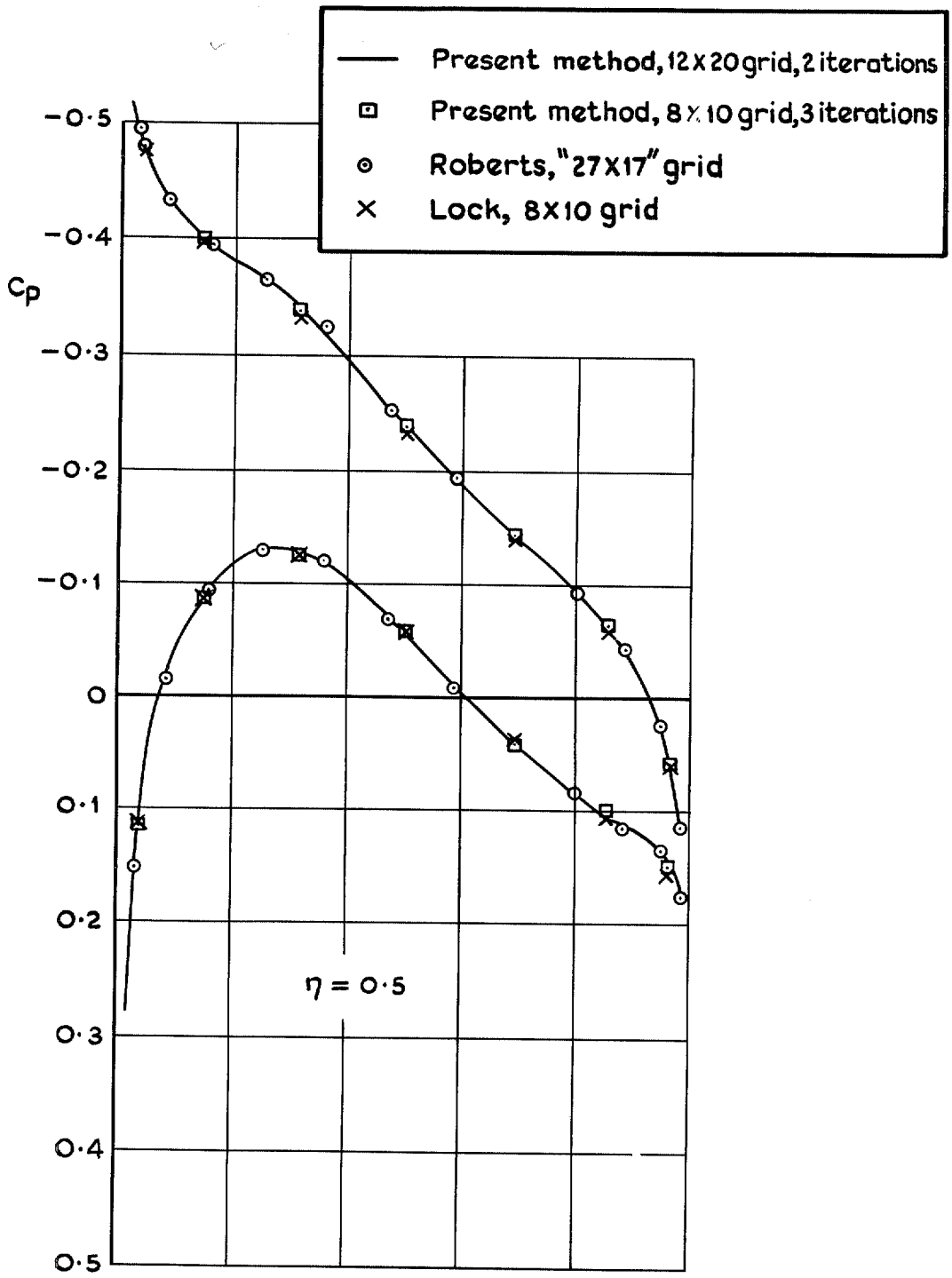

FIG. 13. Comparison of methods at mid-semi-span for R.A.E. wing 'B' at zero incidence, $M_\infty = 0$.

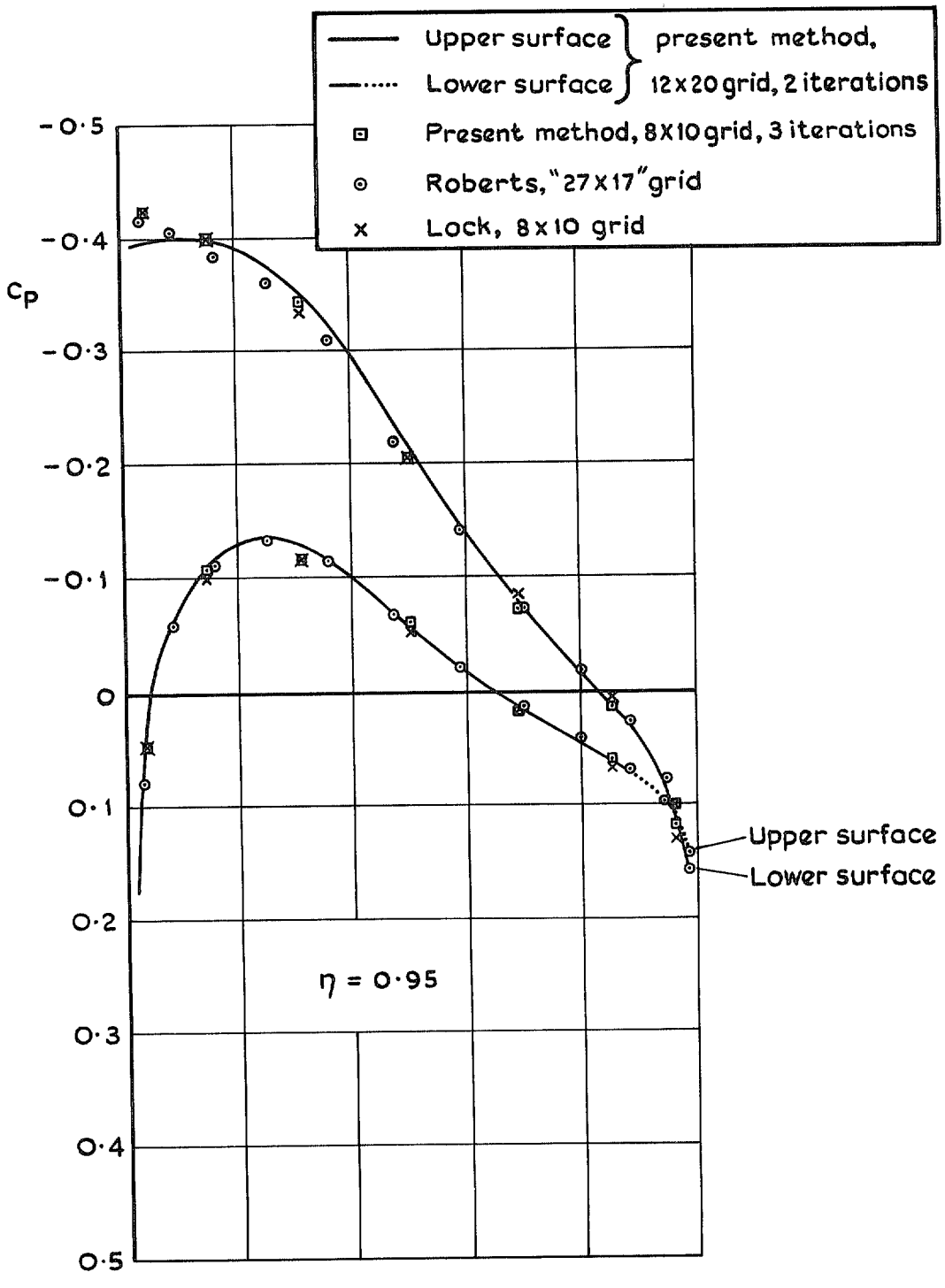

FIG. 14. Comparison of methods near tip for R.A.E. wing 'B' at zero incidence, $M_\infty = 0$.

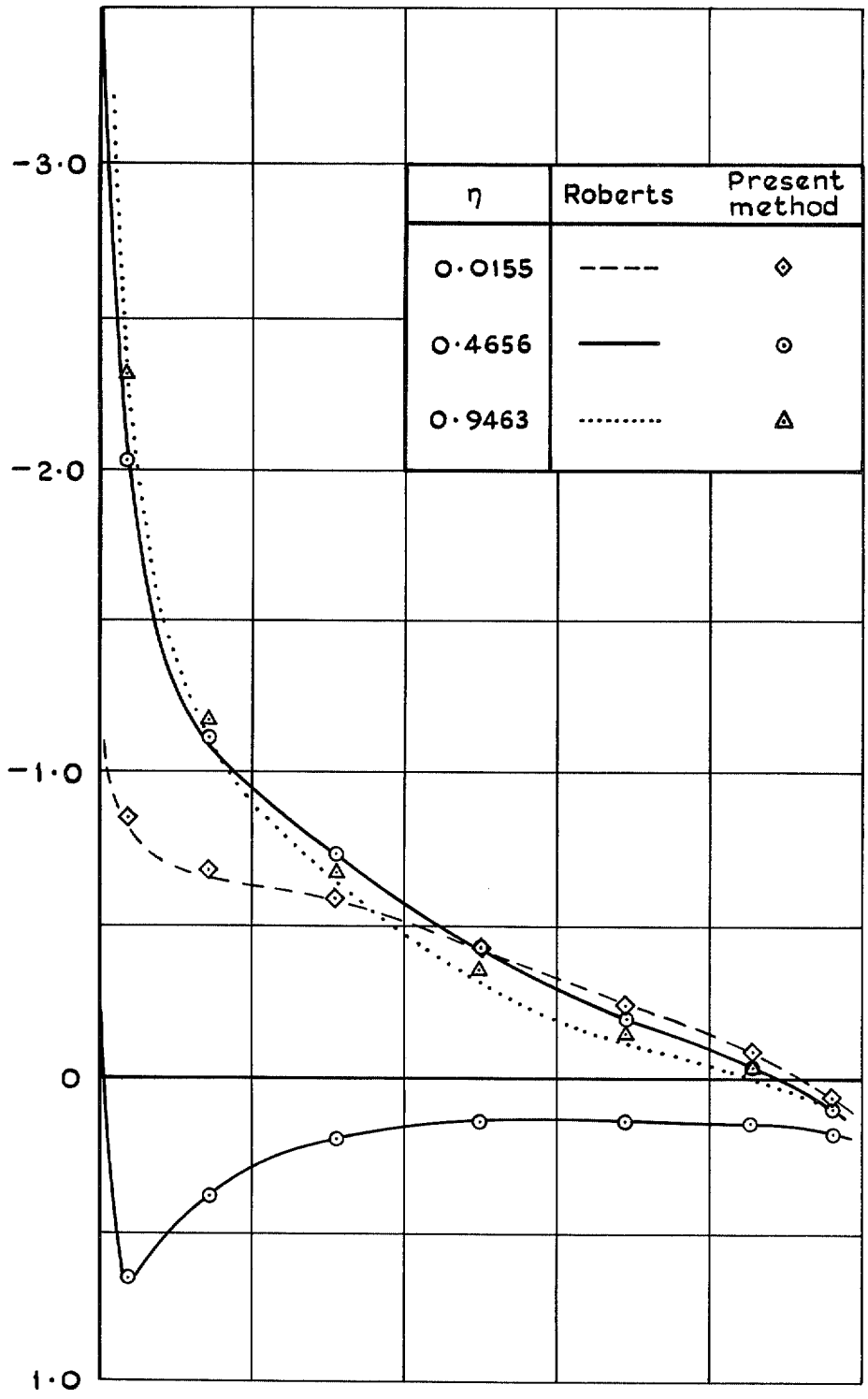

FIG. 15. Comparison of present method with Roberts method R.A.E. wing 'A', $\alpha = 10°$, $M_\infty = 0{\cdot}4$.

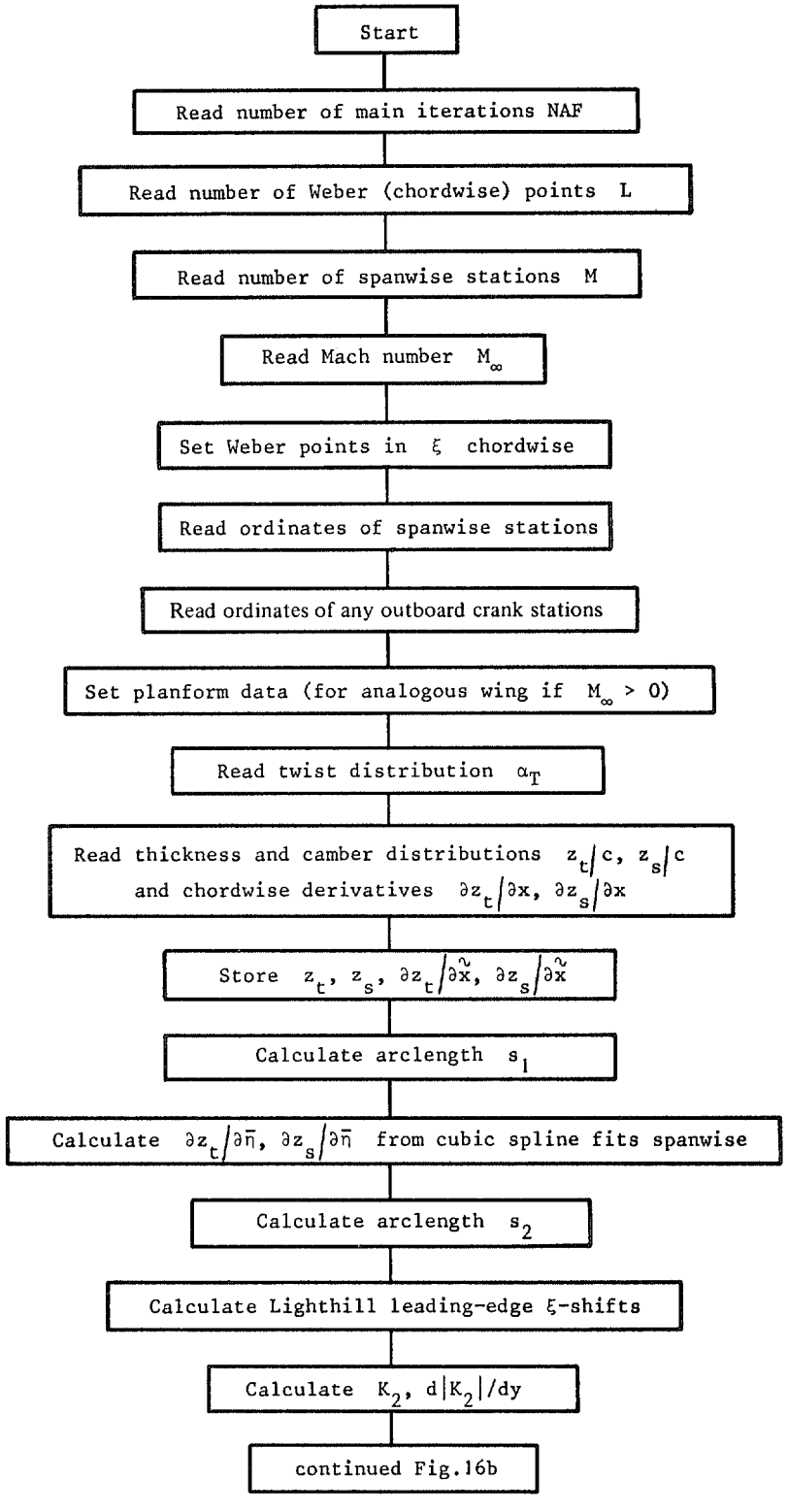

FIG. 16a. Flow diagram of computer program. Preliminaries.

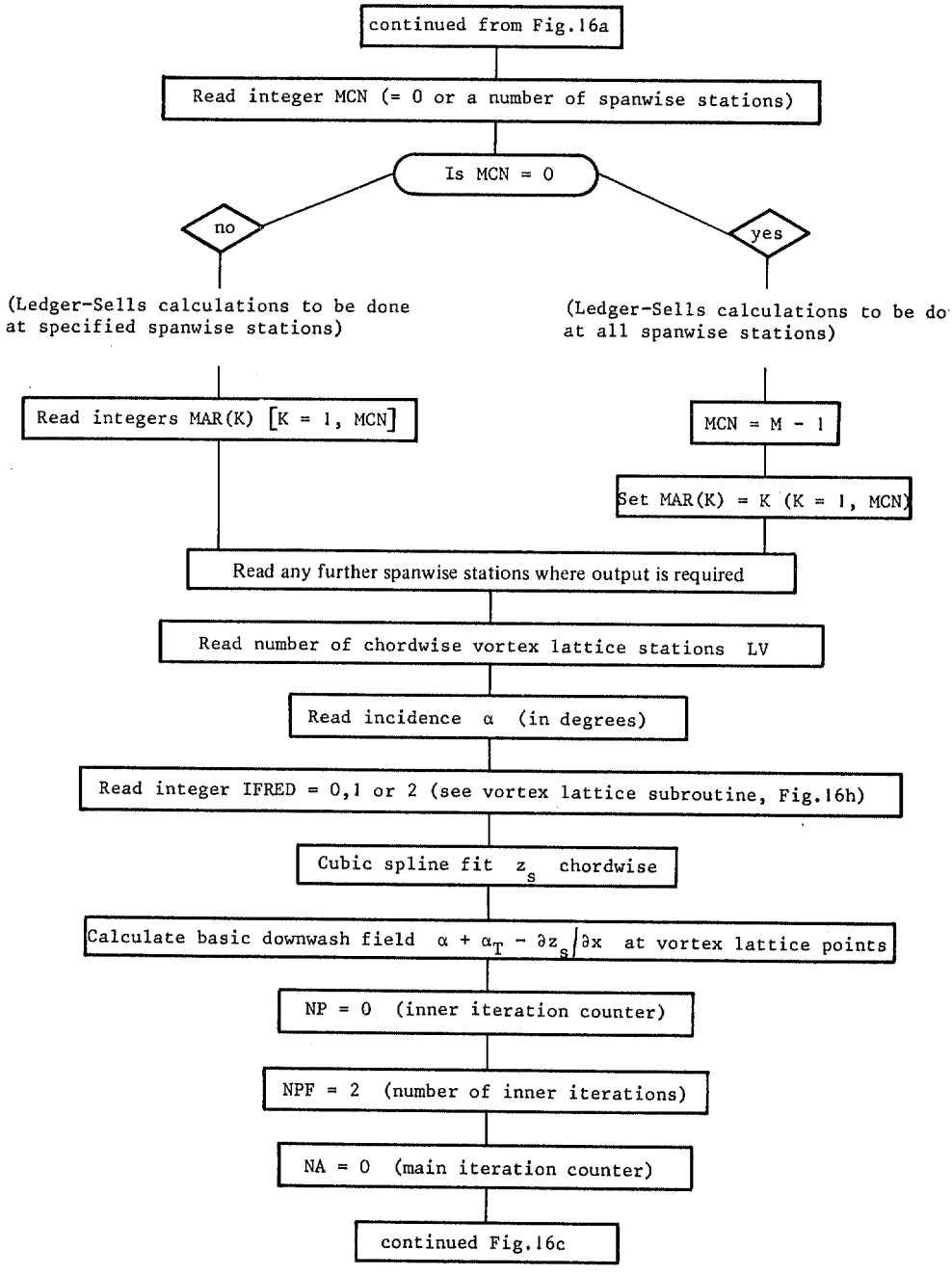

FIG. 16b. Flow diagram. Preliminaries (continued).

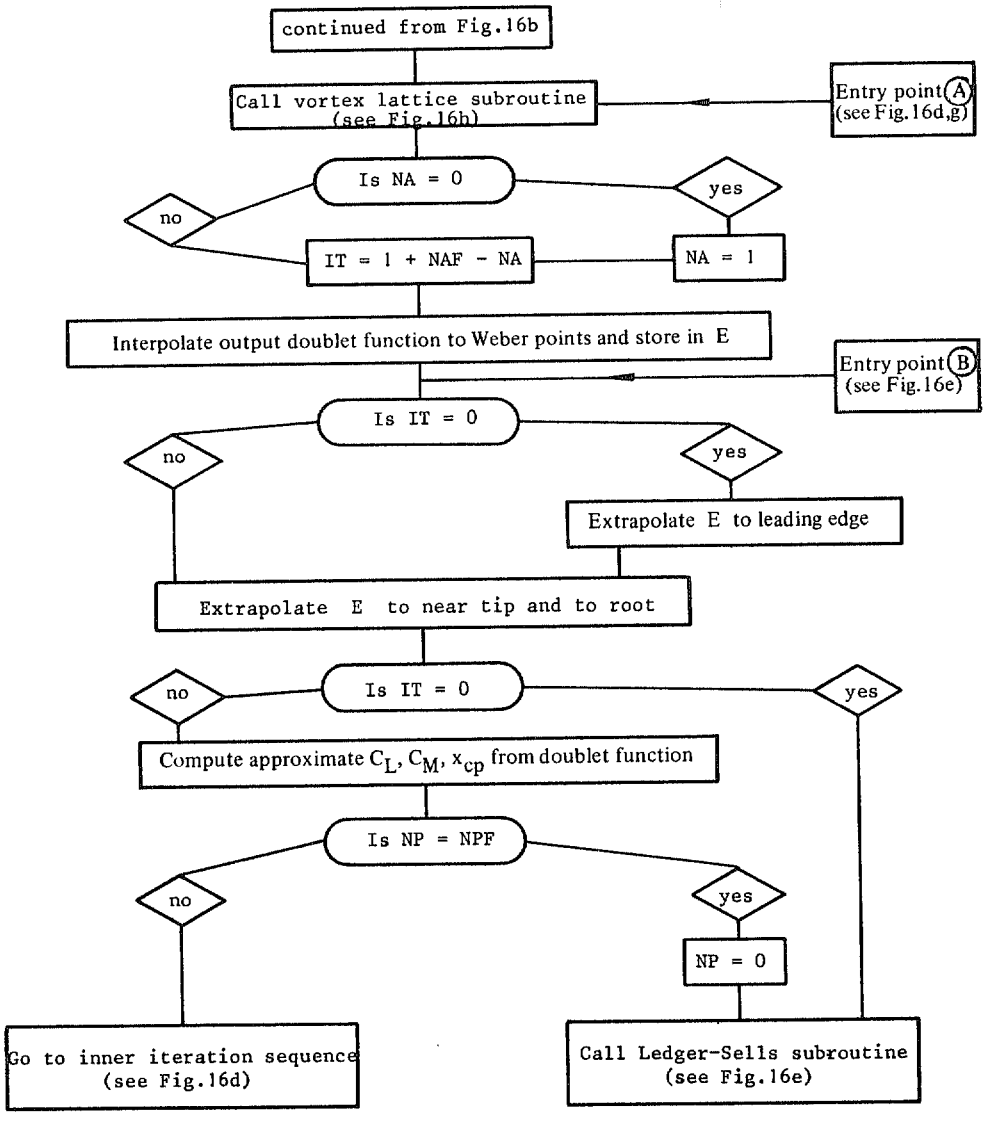

FIG. 16c. Flow diagram. Operations on doublet or source functions.

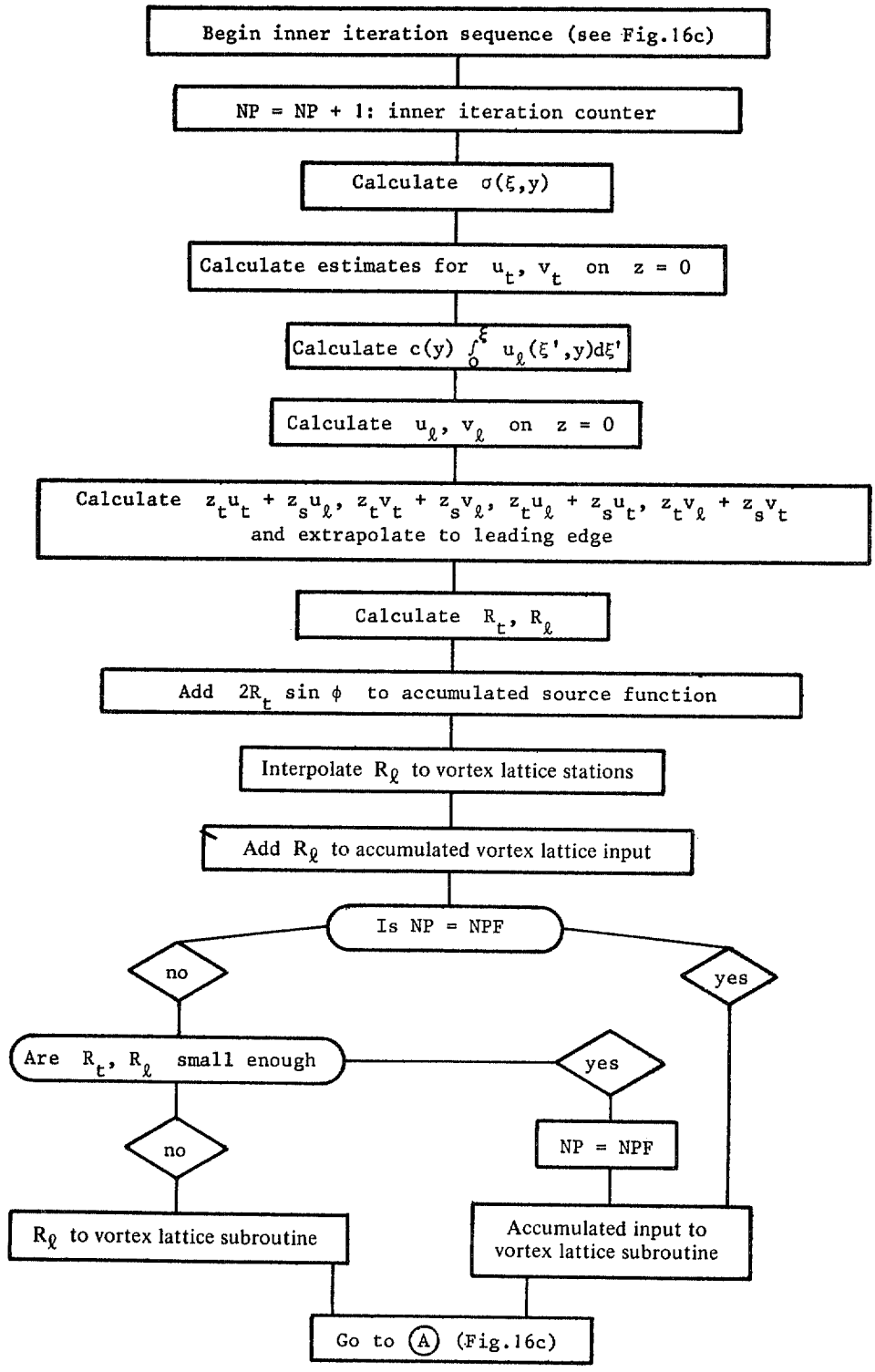

FIG. 16d. Flow diagram. Inner iteration with Maclaurin series.

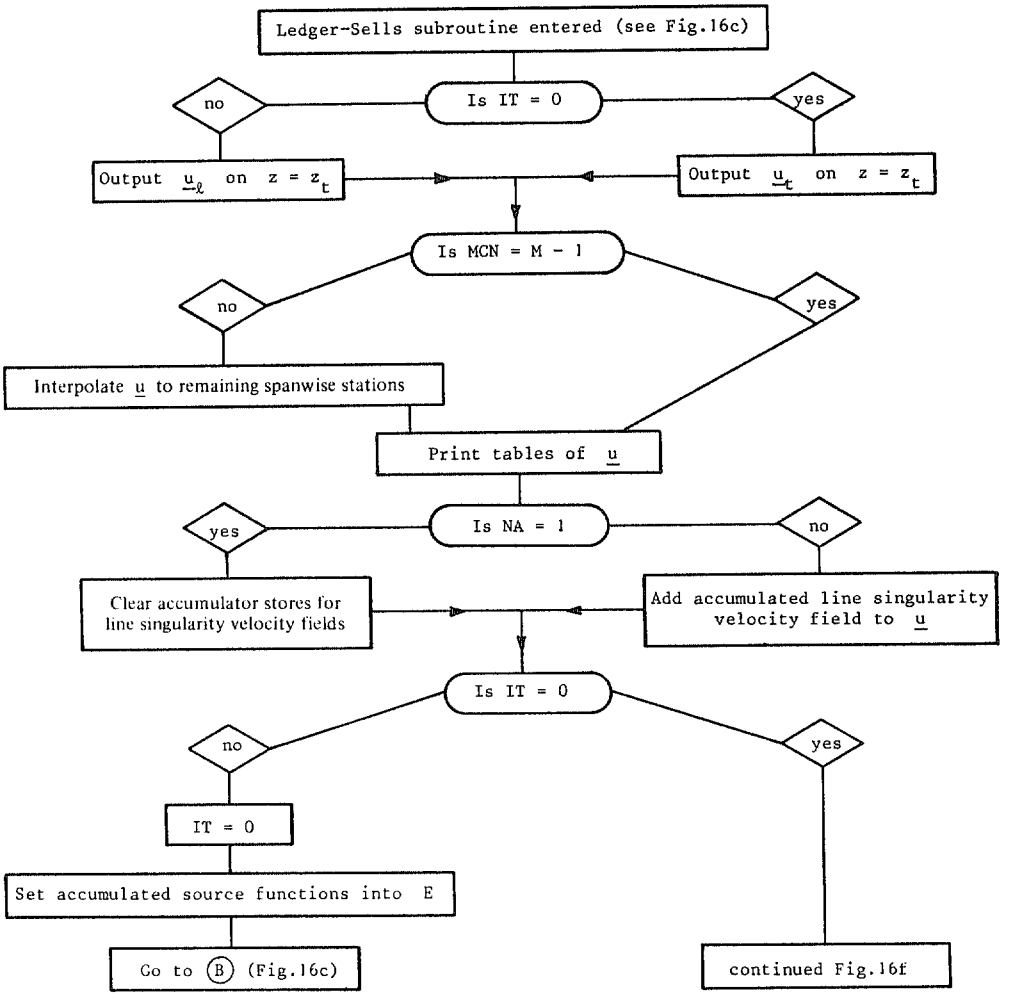

FIG. 16e. Flow diagram. Ledger-Sells and previous line singularity calculations.

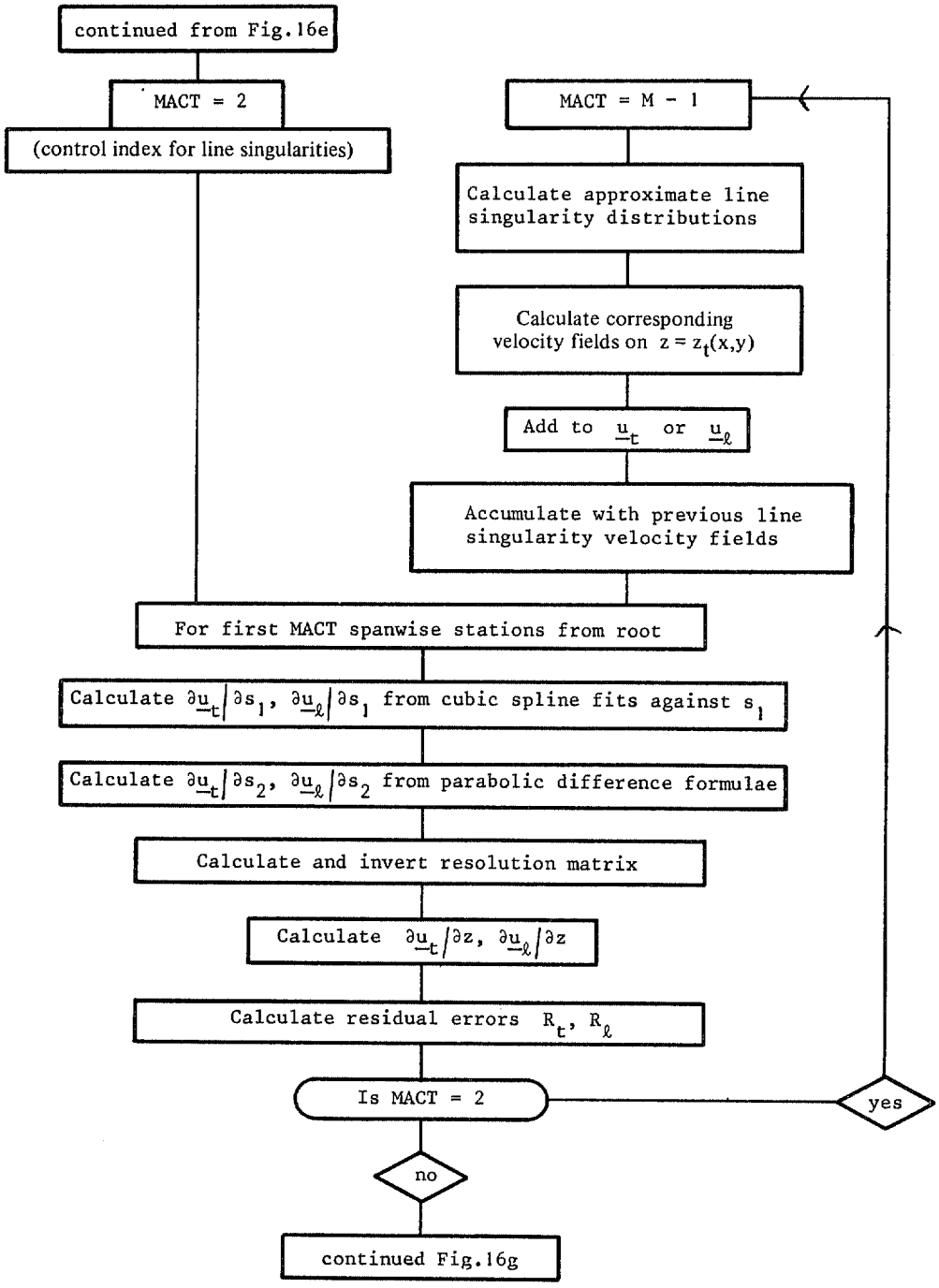

FIG. 16f. Flow diagram. Current line singularity calculations.

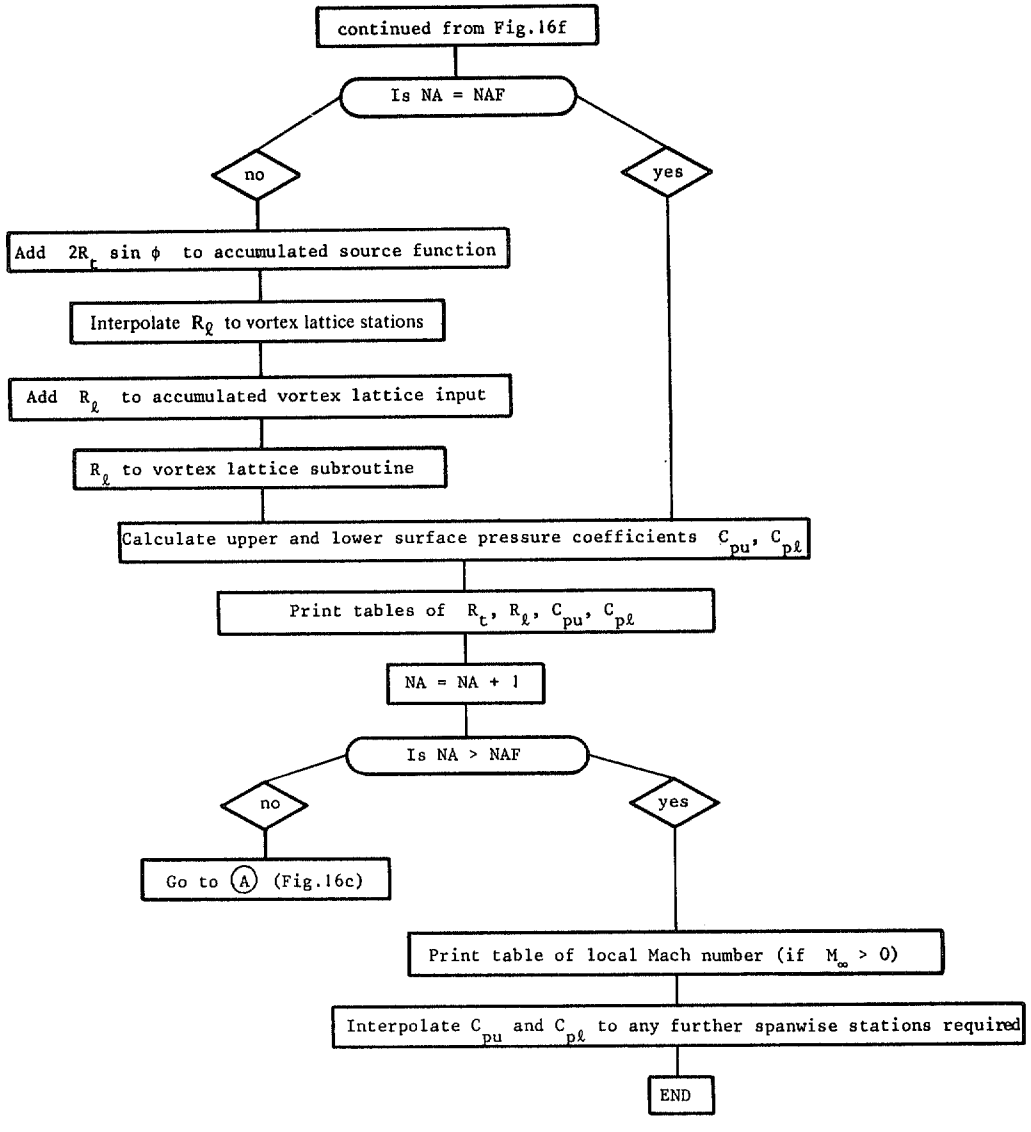

FIG. 16g. Flow diagram. End of main iteration cycle. Results output.

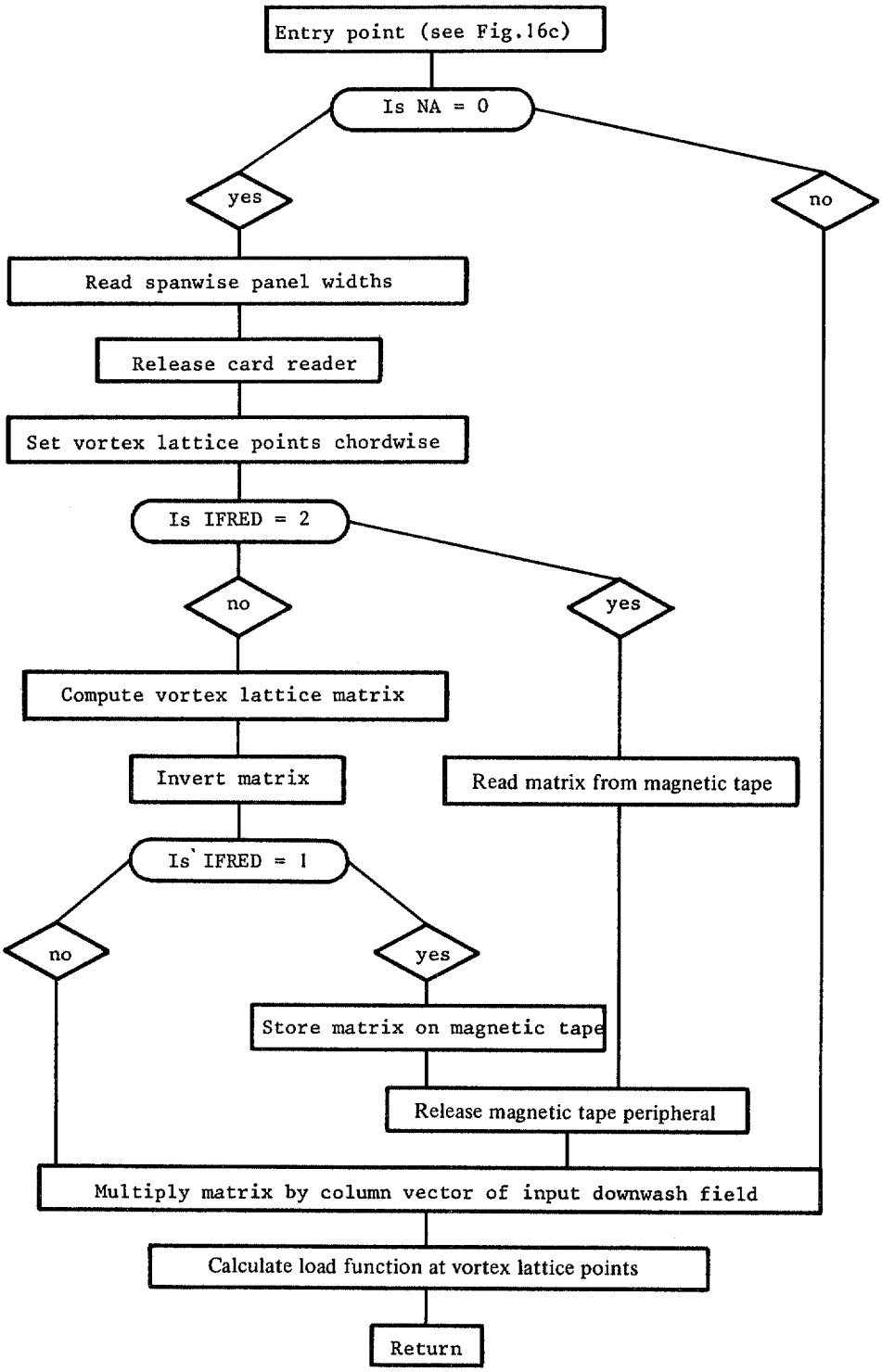

FIG. 16h. Vortex lattice subroutine (called in Fig. 16c).

Printed in England for Her Majesty's Stationery Office by J. W. Arrowsmith Ltd., Bristol
Dd 289031 K5 10/76

HER MAJESTY'S STATIONERY OFFICE

Government Bookshops

49 High Holborn, London WC1V 6HB
13a Castle Street, Edinburgh EH2 3AR
41 The Hayes, Cardiff CF1 1JW
Brazennose Street, Manchester M60 8AS
Southey House, Wine Street, Bristol BS1 2BQ
258 Broad Street, Birmingham B1 2HE
80 Chichester Street, Belfast BT1 4JY

Government publications are also available through booksellers

ISBN 011 470957 2